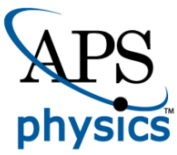

Exploring astrophysics-relevant magnetohydrodynamics with pulsed-power laboratory facilities

S. V. Lebedev, A. Frank, and D. D. Ryutov

Rev. Mod. Phys. **91**, 025002 — Published 25 April 2019

DOI: 10.1103/RevModPhys.91.025002

Exploring astrophysics-relevant magnetohydrodynamics with pulsed-power laboratory facilities

S.V. Lebedev

Blackett Laboratory, Imperial College, London, SW7 2AZ, United Kingdom

A. Frank

Department of Physics and Astronomy, University of Rochester, Rochester, New York 14627, USA

D.D. Ryutov[1]

Lawrence Livermore National Laboratory, P.O. Box 808, Livermore, California 94551, USA

Abstract

Laboratory facilities employing high pulsed currents and voltages, and called generally "pulsed-power facilities", allow experimenters to produce a variety of hydrodynamical structures replicating, often in a scalable fashion, a broad range of dynamical astrophysical phenomena. Among these are: astrophysical jets and outflows, astrophysical blast waves, magnetized radiatively dominated flows and, more recently, aspects of simulated accretion disks. The magnetic field thought to play significant role in most of the aforementioned objects is naturally present and controllable in pulsed-power environments. The size of the objects produced in pulsed-power experiments ranges from a centimeter to tens of centimeters, thereby allowing the use of a variety of diagnostic techniques. In a number of situations astrophysical morphologies can be replicated down to the finest structures. The configurations and their parameters are highly reproducible; one can vary them to isolate the most important phenomena and thereby help in developing astrophysical models. This approach has emerged as a useful tool in the quest to better understand magnetohydrodynamical effects in astronomical environments. The present review summarizes the progress made during the last decade and is designed to help readers identify and, perhaps, implement new experiments in this growing research area. Techniques used for generation and characterization of the flows are described.

[1] Retired

CONTENTS

I. Introduction

This Introduction starts with a brief discussion of the unique elements pulsed power facilities bring to laboratory simulations of astrophysical magnetohydrodynamic phenomena. Especially impressive is a high degree of control of the flow parameters and resultant structures that can be achieved on these facilities. We then proceed to articulate specific examples of objects which have been/can be explored in pulse-power settings. Finally, we address the interdependence of observations, numerical simulations and laboratory experiments in developing a better understanding of phenomena seen on the sky.

Hydrodynamical and magnetohydrodynamical (MHD [2]) phenomena in astrophysics cover an enormous range of spatial and temporal scales. They are the basis for some of the most spectacular astronomical phenomena, like supernovae shocks, accretion discs, and collimated jets. They sometimes occur on a relatively short time-scales allowing for the direct detection of their variability. These dynamically evolving flows may be quite bright, thereby making possible the detection of quite intricate morphologies and fine details. This, in turn, helps in inferring the processes occurring at the sources of these flows, even if those sources are not directly resolvable. Magnetic fields are often detected in these objects, or at least can be inferred from their morphology and dynamics. Despite an enormous diversity of morphologies and spatio-temporal scales, there is one point of commonality in many of these phenomena: they can be described by magneto-hydrodynamics or by radiative magnetohydrodynamics (RMHD).

It was realized decades ago that pulse-power facilities offer a natural platform for the study of these phenomena in laboratory environments. By "pulsed-power" we mean facilities where the plasma motion is triggered by high, short-pulse currents which drive the matter via the "*j-cross-B*" forces though sometimes motions can also be driven by the fast Joule heating of a sample or by a combination of the two processes. High magnetic fields are generated naturally and may become an integral part of the dynamical system.

The ability to generate flows with fields allows researchers to design laboratory experiments where flows that are morphologically similar to their astrophysical counterparts can be generated under controlled conditions and studied by a variety of diagnostic techniques. An expectation is that not only can morphology of astrophysical MHD flows be reproduced, but also one can detect effects that may be hard to resolve and identify in astrophysics. Examples of this would be the development of a small-scale turbulence, or the appearance of non-MHD effects (like the Hall effect). This general philosophy was earlier – and quite successfully – applied to the astrophysically-relevant hydrodynamic experiments based on high-power lasers (Remington *et al*., 1997; Kane *et al*., 1997, Drake, 1999, Robey *et al,* 2001). The first dedicated experiments with the pulsed-power facilities followed a few years later (Lebedev *et al*., 2002).

In addition to the exploration of MHD processes, there are other applications of the pulsed power devices that can benefit astrophysics. Due to their ability to develop high pressure in relatively large diagnosable volumes, pulsed power devices are also used for studies of equations of state relevant to the planetary physics. The ability to generate very bright flashes of radiation has also been used for studies of opacities of various plasmas of interest for astrophysical systems (Rochau *et al*., 2014; Bailey, *et al*., 2015; Knudson *et al*., 2015). In what follows we, however, will focus on the MHD applications.

[2] Definitions of acronyms used in this review are given in Section IX.

Pulsed power devices are not the only platform suitable for the studies of astrophysical MHD: other platforms include high-power lasers and magnetic confinement facilities. Each of these platforms has its own advantages. Lasers are flexible and are capable to deliver enormous energy fluxes into small volumes. Pulsed power systems are typically less expensive and allow for larger experimental volumes. Quasi-steady state plasma devices produce even larger plasma volumes and allow researchers to naturally enter the regimes of low or negligible particle collisionality. This characterization is, of course, quite crude as there may be combinations of elements of more than one approach in a single experiment. We will describe some specific examples later.

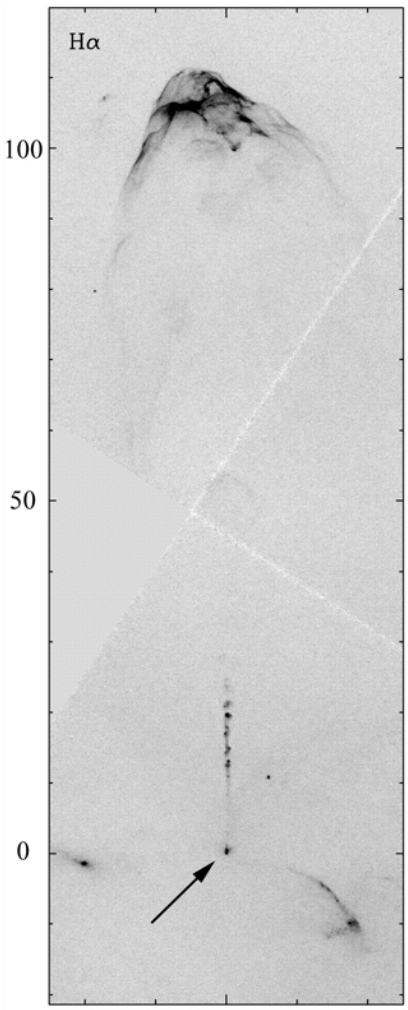

FIG. 1. A jet from a young star. The star situated inside the lowest knot (indicated by an arrow) is obscured by a compact reflection nebula. A knotty structure of the jet is obvious. At the top of the figure a bow shock produced by the interaction of the jet with the ambient medium is visible. For more details see Reipurth et al., (2002). Courtesy B. Reipurth, with permission of AAS.

In general, laboratory astrophysics based on a variety of experimental platforms has experienced explosive growth during the past decade, with several dozens of experimental papers appearing every year. We have chosen to summarize a subset of these results: the studies of astrophysics-relevant MHD with the pulse-power facilities. By narrowing the scope, we gain an opportunity to provide more comprehensive analysis of this area of research which has developed its own efficient techniques for generating and diagnosing dynamical flows morphologically similar to their astrophysical counterparts.

One has to remember that a laboratory experiment can properly reproduce only a relatively narrow subset of processes affecting a particular astrophysical phenomenon. Still, if properly scaled, it provides a reliable test-bed for validating numerical codes used in astrophysics, especially given that the experimenter can vary the input parameters and repeat an experiment many times. The main benefit to astrophysics is the capability of the laboratory experiments to reproduce the observed phenomena and thereby validate the conjectured underlying mechanisms.

A reader who might be interested in a broader view of laboratory astrophysics, can benefit from an older comprehensive review (Remington *et al*., 2006) that covers, in particular, the first

steps in the use of one type of pulsed-power devices, the Z-pinches. Another important publication is a brief review titled "The impact of recent advances in laboratory astrophysics on our understanding of the cosmos" (Savin *et al*., 2012) that summarizes the state of the field as seen from the astrophysicist's perspective. There are available also two studies on the promises of the laboratory astrophysics that have been produced by community-based workshops (Prager *et al*., 2010; Rosner and Hammer 2010), where one can find some brief discussion of pulsed-power approaches to the problem. Broad reviews of the Z pinch physics, technology and applications can be found in (Ryutov et al., 2000; Haines 2011).

To provide the reader with some background regarding astrophysical flows that pulsed power facilities have explored or are currently working on, we present several examples taken from the astrophysical literature; more details and references are provided in the further sections.

Figure 1 shows a jet generated by a young star. Such collimated supersonic streams of plasma driven from a central source are a common phenomenon in astrophysics. Most outflows and jets are thought to be generated near a central engine (e.g. a young, still forming star or a compact object like a black hole) surrounded by an accretion disc. The experimental modeling of all ingredients of this process is still impossible, but significant features like episodic events, intra-jet clumps, the interaction with external medium and others phenomena have been studied in a number of experiments (which we discuss in detail in Secs. II and III).

Creating an analogue of the accretion disc (see an image in Fig. 2) is a harder problem. The intrinsic difficulty here is the impossibility of reproducing the inward gravitational force that causes the disc material to spiral towards the central engine via various types of turbulent viscosity (Shakura and Sunyaev, 1973; Balbus and Hawley, 1991, see also Velikhov, 1959). What is, however, possible in the lab is confining the rotating plasma from centrifugal radial expansion by maintaining the ram pressure of the incoming plasma flow. This configuration will be discussed in Sec. IV.

FIG. 2. Hubble Space Telescope image of HH-30 jet (NASA press release of June 6, 1995). An accretion disk observed edge-on is seen at the top of the image as a dark band between its outer parts illuminated by the central star. The young stellar object is obscured by the densest part of the disk. See Madlener et al. (2012) for the detailed analysis.

A large segment of astrophysical MHD is related to the formation of shocks in supersonic and super-alfvenic flows. In a number of cases the shocks may be of a collisionless nature (Sagdeev and Kennel, 1991). The shocks may also be strongly affected by radiative processes (Drake, 2006). Shocks, including radiative shocks, are discussed in Sec. V.

Thus far we considered single-fluid magneto-hydrodynamics. This may become insufficient even at scales large compared to the particle mean-free path. In such cases one has to switch to two-fluid MHD, that gives

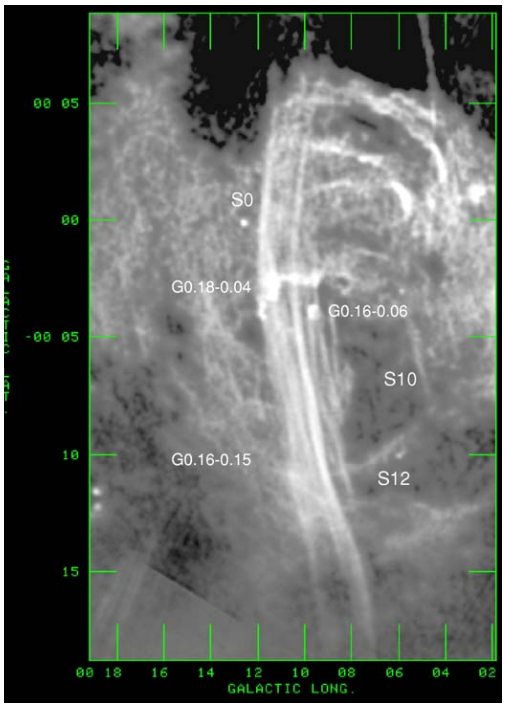

FIG. 3 The image of the fine filamentary structures near the center of our galaxy, consisting of a network of vertical filaments with lengths of about 30 pc (Yusef-Zadeh *et al*., 1984, Yusef-Zadeh *et al*., 2004); it is speculated (Trubnikov, 1992) that those may be disrupting pinches leading to development of high voltages and particle acceleration. The image is taken by the NRAO Very Large Array at the wavelength of 20 cm.

rise to new effects not covered by the "standard" MHD, in particular, to the Hall effect. The Hall effect may play a significant role in the evolution of astrophysical flows, in particular in the jets (Konigl, 2010) and in stellar flares and stellar winds (Mandt, 1994). These issues are discussed in Sec. VI.

Another aspect of non-hydrodynamical effects is the formation of fast particles (high-energy beams and "hot" electron and ion populations). These effects may be important as an injection mechanism for further particle acceleration in cosmic rays. These phenomena lie beyond the boundaries of even a two-fluid hydrodynamics. Still, as high voltages formed in the disruptions of the current channels (see Fig. 3) may be triggered by hydrodynamic instabilities, we briefly discuss fast particles in Secs. III.B and VI.C.

Magnetic reconnection is one more phenomenon affecting dynamics of many astrophysical systems. Depending on the plasma parameters, it may occur via dissipative processes cascading down to the scales much shorter than the collisional mean-free-path, or via development of hydrodynamic turbulence (e.g., Yamada *et al*., 2010; Ryutov, 2015). In the high-energy-density environment of pulsed-power facilities, one can in principle access both regimes. We touch upon this possibility in Sec. VII.

An important issue in simulating astrophysical processes in laboratory experiments is the scalability between the two systems even though their spatial and temporal scales differ by many orders of magnitude. It turns out that the MHD equations allow for a broad class of similarities in situations where fluid viscosity and thermal conductivity are sufficiently low (Ryutov, Drake, Remington, 2000). This occurs in a number of both astrophysical and laboratory settings. Importantly, shock waves are covered by this similarity. A different set of similarities covers aspects of two-fluid description and collisionless phenomena.

In Appendix A we present a discussion of the similarity transformations, and other conditions, which should be satisfied to allow meaningful connections between astrophysical and laboratory phenomena. It goes without saying that it is impossible to create in the lab a fully operating astrophysical object: laboratory experiments can only model a subset of a system for which such a representation is possible. Thus the

successful design of the experimental system requires not only performing the scaling transformations, but also creating appropriate initial conditions and determining a time-interval over which the scaling restrictions remain satisfied such that meaningful connections to astrophysical processes remains valid.
Experiments described in different Sections of this review are at different stages of implementation of the outlined approach. Some of them are at relatively advanced stages, e.g. experiments with laboratory plasma jets (Sec. II, Sec III), and it is possible to discuss the scaling correspondence between the laboratory and astrophysical phenomena. In other cases the experimental systems are still under development and a full scaling to a particular astrophysical system is not possible (e.g. experiments with rotating plasmas, Sec. IV). Experiments discussed in Sections V-VII do not attempt to model particular systems, focusing instead on the physics of fundamental and astrophysically relevant processes such as shocks, non-MHD effects and magnetic reconnection.

These experiments provide data for verification of numerical simulations of the processes. Codes tested in this way can be then reliably used to predict the behavior of an astrophysical system down to certain scale established in a laboratory experiment.

In equations throughout the paper we use SI (mks) units, whereas in the Tables and when presenting experimental data we use mixed units specified in each case.

II. Jets and outflows – weak magnetic field

Hydrodynamic jets with weak fields are an important class of astrophysical outflows. Special experimental techniques developed on pulsed-power facilities allow for high degree of control over lab-scale jets suitable for exploring a variety of their astrophysical counterparts. Scalable experiments on the generation of highly collimated jets, their interaction with the side winds, and their collisions with dense gaseous clouds are described and related to astrophysical observations. Experimental techniques are briefly outlined.

A. Generating plasma streams and plasma jets with wire arrays.

The generation of the astrophysically-relevant jets was probably the most visible and important contribution of pulsed-power facilities to the laboratory studies of astrophysical MHD. An important part of these experiments was their capability to generate and control plasma flows by the use of so-called “wire arrays”, which were initially developed for research in the areas of radiation sources and controlled fusion (see Matzen *et al*., 1999 and references therein). In the simplest case, “a cylindrical array” is made of identical fine wires, from a few microns to few tens of microns in diameter, all parallel to the axis of the cylinder and distributed evenly over its circumference (i.e., an angle subtended by the two neighboring wires is $2\pi/N$, with N being the total number of wires). Such systems allow one to create a well-controlled initial state for fast z-pinches. They have led to the controlled generation of intense pulses of soft and hard X-rays. A general setup of the wire-array experiment can be found in Matzen *et al*., 1999. Figure 4 represents a simple schematic.

Investigation of an early stage of the wire array implosion (Lebedev *et al*., 2001) has revealed that early in the current pulse plumes of plasma with a relatively low density are formed around each wire and begin to expand. This occurs prior to the onset of any radial motion of the wires themselves. This early stage of the discharge is illustrated by Fig. 5 (Lebedev *et al*., 2001). Under the action of a global azimuthal magnetic field, the plasma plumes gain radial momentum, converging to the array axis well before significant motion of the wire cores begins. These separate streams merge somewhere half-way to the axis and form a continuous converging flow. A high resistivity of wire cores means that they do not carry a significant current and remain at their original positions, while majority of the current concentrates in a layer of plasma surrounding the cores. This plasma layer is continuously replenished by the material ablated from the wire cores providing a long-lasting injection of ablated plasma streams accelerated towards the array center by the *JxB* force. The converging cylindrical plasma flow carries some axial current and, therefore, an azimuthal magnetic field. For sufficiently small azimuthal separations between the wires the azimuthal inhomogeneities smooth out at some distance inward from the wire cores, and we get a converging cylindrical plasma stream that is typically supersonic and superalfvenic. It is this smooth radial flow that served as a basis for a number of experiments described in this review, in particular, in Sec. II, III.A, IV, V and VII. Other techniques for producing plasma flows suitable for the studies of the astrophysical MHD phenomena are described in Sec. III.E, V.B and VI.

As an aside, one can mention that formation of the plasma flow propagating inward still allowed for the production of high-quality wire-array implosions used in the applied (fusion, radiation sources) research (Cuneo *et al*., 2006). The current per wire in these experiments was in the range from one kilo-ampere to tens of kilo-amperes, with the rise-time of ~100ns.

The use of the wire arrays allows one to create a diverging plasma flow by putting the reverse current conductor on the axis of a wire array as shown in Fig.6 (Harvey-Thompson *et al*., 2009). This produced an expanding plasma shell outside the wire array. Such a configuration facilitates an access to the experimental zone, which is now situated outside the wire array.

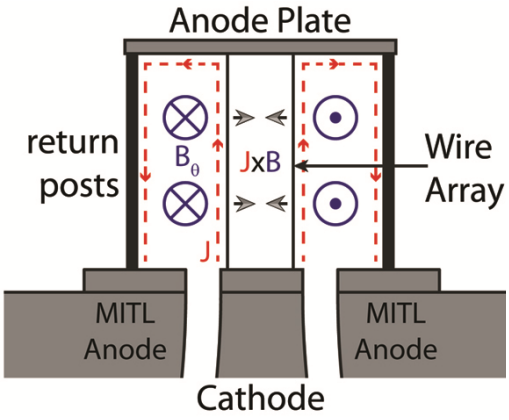

FIG. 4. Schematic of a wire array z-pinch. The cylindrical array of wires is fed through the gap at the bottom of the figure by the current supplied via the pulse-power generator (not shown). The current flows along the wire array (the position of which is show by arrow) and returns through an outer cylinder, usually having holes for diagnostic access or made of separate return current posts. An azimuthal magnetic field present outside the array pushes it inward. In the fusion and radiation applications, implosion of the array leads to a short pulse of extremely high pressure. For the applications considered in this review, the main focus is the early stage of the pulse, when the wires have just started moving towards the axis (Courtesy M.J. Bennett).

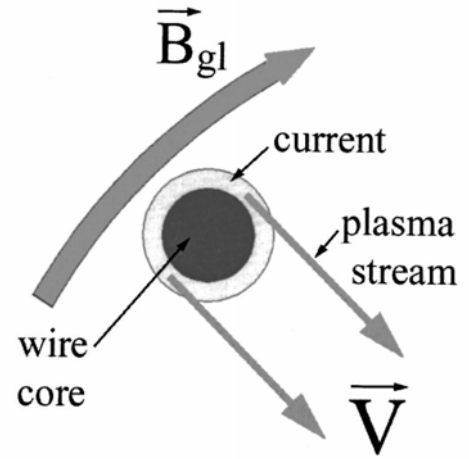

FIG. 5. Formation of a plume of plasma around a wire core (a white annulus around the dark circle). The global magnetic field vector B_{gl} is shown by a grey curved arrow. Interaction of an axial current in the plume with the global magnetic field causes acceleration of the light plume material towards the center. At some distance from the wires, the plumes merge to form a continuous flow carrying some axial current (after Lebedev *et al*., 2001).

Returning to the generation of plasma jets, we describe the corresponding experimental configuration (Lebedev *et al*., 2002), which is illustrated in Fig. 7. Here we have not a cylindrical, but a conical wire array, with the apex half-angle of 15-30 degrees. Accordingly, after the pinch current is turned on, the plasma flow (that moves normal to the array surface) converges on the array axis. The plasma is highly collisional (see below), and the process has to be described as a hydrodynamic phenomenon. As the radial (towards the axis) component of the velocity is highly supersonic, a conical shock forms near the axis, which will redirect the flow momentum in the axial direction (a hydrodynamical "shaped-charge effect", Walters, 1998). Such conical shocks are not a stranger to the astrophysical world. The role of these kind of shock structures has been discussed, e.g., in Canto *et al*. (1988), where the possibility of young stellar object (YSO) jet formation by converging conical shock. In addition, Frank *et al*. (1996), used conically-converging flows in the environment of stellar wind-blown bubbles to create highly collimated flows. In both cases conical flows were explored as a jet formation mechanism years before laboratory experiments were carried out. In the laboratory, dense, strongly radiating jets have also been produced by the irradiation of the inner surface of conical targets by high-power lasers by Farley *et al*. (1999) on NOVA facility and by Shigemori *et al*. (2000) on GEKKO-XII facility.

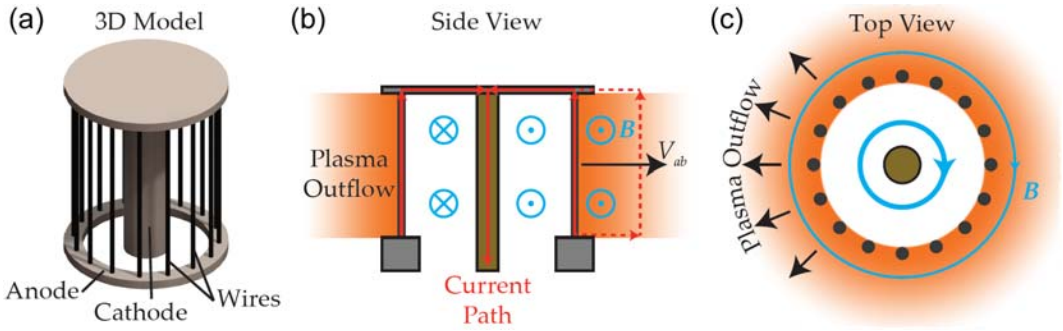

FIG. 6. Inverse wire array. The current comes from the bottom, flows upward along the wires of the array (16 in this case), and comes back through a central post (gray). Diverging cylindrical plasma flow is created due to magnetic pressure acting on the plumes in the outward direction (Courtesy J. Hare)

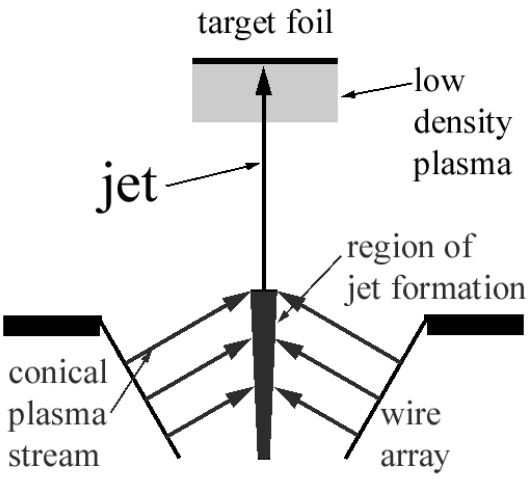

FIG. 7. Generation of the jet in a conical wire array (after Lebedev *et al*., 2002).

The dense plasma formed near the axis in the configuration of Fig. 7 has significant axial momentum and may be additionally accelerated by the pressure gradient in the axial direction. As a result, a well-collimated plasma jet emerges from the cone. Note that the wires in this scenario serve only as a source of plasma for jet generation, and do not significantly participate in the motion (they remain too heavy to be accelerated).

This configuration and its variations allowed the experimenters to produce a broad range of astrophysics-relevant hydrodynamic objects: highly radiative weakly diverging jets; jets propagating through an external medium including emulation of a "side wind"; rotating jets; simulated accretion disks; and others applications. The corresponding results will be discussed in Sec. II.B, II.C and IV. In the next section we describe the use of the just described techniques for the studies of some aspects of the physics relevant to the YSO jets.

B. Hypersonic, radiatively cooled hydrodynamic jets and their interaction with an ambient medium

The configuration of a conical wire array shown in Fig. 7 led to the most astrophysically relevant set of jet experiments from the early stage of the laboratory pulsed power astrophysics research. In this way they served as an early model for what was possible with High Energy Density Laboratory Astrophysics (HEDLA). The first experiments with conical wire arrays (Lebedev *et al*., 2002) have indeed shown the relevance of such jets to astrophysical problems, in particular, to the outflows from young stars which have comparable Mach numbers and radiative cooling parameters. Several wire materials were used in these experiments: tungsten, stainless steel, and aluminium. The wire diameters were 25, 25 and 18 μm, respectively. The number of wires was 16 with a bottom radius of the array set at 8 mm, and an openning angle of the wires at 30^{o}. The length of the array was 1 cm. The velocity of the jet was measured

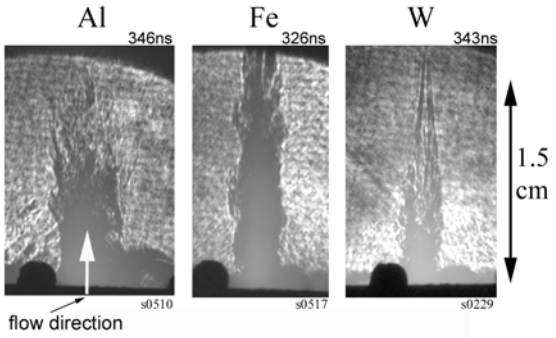

FIG. 8. Laser probing images of plasma jets formed in aluminum, stainless steel, and tungsten wire arrays show that degree of collimation increases for elements with higher atomic number in which the radiative cooling is higher. Lebedev *et al*., 2002.

via laser probing diagnostics and was found to be ~ 150 km/s.

The structure of these jets is shown in Fig. 8 borrowed from Lebedev *et al.*, 2002. The parameters of the jet beyond the upper surface of the array are either measured directly (Lebedev *et al.*, 2002) or inferred from numerical simulations matching the experiment (Ciardi *et al.*, 2002) and are presented in Table I; some most important derived parameters are presented in Tables II and III.

TABLE I. Measured and inferred parameters of the tungsten plasma formed in conical arrays: n_e (electron density); T (common value of the electron and ion temperatures), Z (average ion charge), a (jet radius at the upper surface of the wire array), S (sound speed in the jet plasma), V (jet velocity at the exit from the array), L_C (cooling length, estimated from soft X-ray emission decay along the jet)

n_e†	T*	a	Z*	S	V	L_C
10^{19} cm^{-3}	50 eV	1.5 mm	10	$5\cdot10^6$cm/s	$(1.5\text{-}2)\cdot10^7$ cm/s	0.3cm

†The definitions of the entries are provided in the heading to the Table.
* Parameters inferred from numerical simulations

TABLE II. Derived parameters: λ_{ei}, λ_{ii} - electron-ion (ion-ion) collision length; ν ion kinematic viscosity; D_M magnetic diffusivity, χ_{therm} electron thermal diffusivity; B_0 the magnetic field strength at which the plasma beta evaluated for the thermal pressure would become dynamically significant $\beta=2\mu_0 p/B^2_0=1$.

λ_{ei}	λ_{ii}	ν	D_M	χ_{therm}	B_0
0.1 μm	0.1 μm	60 cm^2/s	10^5 cm^2/s	$4\cdot10^3$ cm^2/s	15 T

TABLE III. Main dimensionless parameters: $\mathrm{Re}=aV/\nu$; $\mathrm{Re}_M=aV/D_M$; $Pe=aV/\chi_{therm}$; L/L_C

Re	$\mathrm{Re_M}$	Pe	$\mathrm{L/L_C}$
$3\cdot10^4$	20	500	2-7

Note that the experiments achieve a remarkably high Reynolds number. The other dimensionless parameters, Re_M and Pe, also significantly exceed the unity. This provides a reasonable degree of confidence that the hydrodynamical phenomena occurring in this laboratory-generated jet will correctly replicate the same phenomena in hydrodynamical astrophysical jets, despite an enormous difference in the scales.

One of the most distinctive features of the YSO jets is their high degree of collimation, with the length-to-radius ratios as high as 10 to 20. In addition the astrophysical flows are characterized by high Mach numbers of M ~10-20. It is thought that such divergence and high values of M are related to the fast radiative cooling of the jets (Blondin *et al.*, 1990; Stone *et al.*, 1993a, 1993b). The observed trend in the divergence of the laboratory-made jets vs. the jet material supports this viewpoint: the tungsten jet is much better collimated than the aluminium jet. The same trend was found

in the earlier laser-driven experiments (Farley *et al*., 1999; Shigemori *et al*., 2000).

Two-dimensional (*r*-*z*) simulations automatically produced azimuthally symmetric outflows due to their imposed azimuthal symmetry. In experiments the converging plasma flow inside the conical array was initially strongly modulated in the azimuthal direction due to the relatively small number of wires used (typically 16, sometimes as little as 8). Nevertheless it was observed that the jets had very good azimuthal symmetry at the exit from the array, which allowed concluding that formation of jet via converging conical flows is stable to the azimuthal perturbations. Note that this was a conclusion that could not be reached from traditional astrophysical studies alone. The characteristic cooling length in the experiments was estimated from the measurements of the soft x-ray emission decay along the jet.

With regard to the magnetic field strength, it was not measured directly in these early experiments, but one could get an upper bound for it by noting that the jet didn't show development of a pinch instability. The absence of this potent instability in a system perfectly describable by MHD could be interpreted as a magnetic pressure that was smaller than the plasma pressure, yielding an estimate presented in Table II. In subsequent experiments the magnetic field was measured directly, yielding the value of a few T, i.e. well below the upper bound given in the right-most column of Table II and, correspondingly, not playing significant dynamical role. We note that in astrophysical jets the magnetic fields appear to become less important at large distances from the region of collimation (Hartigan et al., 2007).

C. Hydrodynamic interaction of the jets with a side wind

The jets described above were truly hydrodynamic in that their plasmas were highly collisional and showed no significant effects due to magnetic fields. In a subsequent series of experiments such jets created by conical arrays were used to study the interaction of hydrodynamical stellar outflows with plasma clouds encountered during their propagation. To generate a miniature analogue of such a cloud, a plastic foil was placed at some distance from the jets axis, at an oblique angle, as shown in Fig.9a. XUV emission from the standing conical shock and individual wires of the array interacted with the foil and led to formation of a plasma flow (plasma wind) crossing the path of the jet (Lebedev *et al*., 2004; Lebedev *et al*., 2005; Ampleford *et al*., 2007).

This setup mimics the interaction of the YSO jet with a cross-wind, a process that is thought to be responsible for the formation of the C-shaped YSO jets, whose observations are summarized in Reipurth and Bally (2001). While there had been a number of analytic and simulation studies of these jet-wind interactions (relevant to the HH110 system, Raga *et al*., 2002), the pulsed power studies described below allowed for theory to be directly compared with controlled experimental studies for the first time.

In the experiment, the presence of the cross wind was shown to cause deflection (bending) of the jet. The jet trajectory/shape was measured using laser probing and XUV self-emission images, and the densities of the jet and the ambient plasma (wind density) were measured by the interferometry. The wind velocity was only estimated, but not directly measured in these experiments. The observed behavior of the jet, its modified trajectory, was then interpreted using results of numerical modeling in which the plasma wind velocity was adjusted to fit the jet trajectory. The typical numbers for the jet (V)

and wind (V_w) velocities, as well as their densities are given in Table IV (taken from Lebedev *et al*., 2004).

The same density/velocity ratios, as well as the jet Mach number were then used to model the bending of *astrophysical* jets by the same mechanism. Simulations (Ciardi *et al*., 2008), in addition to reproducing the overall trajectory similar to predicted by the analytical model of Canto and Raga (1995) show that the interaction also leads to formation of density perturbations (i.e. knots) in the jet. It is important to emphasize that in the simulations both the jet and the wind are initially uniform and smooth, and the perturbations (knots) arise from the development of the combination of Rayleigh-Taylor and Kelvin-Helmholtz instabilities. The duration of the laboratory jet interaction was insufficient to see such a development in the early experiments. Simulations also assessed effects of jet rotation on the morphology of the interaction, suggesting that there could be some observable differences.

TABLE IV. Parameters of the jet and crosswind in experiments (Lebedev *et al*., 2004).

Area	Density (g cm^{-3})	Velocity (cm s^{-1})	T (eV)	Z
Jet	~10^{-4} a)	(10-20) x 10^6	< 50	5-10
Wind	~10^{-5} b)	(2.5-5.5) x 10^6 c)	Unknown	1-2

a) at $n_e \sim 5 \times 10^{18}$ cm^{-3}, $A = 183$, and $Z = 10$.
b) at $n_e \sim 10^{18}$ cm^{-3}, $A = 6$, and $Z = 1$.
c) Velocity of crosswind was determined from the measured delays in the start of jet-wind interaction, observed for different separations between the foil position and the jet axis

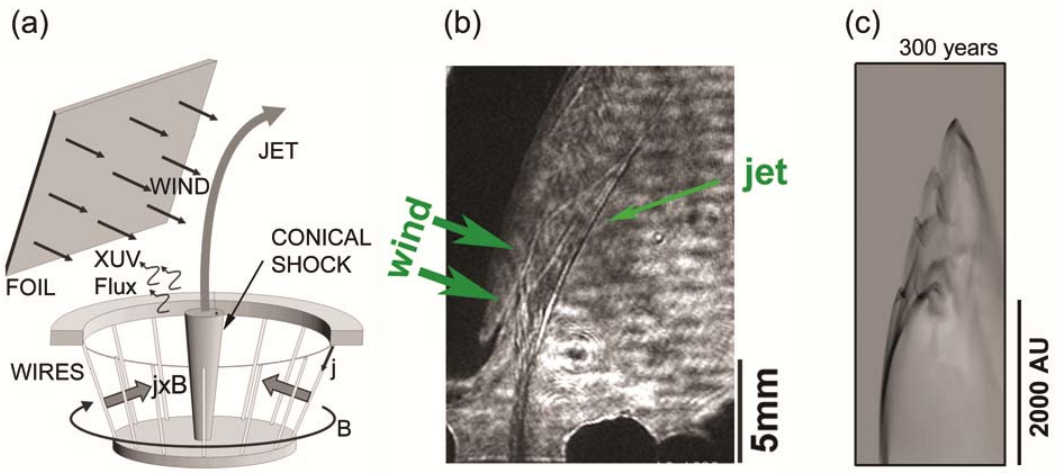

FIG. 9. (a) Schematic of the jet formation in a conical wire array and a side wind generation by surface plasma expansion from the plastic panel; (b) time-resolved laser schlieren image of the jet bending (340 ns after the start of the current); the capability of resolving fine features of the interaction zone makes this platform attractive for selecting the most plausible scenarios of analogous effects in astrophysics; (c) The line-integrated density structure in the jet termination area, from numerical simulations of Ciardi *et al*., 2008. (Adapted from Ciardi *et al*., 2008)

Another common astrophysical configuration is represented by a jet plowing into a stationary gaseous cloud (see, e.g., Fig 1). This occurs in star forming environments when a jet penetrates denser regions of its natal molecular cloud and in galactic-scale jets when they propagate through the clumpy media surrounding the central super-massive black hole. To explore these phenomena in the laboratory, in Ampleford *et al*. (2005) and Suzuki-Vidal *et al* (2012) the ambient medium was formed using a cloud of neutral gas positioned on the path of the jet. The cloud was typically formed using a supersonic gas nozzle. The velocity of the gas flow was, however, significantly smaller than the jet velocity so the gas cloud could be considered as a stationary mass distribution. In this way astrophysically relevant ratios of jet/ambient densities were produced. For laser-based experiments on the interaction of jets with an ambient medium see Foster *et al*. (2005) and Nicolaï *et al*. (2008).

In some of the experiments the gas cloud had a relatively sharp boundary, allowing direct study of the interaction of the jet crossing a density discontinuity. In Ampleford *et al*. (2005) it was observed that the interaction produced a broad bow shock (Fig. 10). The overall dynamics of the working surface (Blondin *et al*., 1990) formed at the head of the jet interacting with the gas cloud was in reasonable agreement with the

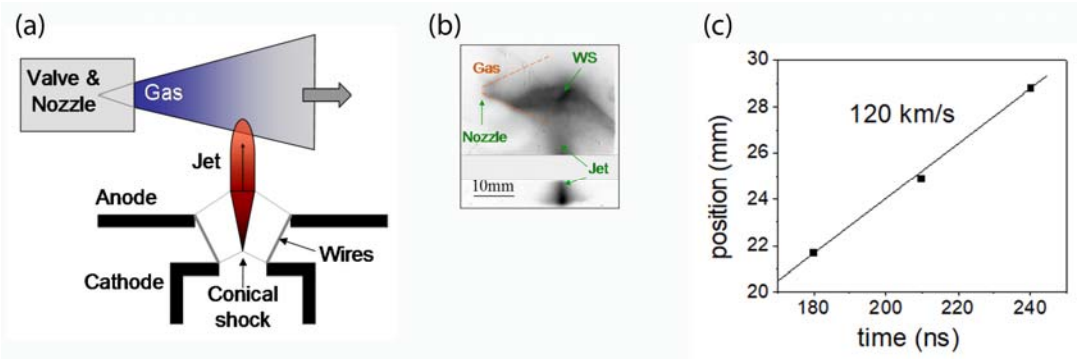

FIG. 10. (a) – Schematic of experiment in which a radiatively cooled plasma jet interacts with a gas cloud. On the time-scale of the plasma jet propagation, the gas cloud can be considered stationary. (b) Self-emission image of a plasma jet (formed from stainless steel wires) interacting with an argon gas cloud. Position of working surface (marked as WS) seen as a region of enhanced emission at the head of the jet is labelled in (b). Velocity of the working surface graphed in (c) is two times smaller than the jet velocity in the absence of the gas cloud, consistent with the jet-ambient density contrast of $\eta \sim 1$. Adapted from Ampleford *et al*., 2005.

standard expressions describing its dependence on the density ratio. In addition, experiments show development of asymmetries in the shape of the bow-shock, and in particular a transverse displacement of the brightest regions of the working surface with time. One possible explanation is the presence of advected B-field in the jets and in the plasma surrounding the jet. The ionization of the gas cloud by the XUV radiation could lead to formation of a new, asymmetric path for the current, which led to appearance of unbalanced JxB force slowly displacing the jet.

D. Highly-collimated jets produced by ablation of the central area of a metal foil

This approach is based on the configuration where the central cathode post is connected with the surrounding cylindrical return current conductor by a thin, vacuum-tight planar metal foil, as shown in Fig. 11. The attractiveness of this technique is related, in particular, to the fact that it allows one to create a setting where the jet is interacting with an ambient medium from the very beginning of the jet formation. This allows one to address an important issue of the effect of ambient medium on the formation and propagation of the astrophysical jets. This question is particularly important as conditions in the medium surrounding an astrophysical jet may not be directly probed by observations so that the medium's conditions (and collimating pressure) may not be directly inferred.

In the experiments the jet is formed because the radial current flowing through the foil between the central post and external cylindrical return current conductor is heating the foil predominantly near the center due to the radial divergence of the current flow. Therefore, intense heating of the foil occurs only near the center, and the ablated plasma column turned out to be highly collimated. This technique was used in Suzuki-Vidal *et al* (2012).

We start from the situation where the ambient gas density above the foil is negligible, and the ablated plasma expands into "empty space." Even in this case, some lower density plasma appears outside the dense central jet due to the heating and ablation of the foil. This "halo" plasma has density a factor of ~10 smaller than that in the central jet but moves with the same axial velocity.

These (and related, Suzuki-Vidal *et al* (2013)) experiments produced jets with a very high degree of collimation: an opening angle of 2-5 degrees is sustained over the distance exceeding the jet radius by a factor of >10, with a sharp density contrast at the boundary between the jet body and the halo plasma (Fig.12). The internal Mach number in these experiments was measured by Thomson scattering (TS) diagnostic: the Doppler shift of the ion feature provided jet velocity. Spectral broadening provided measurements of ZT_e and thus the ion sound speed. From these measurements the Mach number was determined to be only ~2.5, too small to explain the observed very small divergence of the jet (3^0 opening angle would require M ~ 20).

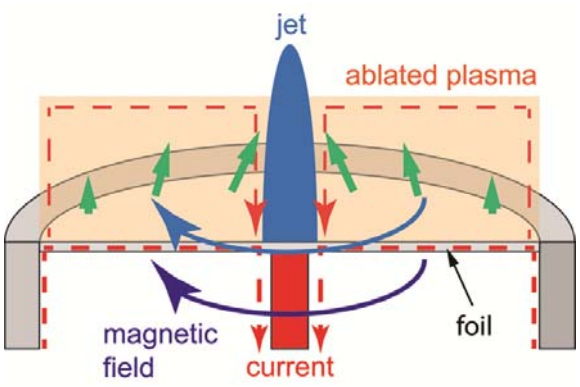

FIG. 11. Schematic of a thermal mechanism of the jet generation on the planar metal foil. A "distributed" magnetic field structure is formed due to advection of magnetic field diffusing through the resistively heated foil. Ablation, strongest near the axis, combined with the magnetic hoop force, leads to the formation of a dense jet surrounded by a lower density plasma flowing upward. (Courtesy F. Suzuki-Vidal).

Explanation of this discrepancy came from MHD simulations (Suzuki-Vidal *et al*

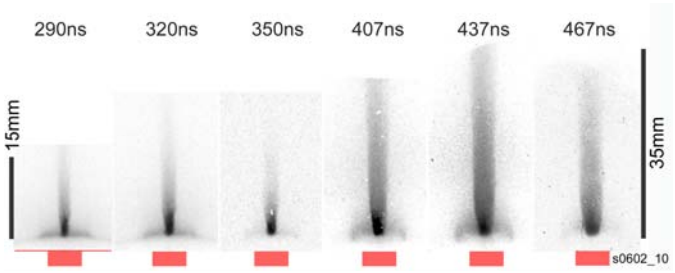

FIG. 12. XUV self- emission images of a jet from a radial foil propagating in vacuum. The images were obtained during the same experiment and times are relative to the start of the current. Position and diameter of the cathode are shown below the jet images, including the initial position of foil in the first image. The jet starts ~1.5mm above the initial foil position due to expansion of the central part of the heated foil. From Suzuki-Vidal *et al*., 2012, Courtesy F. Suzuki-Vidal.

(2012)), which suggest that the halo plasma surrounding the jet carries some level of frozen-in toroidal magnetic field, with the current path responsible for this field closing at the boundary of the halo plasma. The pinch force associated with this B-field produced the inward convergence of the halo plasma. The collimation of the central, dense part of the jet was provided by the ram pressure of this converging flow. What is remarkable in this set-up is that this is essentially a magnetic collimation of the outflow by the "distributed" magnetic field structure. It provides strong collimation but does not destroy the jet stability. In these experiments the maximum observed jet length (≈ 45mm with a length to radius ratio >20) was determined by the duration of the current pulse driving the plasma ablation from the foil, which allowed the jet to propagate distances exceeding the radius of the plasma emitting foil by a factor of 2. The question of how much longer the steady, stable propagation of the jet is possible in this set-up has not been investigated as yet.

As mentioned earlier, the set-up with the use of radial foil provided more flexibility for adding ambient media for jet-plasma interactions, in particular allowing creating a uniform distribution of the neutral gas above the foil. In this case the interaction remains azimuthally symmetric, with formation of a bow shock ahead of the central jet.

As shown in Fig. 13, two distinct features are formed (Suzuki-Vidal *et al* (2012)). Firstly there is a curved shock, gradually becoming a conical shock and driven into argon prefill by the lower density halo plasma. The shock position is determined by the radial profile of ram pressure in the flow and the temporal delay in the plasma formation at the foil (plasma forms earlier at smaller radius as it is driven by a higher current density of the radial current).

Secondly, the bow shock is developing above the central jet from ~300ns and can be seen above the conical ablation shock in the last 5 images of Fig.13a. This is also illustrated by Fig.15a, where the tops of the last three images of Fig. 13a are shown with higher magnification. Fig. 15b shows the images for a different shot – the similarity of the two rows shows the robustness of this feature. The bow shock is driven by the faster axial velocity of the plasma ejected by the high pressure created at the top of the central jet.

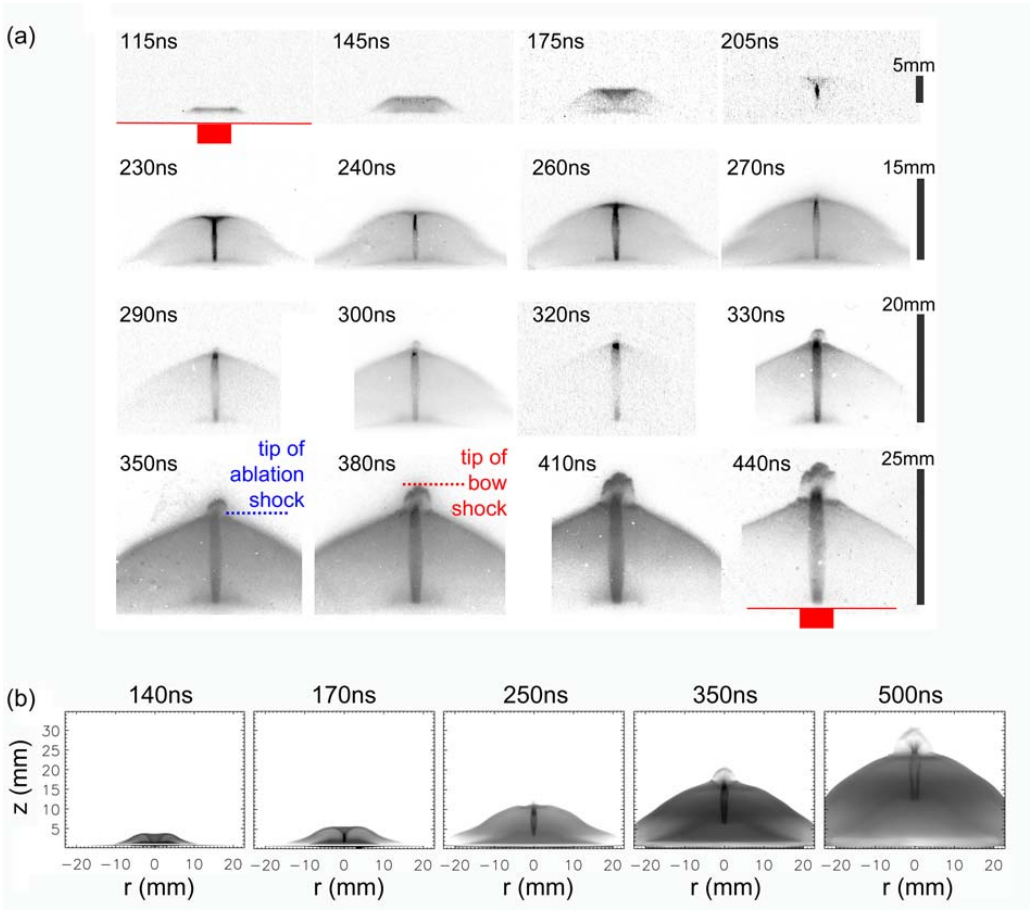

FIG. 13. (a) Sequences of XUV emission of a jet generated via an aluminium foil and propagating in argon, showing the formation and evolution of the jet together with the formation of two distinctive shock features: an "ablation shock" formed at early times, followed by the later formation of a "bow-shock" seen above "ablation shock" from ~300 ns. The diameter and position of the cathode and the foil are shown on the first and last frames. (b) MHD simulations of the experiment reproduce the main features of the jet formation and evolution (synthetic XUV images). Courtesy F. Suzuki-Vidal.

This experiment was modeled with GORGON 3-D resistive MHD code (Chittenden *et al*., PPCF 2004; Ciardi *et al*., PoP 2007), with the simulations accounting for the radiative cooling of the plasma. As can be seen from Fig.13b, which shows synthetic XUV emission images, the simulations were able to reproduce all of the main features of the evolution of the system. Maps of the force densities and the stream lines of the plasma flow (Fig. 14) show that collimation of the central jet is provided by the converging plasma streams: the plasma ablated from the foil is redirected towards the axis by the radial component of the JxB force[3]. The motion of the interface between the

[3] Simulations shown in Fig.14 correspond to the case when a low density ambient gas was added above the foil, but the same mechanism of jet collimation was observed in simulations of jet formation in the absence of the ambient material: in both cases the pinching azimuthal magnetic field was located in the material ablated from the foil.

ambient gas and foil material (the "ablation shock" indicated in Fig.13a) is also magnetically driven, by the JxB force provided by the toroidal magnetic field and current flowing along the ablation shock surface.

The simulations also suggest that the bow shock seen in Fig.13 is formed due to an increase in pressure at the tip of the ablation shock. This is driven to large extent by the enhanced toroidal magnetic field in this region, forming a structure resembling a nozzle. The bow shock driven by the fast plasma flow develops a number of regular, larger scale structures with the size comparable to the bow shock radius. It is interesting to note that very similar structures were recently observed in numerical simulations of the astrophysical bow shocks (Hansen *et al*., 2017) where they were interpreted as due to development of thin-shell instability advected along the bow-shock. Similar structures of bow shock were also seen in computational studies of radiatively cooled astrophysical jets (see e.g. Figure 5 in Blondin *et al*., 1990).

In addition to these large scale features, the experiments also show the development of small-scale perturbation at the bow shock surface. The structure is best observed using laser probing in a shadowgraphy set-up (Fig. 15c), as this diagnostic is sensitive to the gradients of the refractive index (plasma density). Note that the image in Fig.15c provides a high resolution view of the jet's fine details, and can admit the use of correlation analyses and a full parameter study, to be compared with the numerical runs. Similar fine details develop in astrophysical jets (see, e.g., Fig. 17 in Hartigan *et al*., 2011) though in the lab we have the privilege of being able to control their development via manipulation of external parameters. The most probable reason for the development of these structures is the presence of strong radiative cooling. The characteristic spatial scale seen in the experiment is close to the calculated cooling length.

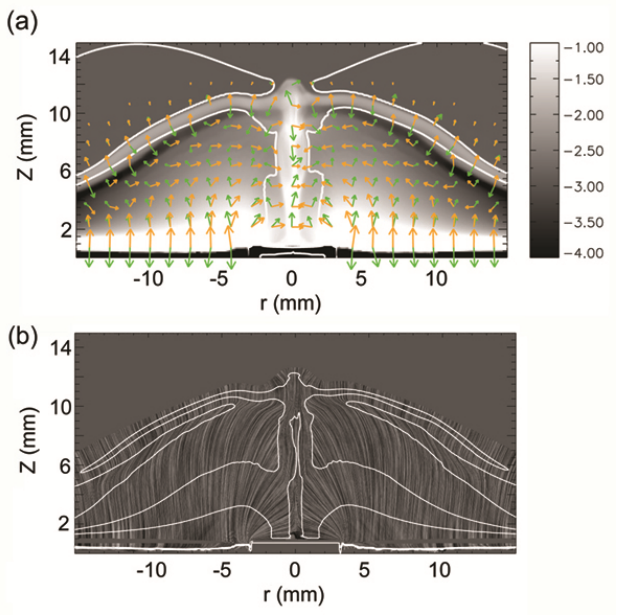

FIG. 14. MHD simulations of a jet from a radial foil propagating through argon ambient gas. (a) - The background shows mass density (in logarithmic scale, in units of kg/m3). Superimposed are contours of plasma β=1. The arrows represent force densities in the plasma, JxB (green) and pressure gradient (orange). (b) - Flow stream lines showing the direction of the plasma flow and contour lines of constant density (with values -4, -2, and -1 of scale shown in part (a)). From Suzuki-Vidal *et al*., 2012, Courtesy F. Suzuki-Vidal.

Comparison of the observed and simulated structures in Fig.15c and Fig.15d shows that though the simulations reproduce the overall structure of the bow shock quite well, they do not show the presence of much smaller, ~200μm scale

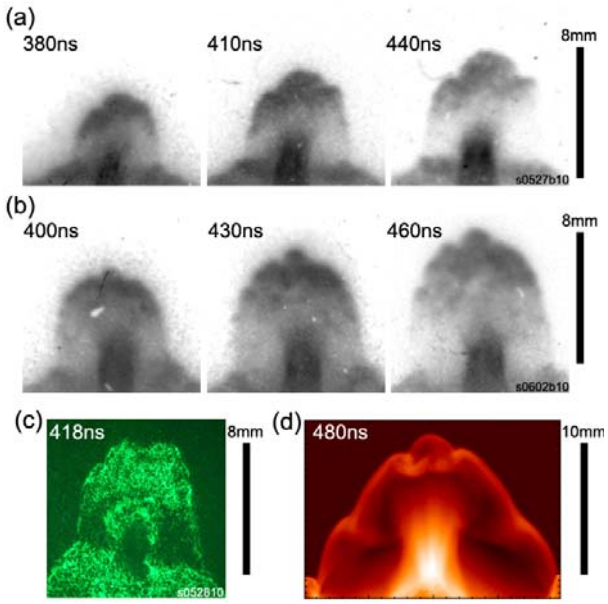

FIG. 15. (a)-(b) XUV emission of the bow-shock ahead of the jet from two experiments. The images show the formation of spatial features at the front of the shock. Both images are centered on the strongly emitting region at the tip of the jet. (c) Dark-field laser schlieren image showing the presence of small-scale structures inside the shock. (d) Simulation results (Suzuki-Vidal *et al.*, 2012) showing the formation of spatial features at the front of the shock.

perturbations seen in the experimental images. The absence of such structures in the simulations comes from the insufficient spatial resolution (100um) in this global simulation which included modeling of the whole experimental system (50mm diameter, 30mm height). This example illustrates the potential for experimental systems to model significantly larger ranges of spatial scales than global numerical model can since numerical diffusion at the grid level effectively reduces the "numerical" Re, Pe, Re_{M} numbers to values much smaller than those determined by the physical parameters of the system.

In conclusion, the use of pulsed power machines allowed for the of production supersonic, collimated plasma flows with weak magnetic field applicable to studies of hydrodynamic aspects of astrophysical jets. The relevance of these laboratory plasma jets to their astrophysical counterparts, in particular to stellar jets at distances far from the central star, is based on the similarity of the relevant dimensionless parameters determining their dynamics. This is illustrated by Table V, which compares typical dimensionless parameters characterising astrophysical stellar jets and laboratory plasma jets described in this section (see Appendix A for a discussion of the scaling issues).

Table V shows that the Re, Re_M and Pe numbers are all much greater than unity, which means that both systems are well described by the equations of ideal MHD and the effects of viscosity, diffusion of magnetic field and thermal conduction are negligible on the global scale L. The noticeable differences in the values of these parameters mean that the ideal MHD description becomes invalid at different relative spatial scales δ/L, which are, however, much smaller than the global scales of the systems, $\delta/L \ll 1$.

Consider two examples: 1) For a model of the Rayleigh-Taylor instability on the background of a smooth density variation with the scale $L \equiv \rho/|\nabla\rho|$, the viscous effects are small for the scales $\delta/L > Re^{-1/2}$ (Ryutov 1999). 2) For the Kelvin-Helmholtz (KH) instability of sheared flow, with a scale L of velocity variation, viscosity is negligible for the perturbations with the scale $\delta/L > (Re/Re_{crit})^{-3/4}$, where Re_{crit}~1000 is the critical Reynolds number for the onset of the KH instability (Landau & Lifsitz, 1987).

Thus for laboratory experiments discussed here the range of the spatial scales δ which can be modelled correctly is orders of magnitude less than the corresponding global scale L, albeit the ratio δ/L is not as small as in the astrophysical jets. It is worth noting here that similar limitations are applicable to computational modelling, where effects of numerical viscosity are equivalent to the relatively small values of effective "numerical" Reynolds numbers (Table V). Therefore, the laboratory experiments provide a good basis for advancement and validation of the astrophysical codes.

TABLE V. Comparison of typical dimensionless parameters characterising astrophysical stellar jets and laboratory plasma jets described in this section.

Parameter	Stellar jets	Laboratory jets
Reynolds number *Re*	$>10^8$	$10^{5\ *)}$
Magnetic Reynolds number Re_M	$>10^{15}$	50-500 *)
Peclet number *Pe*	$>10^7$	20-500 *)
Mach number *M*	2 **) – 20	2 – 10
Density contrast $\eta = \rho_{jet}/\rho_{ambient}$	0.1 – 10	1 – 10
Cooling parameter $\chi = \tau_{cool}/\tau_{dyn}$	0.1	0.1 – 0.001
Spatial scale ***)	15000 AU	10 mm
Relation between time-scales ****) $t_{Ast}=t_{Lab}\cdot(L_{Ast}/L_{Lab})\cdot(V_{Lab}/V_{Ast})$	700 years	200 ns

*) effective values of *Re, Re_M, Pe* numbers for global 3-D simulations, determined by discretisation in numerical schemes, are $Re \sim Re_M \sim Pe \sim 10^3$

**) smaller value of Mach number corresponds to internal shocks in the jets [e.g. Hartigan *et al.*, 2011]

***) characteristic sizes of bow shocks shown in Fig.1 for HH34 object and in Fig.15 for laboratory experiment

****) using the above spatial scales for L_{Ast}=15000AU; L_{Lab}=10mm, and V_{Ast}=200km/s, V_{Lab}=100km/s

There is a close match for the dimensionless parameters which determine the temporal and spatial evolution of the systems. For jets in which magnetic fields are not dynamically significant (plasma $\beta >> 1$), the dimensionless parameters commonly used in

the astrophysical jet literature are as follows: the Mach number (equivalent to the Euler number in Appendix A); the density contrast (equivalent to the similarity in morphology / initial conditions in Appendix A); the radiative cooling parameter (ratio of radiative cooling time to hydrodynamic flow time in Appendix A). Discussion of these dimensionless parameters in the context of numerical simulations of astrophysical jets can be found in e.g. Norman *et al*., 1982, 1983, Blondin *et al*., 1990. As is seen from Table V there is a good overlap between these parameters. Thus the evolution of structures developing in the interaction of laboratory jets with ambient plasma is scalable. Using the transformations discussed in Appendix A, we can determine that the scaling between the laboratory and astrophysical time-scales goes as $t_{Ast}=t_{Lab}\cdot(L_{Ast}/L_{Lab})$. Taking spatial scales corresponding to the characteristic transverse size of the bow shock in HH43 (top part of image in Fig.1), and the size of the bow shock in experiments (Fig.15), we find that a 200ns duration of the laboratory jet evolution corresponds to ~700 years of the astrophysical jet evolution.

III. Jets and outflows – significant magnetic field

In this section we consider experiments relevant to those types of astrophysical jets whose evolution is dominated by magnetic forces. Such jets are prone to a variety of MHD instabilities and may manifest intermittent behavior. Special experimental techniques have been developed to explore these jets in the laboratory. The techniques and experimental results are presented and compared with astrophysical models. The possible role of MHD activity in the generation of high-energy ions is briefly discussed. The section is concluded with description of the merger of multiple current channels that may occur in the atmosphere of magnetically active stars.

A. Magnetically-dominated tower jets

In the previous section, we considered jets and their interaction with the external medium for the cases where magnetic fields were absent or relatively weak (aside from the formation mechanism). We also established the connection with some astrophysical phenomena. In the current section we address the case where the magnetic field becomes critically important in jet creation, propagation, and the interaction with the ambient medium. Both "weak field" and "strong field" scenarios will be realized in astrophysical systems, see Pudritz *et al*. (2007) and Lovelace *et al*. (2002) for further details.

In a number of theoretical models, astrophysical jets are believed to be driven by a combination of toroidal and poloidal magnetic fields, where generation of toroidal components are attributed to the differential rotation in the accretion disc or between the disk and the central star. Launched and collimated by magnetic forces, these jets can propagate distances that are tens to thousands of times greater than their radius. Note also that these jets can be either kinetic or magnetic (Poynting Flux) energy dominated (Lynden-Bell, 2003; Kato *et al*., 2004). Figure 16 illustrates results of numerical simulations of a jet well outside the domain where it was formed. In the experiments described below a single collimated beam is created as opposed to the bipolar jets formed in most astrophysical situations.

The experimental work discussed next is most closely related to the magnetic tower scenario (Linden-Bell., 2003; Kato *et al*., 2004, Uzdensky & MacFadeyn, 2006, 2007). This scenario involves the presence of a magnetic cavity with highly wound-up

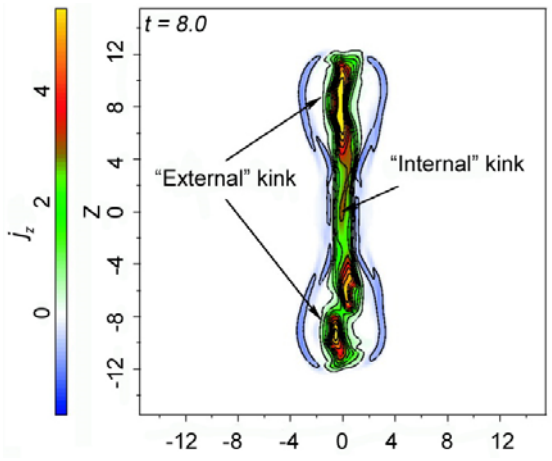

FIG. 16. The results of numerical simulation of a magnetically-driven jet. The "engine" that drives the current through the central column is situated near z=0. The return current flows in the outer shell that forms a characteristic "cocoon" structure. The central jet is unstable with respect to the kink mode. From Nakamura *et al*., 2007.

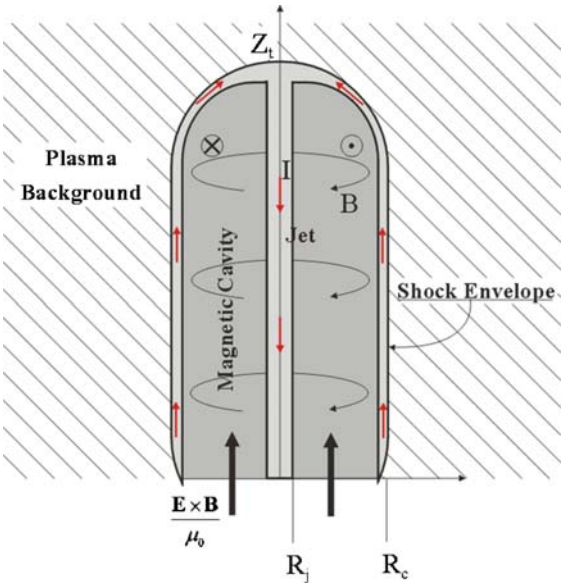

FIG. 17. Schematic of a magnetic tower jet. The toroidal magnetic field in the cavity is supported by the current propagating through the central jet (red arrows). The ambient plasma acts to prevent rapid expansion of the cavity. A Poynting flux through the base injects magnetic energy driving the growth of the cavity. From Ciardi *et al*., 2007.

and predominantly toroidal magnetic field. It is the magnetic pressure of this field which accelerates the outflow. The second key ingredient of this model is the presence of an external ambient medium, acting to confine the magnetic cavity. A simplified schematic of the magnetic tower jet model is shown in Fig.17. The toroidal magnetic field in the cavity is supported by the current propagating through the central jet and the cavity's envelope. The growth of the cavity is driven via injection of magnetic energy at its base. In astrophysical scenarios this is provided by the winding of the initially poloidal magnetic field by rotation of an accretion disc. In laboratory experiments a similar configuration is generated via appropriately configuring the path of electrical current driven by a pulsed power generator as will be discussed below.

One of the experimental approaches to study these jets is based on the use of *radial wire arrays* which consist of a pair of concentric electrodes connected radially by thin metallic wires (Lebedev *et al*., 2005a; Lebedev *et al*., 2005b; Suzuki-Vidal *et al*., 2010), see Fig. 18a for the schematic. The plasma formation and the flow dynamics during the initial stage of the experiment are the same as those observed in conical wire arrays. The main difference in the radial set-up is that the system reaches a stage where the wire cores near the central electrode become completely depleted of material, triggering the formation of a 'magnetic bubble' and a magnetically dominated jet.

The development of the jet in this system is shown schematically in panels (b)-(d) of Fig. 18. During the first stage (Fig.18b) ablated plasma is accelerated axially by the Lorentz **J** × **B** force and fills the region above the radial array forming an ambient medium into which the magnetic tower will eventually expand. As with the conical arrays, the magnetic field and the currents remain confined in the proximity of the wires leading to a relatively high-β background plasma. Thus the magnetized jets that form will propagate into a relatively weakly magnetized medium as is the case in many astrophysical settings. Characteristic parameters for this plasma are: electron densities of ~10^{17}–10^{18} cm^{-3} and temperatures of ~20 eV. Injection of plasma into the upper regions continues until the wires are fully ablated and stop acting as mass sources. The ablation rate is highest close to the axis and at some moment in time the wires near the central electrode will be fully ablated. The disappearance of parts of the wire cores means that the swept-up plasma cannot be replenished, and the current path shown schematically in Fig.18b) is no longer available. Wire breakage thus leads to development of a magnetic cavity in the background plasma, which is pushed by the rising toroidal field loops (Fig. 18c). This is the beginning of the second phase of the experiment: the formation of a magnetically driven jet. The current is now forced to flow along the surface of the cavity and through the central region, where a dense jet-like plasma column develops (Figs.18c

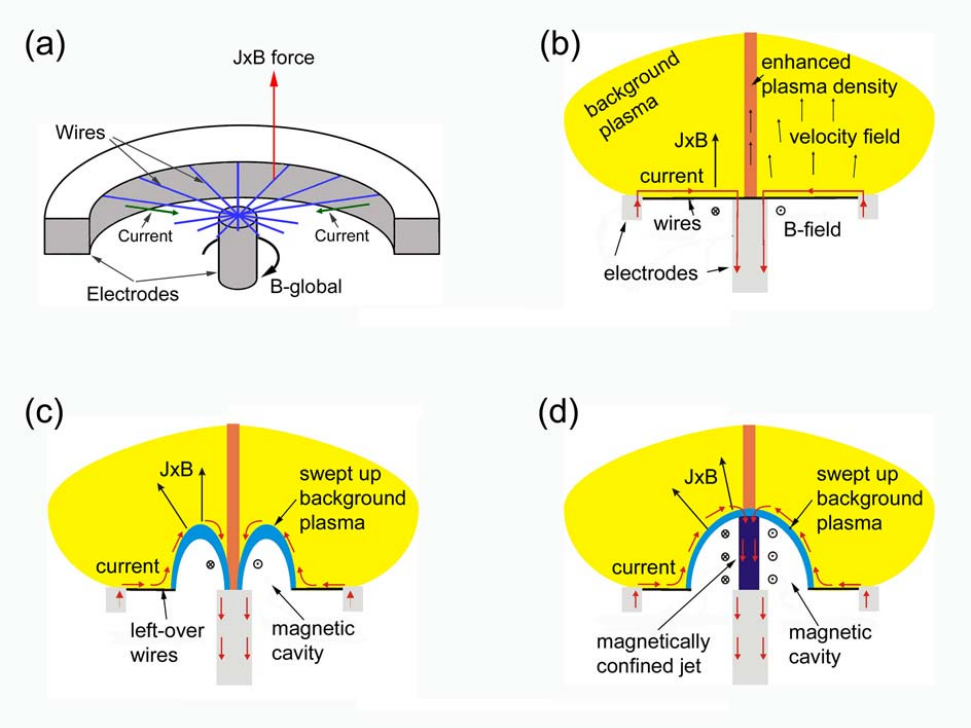

FIG. 18. (a) Schematic of a radial wire array experiment. Currents flow radially through fine metallic wires and along the central electrode, producing a toroidal magnetic field which lies below the wires; typical radius of the radial wire arrays is ~ 1 cm; (b) The ***J*** × ***B*** force acting on the plasma ablated from the wires produces a plasma background above the array; resistive diffusion is slow and the current path remains close to the wires. (c) Full ablation of the wires near the central electrode leads to formation of a magnetic cavity, which evolves (d) into a magnetic tower jet driven upwards by the pressure of the toroidal magnetic field. From Lebedev et al. (2005b).

and 19d). The pressure of the toroidal magnetic field, associated with the current flowing in the plasma column, leads to radial and axial expansion of the magnetic tower and to the axial acceleration of the jet column. Furthermore, the confinement of the magnetic cavity is largely determined by the thermal pressure of the background ambient plasma. This is quite similar to what the models of the astrophysical magnetically-driven jets assume (Lovelace *et al*., 2002; Lynden-Bell, 1996, 2003; Uzdensky & MacFadeyn, 2006).

During the past decade, laboratory experiments of the aforementioned type have produced a number of finely resolved features that are suitable for comparing with corresponding features in astrophysical jets. Parameters characterizing these experiments are summarized in Table VI, and the derived dimensionless parameters are shown in Table VII. The values of the Re, Re_M and Pe numbers are all much greater than unity, meaning that these laboratory plasma jets can be well described by ideal MHD equations. Thus one could expect that the evolution of the laboratory jets should be similar to that in the magnetic tower models of astrophysical jets, occurring on the temporal scales connected via scaling relations discussed in Appendix A.

Table VI. Summary of physical parameters in magnetic-tower jet experiment. [Lebedev *et al*., 2005b]

Parameter	Symbol	Jet	Background plasma
Velocity (km/s)	V	100-200	10-15 *)
Density (cm^{-3})	n_i	10^{18}-10^{19}	10^{16}-10^{17}
Temperature (eV)	T	120	<20
Magnetic field (kG)	B	>500	<50
Ionization	Z	20	10-15
Atomic number	A	184 (W)	184 (W)

*) Sound speed

Table VII. Derived dimensionless parameters for the magnetic-tower jet experiment

Reynolds number, *Re*	Magnetic Reynolds number, Re_M	Peclet number, *Pe*	Mach number, *M*	Plasma β	Cooling parameter, $\chi = \tau_{cool}/\tau_{dyn}$
$>10^4$	20 – 200	5-20	3-5	~1	10^{-3} – 10^{-4}

The main conclusions following from the results of these experiments can be summarized as follows.

The central column on axis is held from radial expansion by the toroidal magnetic field, associated with the axial current. The current then closes through the outer part of the shell, forming a familiar cocoon structure. The axial expansion of magnetic tower occurs with velocity determined by the magnetic pressure inside the cavity and the density of the ambient plasma ahead of the cavity (at Alfven velocity V_A calculated using magnetic field inside the cavity and the ambient density ahead of it). In these experiments the length of magnetic tower reached ~30mm, a factor of 15 larger than the radius at which the magnetic energy was injected through a narrow gap at the base of the magnetic tower (at radius ~2mm, corresponding to R_C in Fig.17).

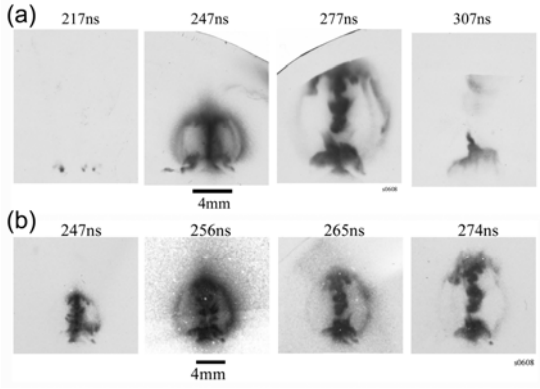

FIG. 19. Time sequence of soft x-ray images (~300eV) obtained during a single shot showing expansion of the magnetic cavity and development of instabilities in the central jet column. The four images in part (*b*) were taken with smaller inter-frame time separations and from different viewing angle. Lebedev *et al*., 2005b.

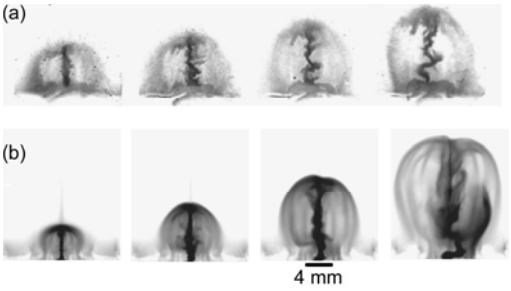

FIG.20. (a) time-sequence of experimental soft x-ray images (~30eV) obtained at four different times in the same experiment and (b) synthetic x-ray images from MHD simulations of the experiment. Ciardi *et al*., 2007.

The high-beta plasma near the axis is generally unstable with respect to necking and kinking instabilities (see e.g. Kadomtsev (1965)). With the jet propagating upward, the corresponding features are advected along the axis. All this is clearly seen in the set of images (Fig. 19) taken from Lebedev *et al*. (2005a). The central jet on the axis of the magnetic tower cavity shows the development of m=0, m=1 instabilities with characteristic wavelengths of ~1mm, comparable to the central jet radius ($kr_0 \sim 5$). Their growth time of ~2ns is consistent with that expected for the MHD modes ($\sim R_{jet}/V_A$), and is significantly shorter than the overall evolution time of the magnetic cavity of ~200ns in these experiments.

On the other hand, Figure 19 shows that these instabilities do not disrupt the plasma acceleration. A well-collimated, though highly structured, outflow is produced. In the experiments the level of instability development is at least partially determined by the balance between the jet acceleration time (cavity expansion time) and the time required for the driving current to "short-circuit" at the base of the jet. This removes, or at least reduces, the axial current in the jet reducing the driving force for the instability. Similar mechanisms may act at the base of an astrophysical disk-driven jet, near the disk surface (Pudritz *et al*., 2007 and Lovelace *et al*., 2002). The fragmentation of astrophysical jets, particularly stellar jets, is well known as observations show the flows to be clumpy on small scales (Hartigan *et al*., 2011).

The observed morphology agrees well with extensive numerical simulations of the tower jets with both laboratory plasma codes and with astrophysical codes (Ciardi *et al*. 2007, Huarte-Espinosa *et al*., 2012). Fig.20 shows a comparison of soft X-ray images from an experiment with synthetic images from simulations using a laboratory plasma code Gorgon [Chittenden *et al*., 2004; Ciardi *et al*., 2007]. The overall evolution and the main observed features are fairly well reproduced. In both simulations and experiments the most intense emission comes from the magnetically confined central jet. The other

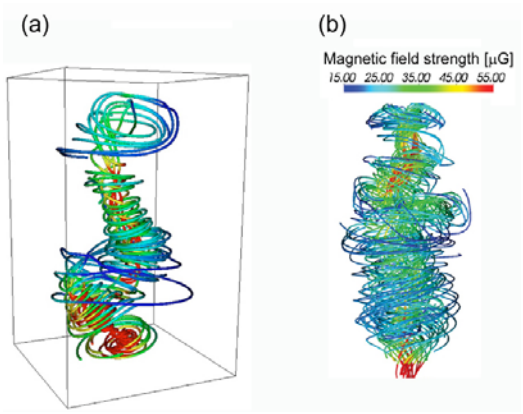

FIG. 21. Structure of magnetic field lines inside the cavity of radiatively cooled magnetic tower jest from MHD simulations; the colors represent the field strength decreasing from red to blue: (a) laboratory experiment, 230ns, jet height ~15mm (Ciardi *et al*., 2007); (b) astrophysical jet, 118year, jet height 300AU (Huarte-Espinosa *et al*., 2012).

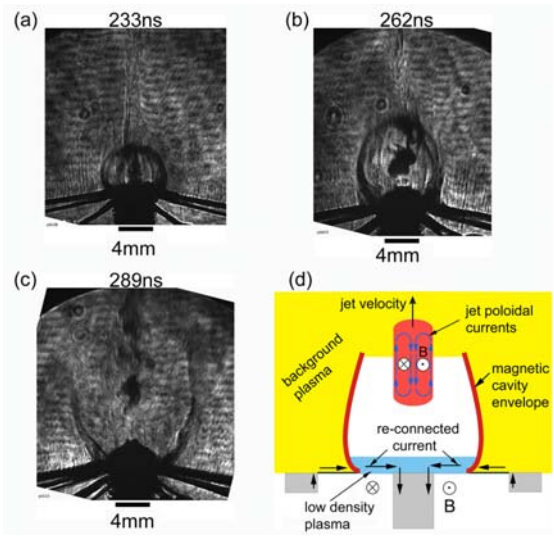

FIG. 22. Laser shadowgraphs of the magnetic jet evolution. (a) At 233 ns the magnetic cavity is well developed. A collimated jet is clearly visible on-axis inside the cavity. (b) The magnetic cavity elongates axially and expands radially. Because of instabilities, sections of the jet on-axis are no longer visible, and the jet assumes a clumpy structure. (c) The upper edge of the magnetic cavity breaks up and disappears. A well collimated clumpy jet is still visible on axis. (d) Schematic of the last stage of the magnetic jet evolution, showing how currents reconnect at the foot-point of the magnetic tower and a jet is ejected with entrained magnetic fields (Lebedev *et al*., 2005a).

prominent emitting region is the shock formed at the envelope of the cavity that is expanding supersonically (M>2) into the cavity confining ambient material .

Simulations (Fig.21) show the formation of tangled magnetic field structures inside the cavity, developing from the purely toroidal field due to the growth of the kink instabilities. This is seen in simulations of both the laboratory and astrophysical magnetic tower jets. The morphological similarity of the field structures in Fig.21 is obvious, despite the very different spatial and temporal scales involved.

The magnetic tower jet scenario creates an outflow propagating away from the region there the driving magnetic field is injected. In Fig. 22, we show an extreme case of separation of the well-formed plasma column from the base. The azimuthal field in the separated part of the jet is maintained by the poloidal current circulating within this separated piece. This section of the flow continues propagation in the vertical direction and forms an isolated "bullet." The current at the foot of the "cocoon" zone is now re-established and can drive the next burst of the plasma. Formation of the isolated plasma bullet is illustrated by the shadowgraphs in Fig. 22. In these experiments the total duration of the electric current pulse generated by the experimental facility was comparable with the time of the magnetic cavity expansion, so only one episode (pulse) of jet formation occurred. A modification of the set-up, allowing

formation of several episodes of magnetic tower jets, is discussed in part D of this Section.

New possibilities of generating larger-scale jets suitable for both the testing of scaling arguments and the introduction of new diagnostics would appear with the higher-power, higher current drivers. The first steps in this direction have been made with the PTS facility in China (Xu *et al*., 2017), where the magnetic tower jets have been produced and characterized with the driving currents of up to 4 MA.

B. Formation of energetic ions in a magnetic cavity

The cavity around the central jet is magnetically dominated, and the magnetic field is sufficiently strong to confine high energy ions (Suzuki-Vidal *et al*., 2013). These ions can be injected into the cavity by potential difference at the base of the cavity (~100 kV, see Burdiak *et al*., 2013 and Suzuki-Vidal *et al*., 2011). Injection may also occur during a clump formation, where the current may experience sharp turns or even complete disruption (Cf. Sec. VI.B). There is a good reason to believe that the ions most susceptible to acceleration are the protons, due to their highest Z/A ratio. The protons are always present in the system due to their residual presence in the metals used in the hardware (Suzuki-Vidal *et al*., 2013), in particular in tungsten wires used in the experiments.

The presence of higher-energy ions with W>100 keV was tested by a variety of techniques, including a magnetic spectrometer and an array of the proton imaging techniques based on the use of the CR-39 radiochromic films (Fleischer *et al*., 1965). The main findings were as follows: the proton spectrum extended from ~100 keV to ~ 3 MeV. The higher-energy (>600 keV) protons clearly originated from the central area of the cavity around the clumpy jet well above the wire array. We take 3 MeV as a reference for the maximum energy. Note that the protons with an energy exceeding 100 keV have a very long mean-free path in the "cocoon" plasma. For the tungsten plasma of T=20 eV temperature $n_e=10^{18}$ cm^{-3} density, and Z=5 the 100 KeV protons have a mean-free path of 60 m. The 100 keV proton slowing length (due to the friction against the electron gas) is also large, ~ 20 cm. These numbers become very large near the cut-off energy of 3 MeV. This means that the high-energy proton formation is not affected by collisions. This is especially true inside the magnetically dominated cavity where the plasma density is smaller.

To get an energy of 3 MeV in one "kick" the proton would have to cross a voltage drop of 3 MV. This is far too high (by factor of 10 to 30) compared to what the circuits involved in the experiments can produce. The maximum inductive voltage drop is ~ 100 kV. Also, the presence of 3 MV drop would show up in the generation of intense electron beams inevitably accompanied by the hard X-rays (up to 3 MeV), which are absent in the experiment. Therefore, we conclude that the ion acceleration cannot occur in one big step, but is rather produced in the multiple ion interactions with time-varying ("moving") magnetic field non-uniformities, very much like in a Fermi mechanism (Fermi, 1949).

Taking as a cut-off energy of accelerated protons the energy of W_{max}=3 MeV, we should consider whether such protons could be confined in a cavity of the observed size and the magnetic field strength. For the current I_{jet} through the central jet of 1 MA, and

the cavity radius of 1 cm, the field strength at its periphery is $B_a=\mu_0 I_{jet}/2\pi a$~20T. For such a field strength the gyro-radius of 3 MeV protons is 1.25 cm, i.e, comparable to the cavity size. Imposing this condition as a rough constraint on the maximum proton energy compatible with the size of the "cocoon", one can write this constraint as:

$$(\gamma_{\max}^2 - 1)^{1/2} < 2I_{jet} / I_{pA}, \tag{3.1}$$

where $I_{pA} \equiv 2\pi m_p c / e\mu_0 \approx 30MA$ is a so called proton Alfven current. We introduced here a factor $\gamma \equiv 1+W/m_pc^2$ in order to be able to cover relativistic energies, if needed (see below). In the non-relativistic case it agrees with the aforementioned estimate of the maximum proton energy in experiment by Suzuki-Vidal *et al*. (2013).

The protons execute complex orbits, with a characteristic orbiting period of $\sim 2\pi a/v_{p,max}$. The presence of random variations of the centroid of the current-carrying column caused by its MHD instabilities, produces random perturbations of the magnetic field with a characteristic time-scale of $\tau \sim r_{jet}/v_A$. This generates random vortex electric fields which can cause diffusion of the protons in velocity space with a diffusion coefficient $D_v \sim (\Delta v)^2/\tau$, (where Δv is the velocity change in each event). The same statement can be rephrased in terms of the second-order Fermi mechanism, where the inductive electric field would be associated with the magnetic features with velocities $\pm\Delta v$, giving small random "kicks" to the protons.

The fastest diffusive acceleration would occur in the vicinity of the jet, since the instability-induced fluctuations of the magnetic field are highest there. For a strongly distorted jet, the changes of the velocity would be on the order of the Alfven velocity itself, with v_A evaluated at the jet surface. Making a standard diffusive estimate for the velocity of protons achieved within some time t,

$$V^2 \sim 2D_v t, \tag{3.2}$$

one finds that

$$V \sim v_A \sqrt{2v_A t / r_{jet}}. \tag{3.3}$$

This part of the discussion pertains to a non-relativistic case as in (Suzuki-Vidal *et al*. (2013)). Taking the numbers typical for this experiment, $v_A \sim 4\times10^7$ cm/s, r_{jet}~0.1 cm, and t~250 ns, we find $V \sim 6\times10^8$ cm/s corresponding to the proton energy W~150 KeV. Obviously, this number is significantly smaller than the maximum energy of 3 MeV. However, the Gaussian tail of the diffusive distribution would extend at least a factor of 2-3 over the r.m.s. value of $V \sim 6\times10^8$ cm/s, easily yielding an energy of 600 keV. In this regard the number looks consistent with the spectral information from the experiment (Fig. 23).

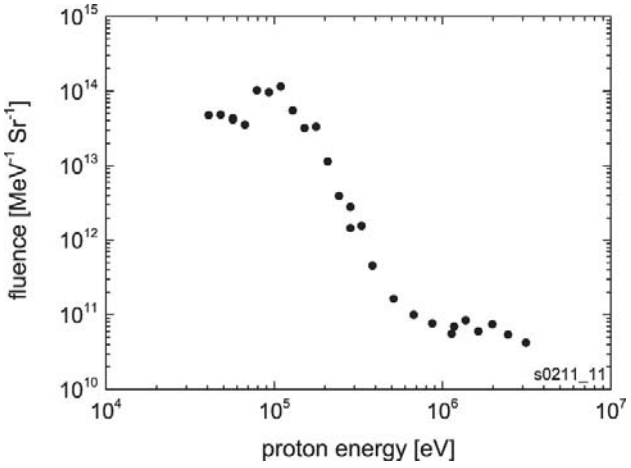

FIG. 23. Proton spectrum from the magnetic spectrometer (Courtesy Suzuki-Vidal)

With regard to the highest detected energies (~ 3 MeV) some

non-Gaussian effects may play a role, in particular, related to special choice of the initial phase-space characteristics of the accelerated particle (location and three velocity components). One can then get a non-diffusive acceleration (first-order Fermi), limited only by the particle confinement within the "cocoon", as mentioned above ("Hillas constraint", Hillas, 1984). Although the first-order mechanism has been studied in great detail (e.g. Longair, 2011) its existence and efficiency in the cocoon setting described above has not been proven yet. If this mechanism turns out to work for the astrophysical jets, higher-energy protons should be generated there as well. The maximum (cut-off) energy would still be determined by Eq. (3.1). In the astrophysical setting the jet current can easily reach $(10^3\text{-}10^5)I_A$. If the basic physics behind the clumpy high-current jets remains similar to that described in Sec. III.A-C, then the magnetic tower jets should correlate with the sources of relativistic protons and be considered as injection points for cosmic ray acceleration. We note that astrophysical jets, particularly relativistic flows associated with gamma ray bursts have often been suggested as particle acceleration sites (Bosch-Ramon and Rieger, 2012). A strong support to the mechanism discussed above would be experimental scaling of the maximum proton energy vs. the pinch current, as described by Eq. (3.1). Such experiments have yet to come.

C. Possible role of an axial magnetic field

In the physics of the jet launching from the central part of an accretion disk, an important issue is that of the relative role of the toroidal and axial components of the magnetic field (Pudritz *et al*., 2007 and Lovelace *et al*., 2002). Experiments with radial wire arrays provide a natural platform to address this issue experimentally. In the study of Suzuki-Vidal *et al*. (2010a) the axial field was added using a solenoid connected in the path of current driving the radial wire array. The axial field produced near the center of the launch area was B_Z~5 T. Because of a significant magnetic Reynolds number of this experiment (Re_M ~20, Table VII), the field was line-tied to the plasma of the emerging jet and compressed together with it.

The contribution of the axial field pressure limited the jet compression at the radii somewhat larger than in the absence of the field. The maximum value of the axial field was as high as 200 T, comparable with the magnitude of the drive field (100T). The limit to the achievable degree of compression should have led to lower plasma temperatures (compared to the no B_Z case); indeed, an increase of the minimum jet radius and reduction of the x-ray emission intensity at compression are observed.

The axial magnetic field of the achieved values is not sufficient to stabilize the fastest-growing modes of MHD instability of a current-carrying column. So, the formation of clumps was not noticeably affected. The main conclusion from this discussion is that (compressed) axial fields even those as high as the drive toroidal field, do not have any dramatic effects on the jet launching.

To address the role of the jet instabilities on the global properties of the magnetic cavity growth and jet propagation (in the setting with the anode made of a thin foil), a thin metal needle (stainless steel, 400 μm diameter, 1 cm long) was added above the foil along the axis of the system (Suzuki-Vidal *et al*., 2010b). The presence of the needle provided a well-defined, fixed path for the current which was not affected by the instabilities. This prevented radial displacements (wiggling) of the jet and excluded

disruptions of the current. The needle made an early stage of the discharge more smooth and led to faster growth of the magnetic cavity (~ 40% faster in both radial and axial directions), which is consistent with the larger value of current flowing through the central jet.

Current-driven instabilities of the central column were also experimentally observed and numerically simulated in Gourdain *et al*. (2012) for a thin (10 μm) Al foil driven through a small-diameter (0.5 mm) "pin" cathode. The development of kink mode was clearly identified and they observed that insertion of a metal needle on the axis of the system led to suppression of this mode and to general symmetrization of the discharge. In general, experiments with the central needle suggest that the development of MHD instabilities in the central plasma column could provide a feedback for the process of episodic formation of magnetic cavities.

D. Episodic magnetic tower jets

In the magnetic tower jet model (Linden-Bell, 2003) the formation of the magnetically driven jet / cavity is intrinsically transient, and experiments described in Section IIIA investigated properties of the outflows formed during a single episode of the magnetic cavity expansion. A closure of the gap through which the magnetic flux is injected into the cavity by a plasma could lead to current reconnection at the jet base (Fig. 22d.). Such reconnection restores the initial magnetic field configuration, providing conditions for a new episode of magnetic tower jet formation as schematically illustrated in Fig.24. The possibility of episodic magnetic tower jet activity was investigated using a modified experimental set-up in which the radial wires were replaced by a thin radial foil (Suzuki-Vidal *et al*., 2009; Ciardi *et al*., 2009). Average mass per unit area decreased in the radial direction of a radial wire array, whereas for a foil of constant thickness, the same parameter didn't depend on the radius. The foil was therefore ablated and pushed up to form a cavity in a narrower region near the axis leading to ejection of a bubble of smaller radius and energy content. The smaller radial extent where all foil material was ablated created conditions for more frequent "reconnection" of the current at the base. This lead to generation of several subsequent magnetic cavities / jets (Suzuki-Vidal *et al*., 2009; Ciardi *et al*., 2009). A detailed experimental characterization of the processes occurring in the foil during the discharge can be found in Gourdain *et al*. (2010) based on the COBRA pulsed power device at Cornell University.

After the reconnection event had occurred and led to a separation of the jet from the base (similarly to what is shown in Fig. 22), a new cavity could start growing, with a new jet emerging from the base. This was accompanied by episodic burst of soft x-rays generated during compression of the central jet. The time evolution of the jets and bubbles is presented in Figure 25. A succession of multiple cavities and embedded jets are seen to propagate over length scales spanning more than an order of magnitude – from the smallest to the largest bubble. The central jet in each of the subsequent cavities is unstable to current driven instabilities, with the characteristic growth-time of a few nanoseconds. This corresponds to the Alfven propagation time across the jet radius. The second time-scale in this experiment is the magnetic cavity ejection period, which was a factor of 10-20 longer and linked to the temporal variability of the Poynting flux feeding the cavities. It is important to note that episodic jet formation appeared in several

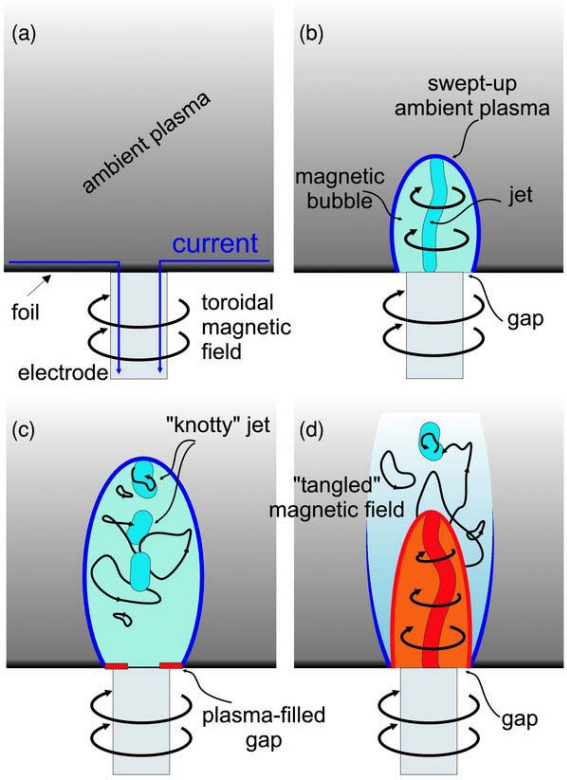

FIG. 24. Schematic illustrating formation of episodic magnetic tower outflows in experiments. Filling of the gap at the base of the magnetic cavity by plasma restores the initial magnetic configuration. A new jet and bubble (shown in red) then formed (panel (d), which propagate and interact with the plasma and "tangled" magnetic field left by the previous ejection event (shown in blue) (Courtesy A. Ciardi)

numerical simulations of young stellar objects jet launching (Goodson et al., 1997; Goodson et al., 1999; Goodson and Winglee 1999; Romanova et al., 2006).

The resulting flow observed in the experiments is heterogeneous and clumpy, and is injected into a long-lasting and well-collimated channel made of nested cavities. It is worth remarking that the bow-shaped envelope is driven by the magnetic field and not hydrodynamically by the jet. Another interesting observation was the increase of the axial expansion velocities of the subsequent cavities. This occurs due to their propagation through a smaller density as substantial part of the plasma was "swept" to the central column in a previous episode (Ciardi *et al.*, 2009). The subsequent clumps may have higher axial velocity than the preceding ones, this leading to an overtaking effect and formation of the internal shocks in the clumpy outflow. The characterization of

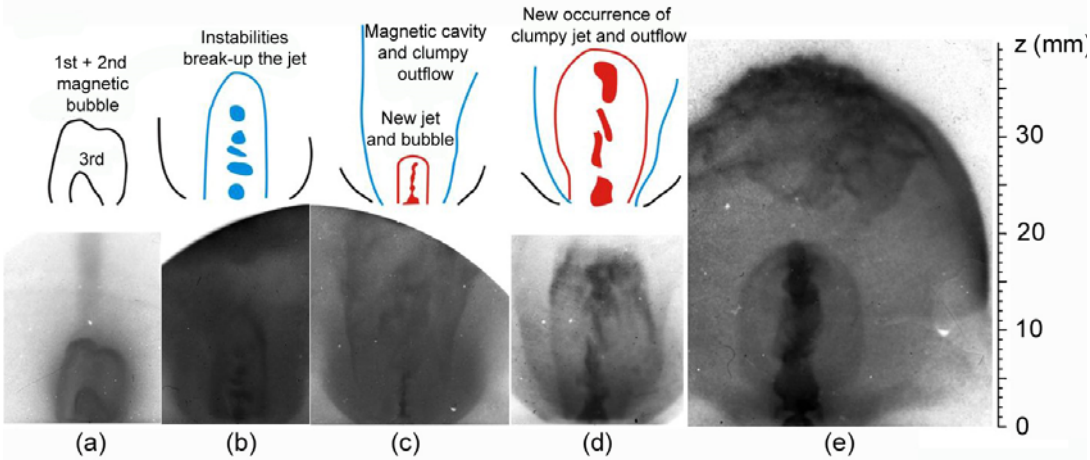

FIG. 25. Time sequence of soft X-ray images showing evolution of episodic magnetically driven jets, with images taken at (a) 286 ns, (b) 346 ns, (c) 376 ns, (d) 406 ns, and (e) 487 ns after the driving current start. The schematic cartoon serves to guide the eye; the features are described in the main text. (Ciardi *et al.*, 2009)

knots in many astrophysical jets also shows them to be propagating into environments that are already in motion (Hartigan *et al*., 2011). Thus the experiments allow researchers to explore a key aspect of astrophysical jet evolution.

The dimensionless parameters characterizing this experiment are similar to that shown in Table VII and a similar scaling can be applied to consider astrophysical implications of the results of this experiment. This was discussed in Ciardi *et al*., 2009 and Suzuki-Vidal *et al*., 2010, where the authors suggest that the scaling of the experiment to the parameters of protostellar jets indicates that the presence of multiple bubble-like features should be observed on scales of few hundreds of AU from the source, while the non-axisymmetric features from the current-driven instabilities should appear within tens of AU. This is consistent with the observations of outflows from e.g. DG Tauri star which demonstrate many morphological features similar to the observed in the experiments: ejection variability, limb-brightened bubble-like structures and the presence of wiggles in the optical jet evident on scales ranging from tens to few hundreds of AU from the source (Bacciotti *et al*., 2000, 2002; Dougados *et al*. 2000). Some possible connections between the results of the episodic magnetically driven jet experiments and the astrophysical observations and numerical models were discussed in [Agra-Amboage *et al*., 2011; White *et al*., 2014; Pascoli and Lahoche, 2010; Moll 2010; McKinney *et al*., 2009; Savin *et al*., 2012; Federrath *et al*., 2014; Ciardi and Hennebelle, 2010].

E. Magnetic arches and their stability

Interesting features of astrophysically relevant jets have been revealed in the experiments by the Caltech group based on the pulse-power techniques related to the spheromak magnetic configuration, see Bellan (2000) and references therein. The dimensions of the plasma objects in these experiments reach tens of centimeters, and the evolution time of the plasma objects exceeds several microseconds, i.e., orders of magnitude larger than in the fast z-pinches. Still, the basic physics underlying the evolution of the jets remains the same and some of the images are very similar to their mm-size counterparts. This once again indicates the potential of the scalings and similarities in relation to astrophysics. A detailed comparison of the spheromak-produced laboratory jets with astrophysical models can be found in Bellan (2018a, 2018b). See also You *et al*., 2018.

The basic configuration of the Caltech experiment is shown in Fig. 26 (Bellan *et al*., 2005). The poloidal magnetic field threads two

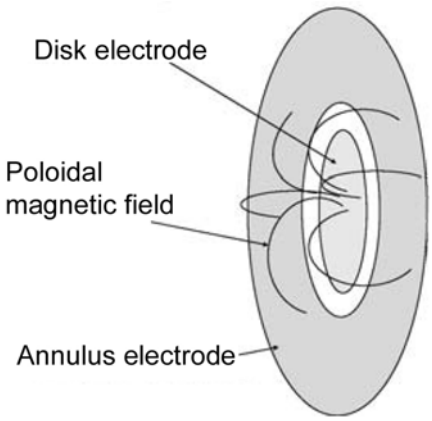

FIG. 26. Schematic of the Caltech experiment on the merging of current channels and formation of an axial jet. This structure is attached to a large vacuum chamber (not shown) extending by ~ 1.5 m to the left, with diameter ~ 1.4 m. The formed plasma objects are observed through several ports in the chamber; magnetic probes are used for in situ measurements of the magnetic field. Figure courtesy P. Bellan.

electrodes, the inner disc (cathode) and the outer annulus (anode). In several points (roughly at the foot-points of those field lines that are shown in the figure) the working gas is injected, and the voltage of a few kV is applied between the inner and the outer electrodes. As breakdown occurs the current starts flowing predominantly between the footpoints ending at the location of the gas inlets. The poloidal current causes mutual attraction of the inner "stems" of the current channels and, at the same time, pushes the outer stems outward, similarly to the magnetic tower jet configuration discussed earlier. This dynamics is reflected in the optical images shown in a set of consecutive snapshots in Fig. 27 (from Hsu and Bellan, 2002).

In the first few frames, one sees a process of merging of the inner stems and formation of one bright current channel; the current is closed through the outer shroud which grows in size and eventually leaves the field of view. The central jet propagates away from the electrodes. As it propagates it shows signs of kinking and then, eventually, dissipates. The characteristic plasma parameters in this experiment were (Hsu and Bellan, 2002): plasma density (hydrogen) $n_e \sim 10^{14}$ cm^{-3}, T_e , $T_i < 5$–20eV, B=0.2 – 1 kG, the duration of the shot ~15 μs. The length of the jet at t=10 μs is $L \sim 50$ cm. The Coulomb mean-free path for $T_e = T_i = 10$ eV is 3 cm, i.e., the plasma is mildly collisional.

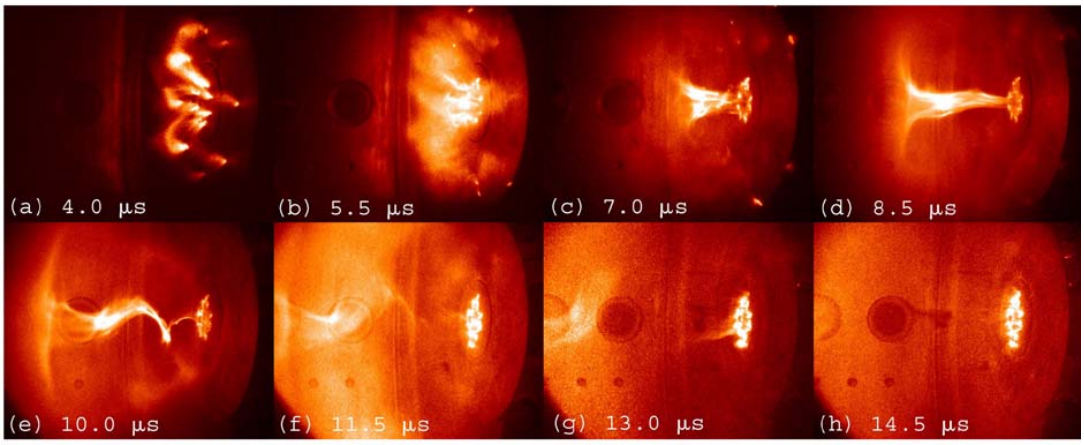

FIG. 27. A sequence of the snapshots showing an evolution of the plasma. The time after applying the voltage between the electrodes is shown in each frame. Courtesy S. Hsu.

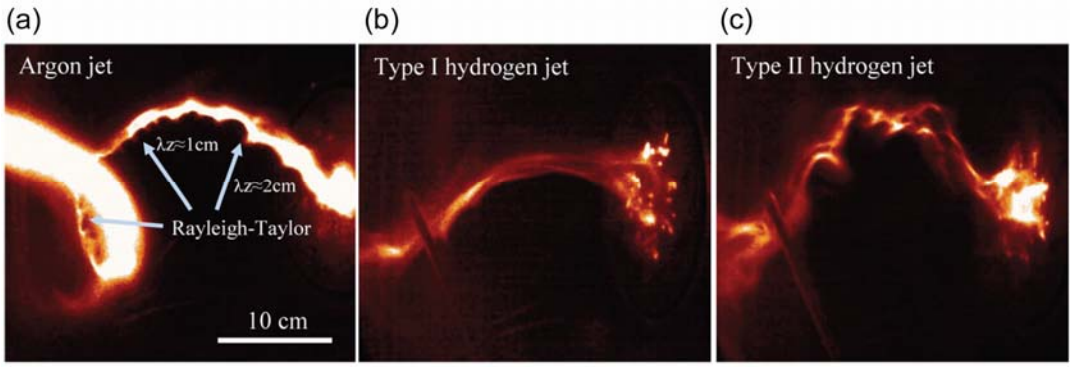

FIG. 28. Development of finer structure on the twisted jets, experiencing lateral acceleration. Courtesy X. Zhai and P. Bellan.

The ion gyro-radius for T_i=10 eV and B=0.5 kG is ~ 1cm, i.e. less than the jet radius. The magnetic diffusivity D_M is ~10^5cm^2/s, i.e, the magnetic diffusion time τ_{diff} over the jet radius of r~3 cm is $\tau_{diff} \sim r^2/2D_M$~30 μs. Thus an MHD approach can be used in the analysis of the jet behavior, at least qualitatively. The jet kinking is a part of the MHD predictions, although specific results may depend on such factors as axial current distribution over the radius, as well as possible effect of the velocity shear, similar to those discussed in Sec. III.F.

As the authors emphasize, applying a voltage between the electrodes in the pre-imposed poloidal field is equivalent, in terms of the effects produced, to the rotation of the electrodes. Therefore, the setting of Fig. 26 imitates processes occurring near the foot of the jet and related to the presence of the differentially-rotating accretion disk (see Bellan, 2018). This kind or phenomena has been a subject of considerable interest in astrophysical disk simulations (Romanova *et al*., 2004).

Higher resolution optical imaging used in recent experiments of the Caltech group allowed them to detect some finer features on the jet images (Fig. 28 that contains snapshots of a shorter segment of the jet seen in Fig. 27). In the course of violent lateral motions generated by the kink instability, the surface of a jet may also experience high lateral acceleration. This creates conditions for the Rayleigh-Taylor instability at the interfaces. Moser & Bellan (2012) and Zhai & Bellan (2016) attribute the features shown in Fig. 28 to this instability. In these experiments both hydrogen and argon plasma was used. In an argon plasma (Fig. 28a) the lateral acceleration of 10^{10} cm/s^2 generated this effect quite reproducibly. In hydrogen, with the same acceleration the effect was not detectable (Fig. 28b); however, at higher acceleration of 10^{11} cm/s^2 it re-appeared as shown in Fig. 28c.

F. MHD equilibria stabilized by the shear flow

A plasma column where the plasma pressure is balanced by the magnetic pressure is often considered as a reasonable representation of magnetically dominated astrophysical jets. However, it is well known that an equilibrium pinch is unstable with respect to formation of "necks" (m=0), as well as "kinks" (m=1). These instabilities are identified as a common occurrence in the dynamics of long, thin, current-carrying astrophysical jets (see e.g. Benford, 1978; Begelman, 1998; Reipurth & Bally, 2001; Nakamura & Meier, 2004). The growth of both modes is associated with the release of the magnetic energy due to changes in the current distribution and can be evaluated on the basis of the MHD energy principle, see review by Kadomtsev (1965). The growth rate Γ is highest for the perturbations with the axial length scale $1/k_z$ comparable to the equilibrium pinch radius a, (i.e., for $k_z a$~1), and is roughly equal to $\Gamma \sim v_A / a$, where v_A is the Alfven velocity. Note that there are special pressure distributions (Kadomtsev's profile) for which the instability is stabilized (Kadomtsev, 1965); however, if the pinch equilibrium is not specially tailored from the outset, this profile does not form automatically.

A possibility to stabilize such MHD instabilities by introducing a sheared axial flow velocity (v_z(r)) was investigated in experiments with so-called "flow pinch", described in the context of the laboratory astrophysics in Shumlak *et al*. (2007, 2017). The parameters of the hydrogen plasma in these experiments are (Shumlak *et al*., 2007):

plasma radius a=1 cm; plasma length 100 cm; plasma density $n=10^{16}$ cm^{-3}; plasma temperature T=100 eV, flow velocity on axis v=10^7 cm/s. The azimuthal magnetic field is zero on axis and reaches 25 kG on the pinch radial boundary. The particle mean-free path (3 cm) is somewhat larger than plasma radius. Importantly, the plasma flow has significant shear in the radial direction, with the flow being faster on axis and slower on the periphery. The presence of velocity shear leads to stabilization of the sausage instability. It is noteworthy that such shear flows are likely to occur in jets from accretion disks as the footpoints of flow rotate at the local Keplerian velocity (e.g. Ferreira *et al*., 2006). The characteristic growth-rate of the sausage instability in this experiments is ~v_A/a and stabilization occurs if the radial shear, dv/dr, is sufficiently high, $dv/dr > v_A/a$. The qualitative explanation of the shear stabilization is that the shear destroys radial coherence of the mode, by stretching the perturbation along the axis. This, perhaps, may serve as one of the factors explaining a remarkable length of some of the astrophysical jets.

IV. Rotating plasmas – towards an accretion disk experimental platform

Momentum transport in accretion disks is among the most intriguing issues of the modern astrophysics. Is the momentum transport caused by the plasma turbulence? If so, what kind of turbulence is involved? Is the magnetic field a significant player? Novel techniques developed on pulsed power facilities have allowed experimenters to make first steps in producing rotating plasma disks whose behavior may help in answering some of the aforementioned questions.

Accretion disks (e.g., Pringle, 1981) are formed around a variety of celestial objects, from young stars to supermassive black holes in the center of galaxies. They "feed" central objects and are also thought to be responsible for the formation of jets that emanate from the vicinity of the central object. To feed a central object, meaning to allow accretion to occur, some viscous mechanism is needed for transferring angular momentum from the inner to outer parts of the disk. Despite a very high Reynolds number (>10^{10}), purely hydrodynamic turbulent viscosity is insufficient to produce the necessary momentum transfer (e.g., Shakura, Sunyaev, 1973; Balbus, 2011). Magnetic fields are thought to play an important role in this process through the creation of new unstable modes such as the Magneto-rotational Instability (Balbus & Howley, 1991; see also Velikhov, 1959). The interaction of gravity, shear flows, and magnetic fields creates a complex dynamical system that is the subject of active study observationally, theoretically and numerically. The role of the fluid turbulence, magnetic fields and disk vertical structure are all examples of open questions in the study of accretion disks (e.g., Thompson, 2006; Käpylä *et al*., 2010; Balbus, 2011).

Unfortunately, laboratory experiments, including those using pulse-power devices, cannot reproduce the gravity of the central object, and this limitation makes laboratory simulation of full accretion disk physics impossible. Still, as was shown in recent years, it is possible to reproduce key aspects of the sheared rotation of magnetized plasmas and transformation of the radially convergent flow into the bipolar jets (Ryutov, 2011). This experimental approach allows studies of fast phenomena occurring on a time-scale of one rotation period. Modeling phenomena that develop on time-scales of many (~100) rotation periods remains beyond the current capabilities of pulsed power or laser driven experiments.

In spite of this limitation, plasma effects occurring in a turbulent rotating plasma disc during a single rotation period are of interest as these can occur in the zone in the inner-most part of the astrophysical disc-jet system, including the launch of jets and the transfer of angular momentum to these jets. Specific aspects of accretion disc physics which could be amenable for laboratory study include turbulent anomalous viscosity, the interaction of differentially rotating discs with a magnetic field, and the formation of axial outflows from the inner boundaries of the disc.

First steps in creating plasma flows with non-zero angular momentum were made in Ampleford *et al*. (2008) using a "twisted" conical wire array (Fig. 29) to add spin to a jet. Compared to untwisted arrays, in this case some axial magnetic field was generated by the azimuthal component of the currents appearing due to the twisting. The plasma streams flowing towards the axis received a finite angular momentum from the global *axial* magnetic field (in addition to the radial momentum that they receive from the global *azimuthal* field). Converging near the axis, these streams merged into the plasma jet spinning around its axis and propagating upwards, as was described in Sec. II.A,B. The difference between the jets exiting the wire arrays in a twisted (Fig. 29b) and untwisted (Fig. 29a) cases is obvious. The larger diameter of the rotating jet is related to the effect of the centrifugal force. Typical flow parameters in the jets formed from tungsten wires were: A=183, Z=5, $n_e=4\times10^{16}$ cm^{-3}, T_e=20 eV, jet axial velocity at the upper end of the array V=10^7cm/s, rotation velocity 25 km/s (all values were inferred from MHD simulations, shadowgraphy and interferography). As seen from these numbers, the jet is made of a highly collisional plasma (λ_{ei}~60 μm, λ_{ii}~ 2.5 μm) that can be accurately described by the standard MHD equations. Dimensionless parameters characterizing the jets are similar to those reported for young stellar object jets (as discussed in Chapter II), including the ratio of rotational and axial velocities of 10-25% (Coffey *et al*., 2004).

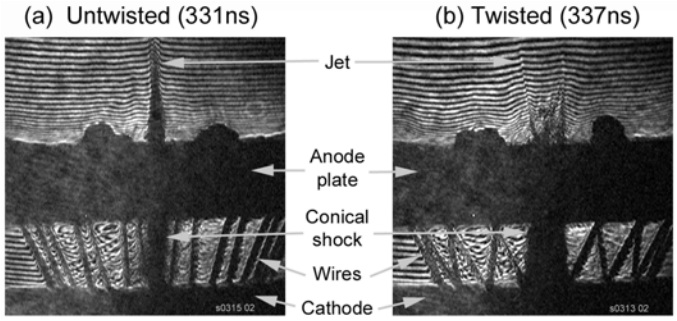

FIG. 29. Schlieren images of the plasma flows in a non-twisted (a) and twisted (b) Al wire arrays. The jet is a dark feature near the axis. Also seen are wires and upper and lower electrodes. Note that the jets look dark due to high density gradients within them. The presence of plasma rotation in the jets is inferred from the twisted filamentary features visible on the shadowgrams at higher magnification (see Fig. 4 in Ampleford *et al*., 2008).

Formation of "braids" in the rotating jets is related to the discrete nature of the sources; aforementioned twisting of the braids (visible in Fig. 29b and, more clearly, in Fig. 2 of the original paper Ampleford *et al*. (2008)) is caused by the plasma rotation and can be used for determining the pitch of the rotating flow, allowing for the estimate of the azimuthal velocity. The larger width of the rotating jet is consistent with the centrifugal effect. Taken as a whole this configuration provides an interesting platform for developing a better understanding of the physics of rotating jets. For example, numerical simulations of astrophysical jets interacting with ambient media suggest that jet rotation could lead to observable differences in the morphology of interaction (Ciardi *et al*., 2008), and experimental platform allow one to test such predictions. We note the

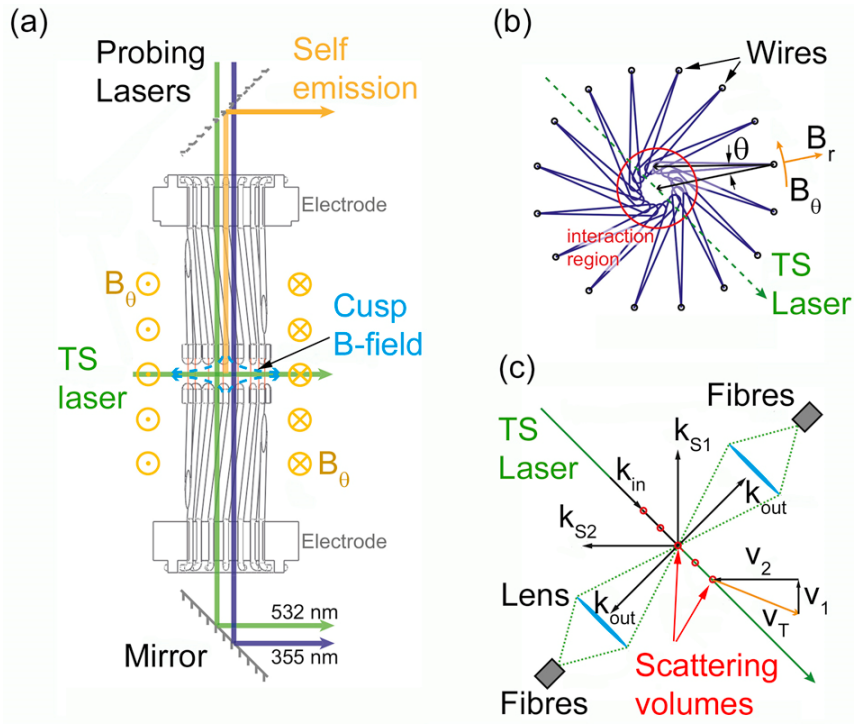

FIG. 30. Generation of a rotating plasma disc (From Bennett *et al*., 2015). a) The wire array (16 Al wires) is only 4 mm tall and occupies a short section in the middle of the whole structure, whose diameter is 16 mm. Therefore, the plasma would indeed form a disc. The rest of the hardware is made of two sets of 1-mm diameter conductors supplying a current separately to each wire. The upper and lower sets are twisted in the opposite directions but match the positions of the wires of the wire array. The presence of the twists in the upper and lower structures leads to formation of an axial magnetic field directed oppositely above and below the mid-plane. This causes formation of a cusp magnetic field around the mid-plane, with the field being almost radial at the location of the wires. b) The flow, formed by the plasma ablated from the wires, streams toward the center with some off-set, caused by the "kick" produced by the azimuthal force $\propto j_z B_r$. As a result, a rotating plasma disc is formed that is held from the expansion in the radial direction by the ram pressure of the incoming plasma (cf. Ryutov, 2011); c) The orientation of the incoming and scattered light in the Thomson scattering system that allows measuring the rotation velocity and plasma temperature.

importance of such flows in astrophysical studies where observations have measured the rotation rates for a number of YSO jets. These rotation rates have then been used to distinguish between different jet launching models (i.e. physics occurring in the accretion disks, (Bacciotti *et al*., 2002; Coffey *et al*., 2015; Frank *et al*., 2014, Lee *et al*., 2017).

The next important step was to limit the axial extent of the rotating plasma and thereby to produce a rotating disc. This was attained by using a novel configuration (Bennett *et al*., 2015) of conductors and wires, illustrated in Fig. 30 where explanations of the operation are given in the figure caption.

Self-emission optical and XUV images indicate formation of a disc of diameter 3 mm near the axis (with the diameter of the array of 16 mm!), Fig. 31. The Thomson scattering measurements of the rotation velocity yield $v_{rot}\sim 6\cdot 10^6$ cm/s. Fine structure appearing at the images late in time and reminiscent of spiral arms may be driven by shear-flow instabilities. Note that between the first and last frames, the plasma makes a full rotation around the axis.

There is, of course, no gravity, but the disc is confined radially by the ram pressure of the incoming streams. Since there is no confinement in the z direction, a bipolar plasma outflow is formed, very similar morphologically to outflows from astrophysical discs where gravitational "confinement" cannot counter the combination of the magnetic and thermal pressure pushing plasma away from the center along the vertical axis.

MHD simulations (Bocchi *et al*., 2013) of these experiments reproduce the main features of the overall evolution of the rotating plasma discs and the formation of bipolar outflows (Fig. 32). Characteristic plasma parameters in a disc made by ablation of copper wires are as follows (at 160 ns from the driving current start): radius of the spinning disc $a\sim 1.5$ mm; electron density $n_e\sim 3\cdot 10^{17}\text{cm}^{-3}$; temperature $T\sim 15$ eV; rotation velocity $v_{rot}\sim 6\cdot 10^6$ cm/s; axial velocity $v\sim 3\cdot 10^7$ cm/s; $A=64$; $Z\sim 3$. For this set of parameters we find the magnetic diffusivity $D_M\sim 2\cdot 10^5$ cm^2/s and kinematic viscosity $\nu\sim 10$ cm^2/s. Note we have used simple approximate expressions of Ryutov, 2015 (note also a typo in Eq. (27) of that paper, where the exponent of the temperature should be 5/2 instead of 3/2 though the numerical coefficient is correct).

The corresponding dimensionless parameters are: $Re_M=av_{rot}/D_M\sim 5$; $Re=av_{rot}/\nu\sim 10^5$; $Pr = Re_M/Re \sim 5\cdot 10^{-5}$. The small value of magnetic Prandtl number is relevant to conditions expected in the inner parts of protoplanetary discs (Balbus and Henri, 2008). The magnetic Reynolds number exceeds unity which means that the radial magnetic field embedded in the rotating disc will experience significant stretching by differential rotation. Such "winding" of the field is an essential step in so-called α–Ω dynamo models which are expected to be a principal means

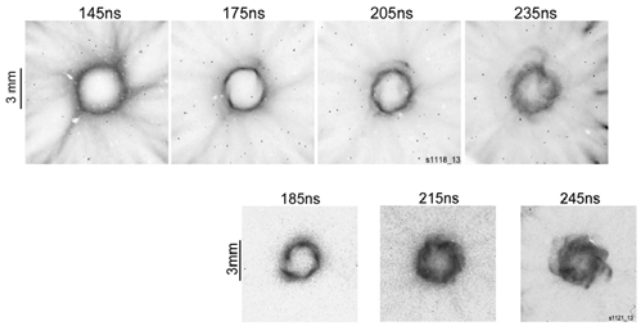

FIG. 31. XUV images of the disc obtained in two identical shots (top and bottom rows, respectively) with aluminum wire array, 16 wires, 30 mm diameter. From M. Bennet *et al*., 2015.

by which fields are generated in disks (e.g., Moffatt. 1978). Experiments on higher-current facilities, like the PTS facility in China (Xu *et al*., 2017), could allow production of discs with higher values of magnetic Reynolds number.

The large Reynolds number implies that hydrodynamic turbulence in the experiment can be fully developed. The rotating disc formed in these experiments is initially smooth, but then demonstrates the development of azimuthal perturbations which start at the longest spatial scale (m=2 azimuthal mode) and rapidly progress towards much shorter scales (Fig.31). Even more important, the late-time images in Fig.31 show a significant inward expansion of the inner boundary of the disc, which occurs on a time-scale of only ~50ns (~ 0.5 of rotation period). This time-scale is significantly, (by 4-5 orders of magnitude), smaller than the diffusion time ($t \sim a^2/\nu_{Sp} \sim 2\text{x}10^{-3}$s) calculated for the classical (Spitzer) viscosity. The observed fast inward expansion of the rotating disc can be interpreted as an evidence of the development of anomalous viscosity in this system. Indeed, for *Re* >> 1 the growth rate of shear-flow instabilities is of order $\Gamma \sim v_{rot}/a$ (e.g., Landau and Lifshitz 1987). Thus one revolution time ($2\pi a/v_{rot}$) would provide a significant growth factor, $\sim\exp(2\pi\Gamma a/v_{rot}) = \exp(2\pi)$. Given that initial perturbations are

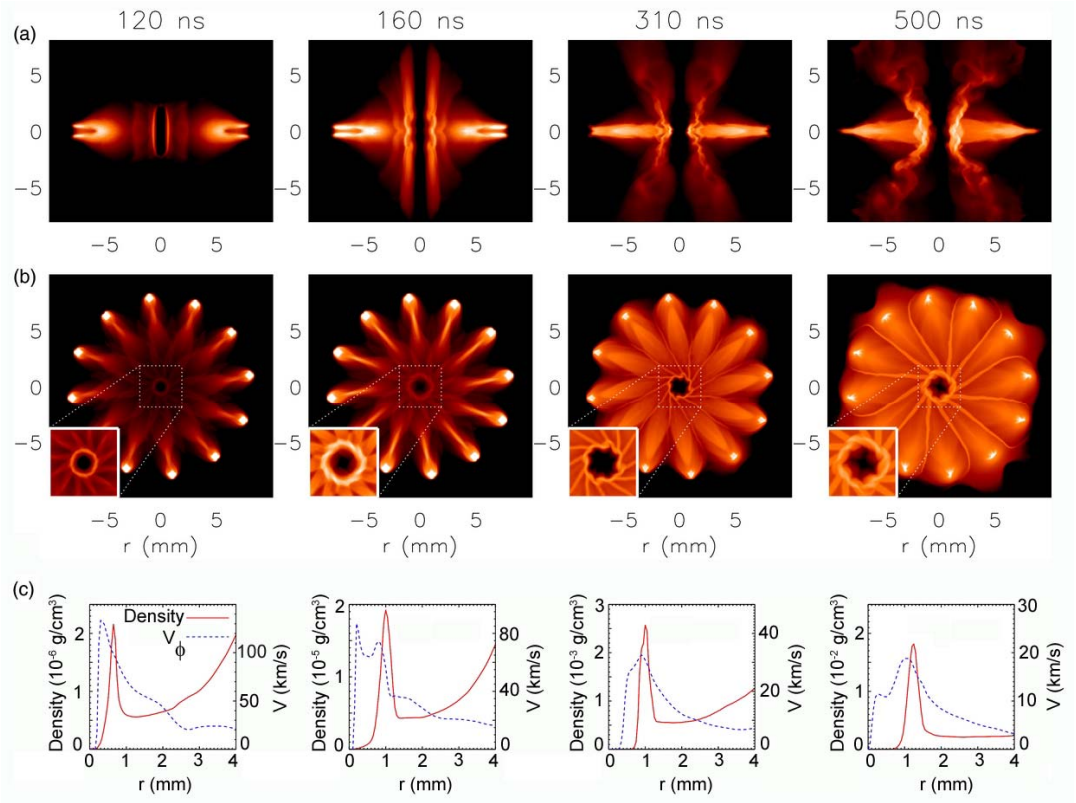

FIG. 32. Results of the reference case simulation (50 μm resolution). (a) Time sequence of slices of mass density on the XZ plane. From left to right: 120, 160, 310, and 500 ns. Only part of the computational domain is shown. The color scale is logarithmic, ranging from 10^{-7} g cm^{-3} (darker tones) to variable levels (lighter tones) to highlight structures. (b) Same as (a) but for the XY plane instead. The inset in the bottom left corner is a magnified version of the central region. (c) Time sequence of average radial profiles of density (red solid line) and toroidal velocity (blue dashed line). The times are the same as in (a) and (b). Courtesy M. Bocchi.

large due to the discrete nature of the plasma streams forming the disc, the development of turbulent viscosity should be possible on the time-scale of the experiment. It is interesting to note that the value of viscosity required to explain the fast inward material transport observed in this experiment, $\nu_{tr} \sim 10^5 \nu_{Sp}$ corresponds to the value of the α parameter in the α-prescription ($\nu_{tr} = \alpha C_S H$) of Shakura-Sunaev (1973) of $\alpha \sim 0.1$.

Although the laboratory experiments investigating accretion disks are in their initial stages, they provide a promising platform for future studies of a number of physical processes affecting real astrophysical accretion discs.

V. Astrophysics-relevant shocks

Shock waves form naturally in many dynamical astrophysical environments. They appear wherever large energy releases occur or where the supersonic/superalfvenic plasma streams collide or meet other obstructions. Shocks effectively convert the flow's kinetic energy into thermal energy and radiation. They are also thought to play important role in particle acceleration. Pulsed-power techniques provide an excellent opportunity to study the physics of magnetized shocks of astrophysical relevance. In particular, issues related to a number of problems have been explored such as: i) blast waves and radiative precursors; ii) blast wave instabilities; iii) the structure of intra-jet shocks; iv) interaction of shocks with obstructions.

A. General comments

Shock waves are an integral part of supersonic hydrodynamical and magneto-hydrodynamical flows and appear in a variety of forms, including blast waves following SN explosions, termination shocks formed at transition of supersonic to sub-sonic expansions, bow shocks forming in the interaction of supersonic flows with impermeable obstructions, and many others. Of a particular interest are the effects of radiation on MHD shock structure and shock stability. Pulsed-power techniques provide an excellent opportunity for studies of shocks and, in particular, magnetized shocks of astrophysical relevance. Specific examples are presented below.

Shocks appearing at the tips of astrophysical jets, as well as intra-jet shocks (called "working surfaces", Sec. II) caused by the variability of the flow velocity have been discussed in some detail in Sec. II, as they are an integral part of the jet physics. Below, we cover broader aspects of astrophysical shocks: blast waves of various kinds, shocks in a magnetic field and radiative effects in shocks. We also discuss instabilities with a particular emphasis on thermal instabilities of the shocked flow.

In the ideal MHD description, shocks appear as sharp discontinuities in the flow; i.e. the transition width is assumed to be infinitesimal (e.g., Landau and Lifshitz, 1984, 1987). In reality the width of the shock transition in density is determined by the particle mean-free path (m.f.p.) and – for the magnetic field – by the resistivity of the medium. If both scales are small compared to the global scale of the flow, then MHD, with shocks included, provides a valid description of the global flow. An example of the situation where such description is valid are shocks propagating through an expanding supernova material (Arnett, 1996). Plasmas produced in pulsed-power experiments are typically highly collisional, with the m.f.p. significantly shorter than the global dimensions of the flow. Thus pulsed power experiments deal here with the canonical MHD shocks.

The main dimensionless parameter that characterizes the presence of the shock is the width of the shock transition compared to the global scale of the underlying flow: the former must be much less than the latter. The shock strength is characterized by the Mach number. In the case of flows with significant radiative loss, the cooling time of the shocked material with respect to the hydrodynamic time scale are of significance. In partially ionized gas, the degree of ionization affects equation of state and thereby a Mach number. These effects and corresponding dimensionless parameters are discussed below in relation to specific types of shocks and corresponding effects.

In astrophysics, one can meet also situations where flows occur in media having very long m.f.p. An example is a late stage of expansion of supernova remnants into the interstellar medium (see, e.g., images and plasma parameters for SN 1006 remnant in Ghavanian et al, 2002; Bamba et al, 2003). In this case, the collisionality of the medium may be re-instated due to development of microinstabilities of the interpenetrating plasma flows. In this way so called "collisionless" shock can be formed (see a summary in Sagdeev and Kennel, 1991). Although the properties of these shocks are somewhat different from the "canonical" collisional shocks (in particular, the concept of the adiabatic index has to be modified), the global structure of the flow will still be similar to that occurring in a collisional medium. The general morphology of the collisionless shocks could then be reproduced in the collisional flows generated in pulse-power facilities.

There is a significant on-going effort in the generation of collisionless shocks in the lab as well as studies of their internal structure. Many of these experiments are based on laser-generated plasma streams (e.g., Fox *et al.*, 2013; Huntington *et al*., 2015), thus any substantive discussion of these experiments would bring us well beyond the scope of this review.

B. Blast waves and radiative precursors

A blast wave is usually defined as a diverging shocked flow initiated by a sudden energy release in a small initial volume. The ensuing structure then consists of a hot core expanding into the surrounding medium and driving a strong (but gradually weakening) shock. Depending on the density distribution in the ambient medium, there may appear a reverse shock in the hot driver that may be propagating backwards towards the center. This reverse shock may have a smaller velocity than the expanding gas and be advected outward. There exist many good tutorials on blast wave structure and these flows are also described by the well-known Sedov-Taylor self-similar solution (e.g., Landau and Lifshitz, 1987).

The Sedov-Taylor solution shows that the matter in front of the shock is compressed to a thin shell that, in the frame of the blastwave, accretes the pre-shock material. The shell thickness depends on the equation of state of the gas and on the intensity of radiative losses in the case of an optically-thin shell. A number of instabilities can develop in the propagating shock, and the presence of small scale structures is visible in the images of many of the supernova remnants, see Fig. 33 as an example.

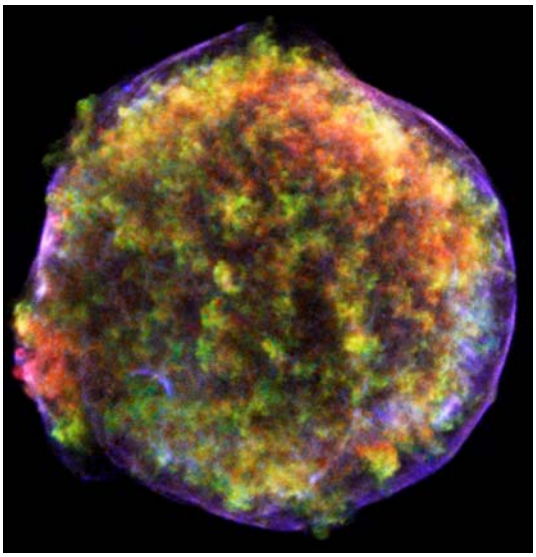

FIG. 33. Tycho's (1572) supernova remnant X-ray image (false colours); Chandra X-ray telescope. The highly structured surface of the blast wave is thought to be a result of a variety of instabilities. NASA/CXC/Rutgers/J.Warren & J.Hughes et al. - http://chandra.harvard.edu/photo/2005/tycho/

The shell may experience ripple instabilities (Vishniac instability, Vishniac, 1983); a qualitative assessment of those for the Z-pinch setting can be found in Ryutov et al. (2000), Eq. (4.32). In astrophysical environment, the Vishniac instability is important in a number of situations (Ostriker and McKee, 1983).

A complementary (conjugate) configuration of a blast wave is a c*onverging* strong shock that can be produced by turning on a high pressure on the spherical or cylindrical surface and pushing an imploding shell inwards. The physics behind the diverging and converging (imploding) thin shell is similar in many respects, in particular, in the properties of the Vishniac instability as long as perturbations of the scale smaller than the curvature radius are concerned.

Systematic studies of the converging blast waves have been carried out on the MAGPIE pulse-power facility (Imperial College), (Burdiak *et al*., 2013a; Burdiak *et al*., 2014; Burdiak *et al*., 2015), with Ne, Ar, and Xe. A schematic of one such experiment is shown in Fig. 34. A cylindrical shock was launched from the inner surface of an Aluminium cylinder of 5.8 mm inner diameter and 14 mm long. The wall thickness was 0.09 mm. The axial current of 1 – 1.4 MA caused some inward displacement of the inner surface that pushed the gas and generated a strong converging shock. [Specific details of the processes that caused the inward push are still under study.] The temperature increase at the shock front created a radiation field that could ionize the pre-shock gas (a radiation pre-cursor, see e.g., Drake, 2006). The initial mass density of the gas fill was $1.3\cdot10^{-5}$ g/cm^3 in all cases. This corresponded to the particle density of $6\cdot10^{16}$ cm^{-3} for Xe. Given that atomic collision cross-section for Xe is ~ 10^{-15} cm^{-2}, this corresponded to mean-free paths of ~ 0.15 mm for Xe, so that the anticipated shock thickness was much less than the inner radius of the tube (2.9 mm). The shock velocity was ~ 20 km/s, so that the post-shock temperature reaches a few eV. Such temperatures cause partial ionization of the gas and excitation by electron impact. This, in turn, produces a flux of intense ionizing radiation from the shock – a radiative precursor. The ionization states in a shocked region reach Z~2.

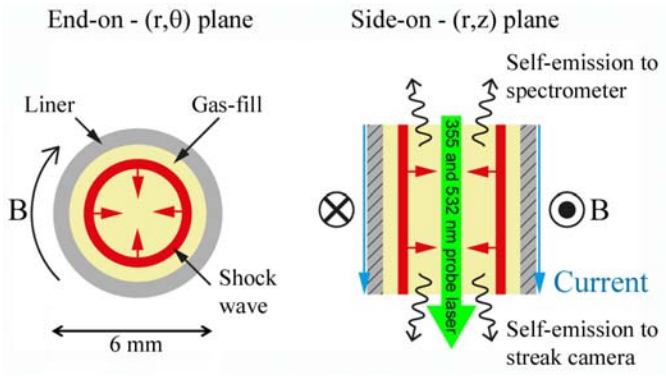

FIG. 34. Schematic of the blast-wave experiment from Burdiak *et al.* (2015). Note that the liner (shown in grey) is not imploding as a whole; however, its inner surface gives a strong kick to the gas inside, thereby driving a converging blast wave (red). The density distribution during the implosion was found by the end-on interferometry. Courtesy G. Burdiak.

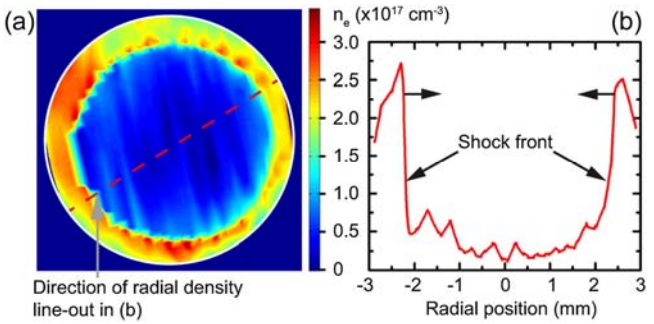

FIG. 35. (a) The electron density distribution reconstructed from the end-on interferometry (Ar, 182 ns after the start of the current pulse); (b) Radial electron density distribution at that time. The radiative precursor extending far beyond the shock transition is clearly visible. From Burdiak *et al.* (2013a), Courtesy G. Burdiak.

The electron (and ion) density at the shock transition produced a characteristic peak typical of the blast wave (Fig. 35b). Instabilities of the front show up very clearly (Fig. 35a). The high azimuthal mode number and the localization near the blast wave may indicate the presence of the Vishniac-type instability (Vishniac, 1983), although the thermo-radiative instabilities behind the shock are also possible. The measured shock velocity of ~20km/s corresponds to Mach numbers of M=60 for Ar and M=110 for Xe with respect to the sound speed of non-preheated gas. However, the significant pre-heating of the upstream material by the radiation from post-shock plasma reduces the Mach number to M~7 (Burdiak *et al.*, 2013a). The radiative cooling of the post-shock plasma is significant: the radiative cooling time of 5-10ns (Rodriguez *et al.*, 2012) is a factor of 10-20 shorter that the shock propagation time.

On larger scales, radiative precursors have been studied on the Z facility at SNL (Rochau *et al.*, 2008). The precursor was driven into a CH_2 foam by the imploding inner liner in a nested arrays Z pinch. The shock velocity exceeded 250 km/s, and the shocked foam temperature reached 400 eV. Under these conditions, the shock radiated 30-50 GW into the un-shocked foam, leading to its ionization prior to the shock arrival. An extensive set of data presented in Rochau *et al.* (2008) allows one to obtain opacity data suitable for benchmarking astrophysical radiative codes against the experiment (e.g. Falcon *et al.*, 2015).

C. Shocks in the colliding streams

As has been discussed in Secs. II and III, in clumpy jets one can often encounter a situation where one of the later clumps moves faster than the previous one and eventually overtakes it. As the Mach numbers are quite high (especially in the presence of radiative cooling), the Mach number for the relative velocity is also high, and the interaction of colliding clumps leads to a formation of intricate shock structure often referred to as "working surfaces" (Section II, see also Hartigan, 2005).

The process of collision of two non-identical clumps was simulated in a dedicated experiment (Suzuki-Vidal *et al*., 2015). This was done by investigating interaction of two counter-streaming plasma jets. The set-up shown in Fig. 36 produced currents flowing in the opposite direction in the lower and the upper foils. This is a situation where the Hall effect should lead to a difference in the densities and velocities of the two jets (see details in Sec. VI.A). Indeed, the upper jet turned out to be faster and denser than the lower one, thereby creating a desired situation of collisions of two non-identical jets.

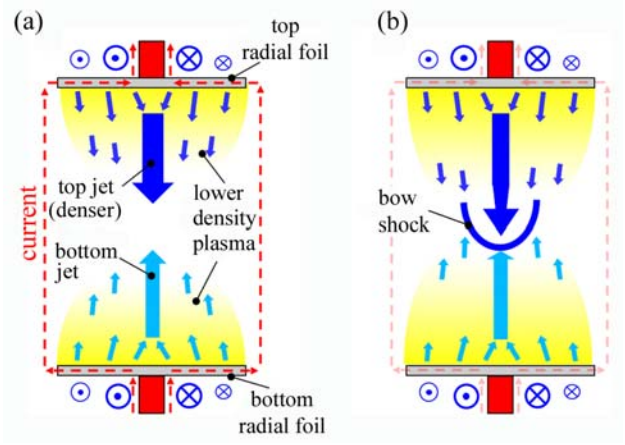

FIG. 36. Schematic experimental configuration to study the formation of a bow shock from the interaction between two counterstreaming jets with different axial velocities, represented as opposite vertical arrows on axis. The schematic depicts a side-on (radial), cut view of the system, which has azimuthal symmetry. The dashed (red) arrows represent the path of the current that drives the two plasma flows. The (blue) arrows pointing into and out of the page correspond to the azimuthal magnetic field generated by the current, which provides the driving force for the two outflows. The jets are surrounded by lower-density plasma (yellow regions), which moves with the same axial velocity as the jets. Smaller arrows in these regions represent the plasma flow direction. The images depict the two counterstreaming outflows (a) before their collision and (b) after they collide, triggering the formation of a bow shock moving toward the bottom foil. (Suzuki-Vidal *et al*., 2015)

The resulting configuration (Fig. 37), if considered in a reference frame moving with the average jet velocity, is equivalent to the interaction of the faster part of an astrophysical jet catching up with slower moving jet material. The emerging bow shock is initially smooth, but the development of small-scale structures is subsequently observed. The spatial and temporal scales are consistent with those expected for the thermal instabilities, developing at the appropriate slope of the radiative cooling curve. The dimensionless parameters characterising this experiments are similar to that discussed in Section II.D. Suzuki *et al.* (2015) discussed the scaling of the observed shock evolution to the conditions of shocks in Herbig-Haro (HH) objects. The temporal scale of the shock fragmentation in these experiments (~30ns) corresponds to ~15 years for plasma conditions typical for the shocks in HH

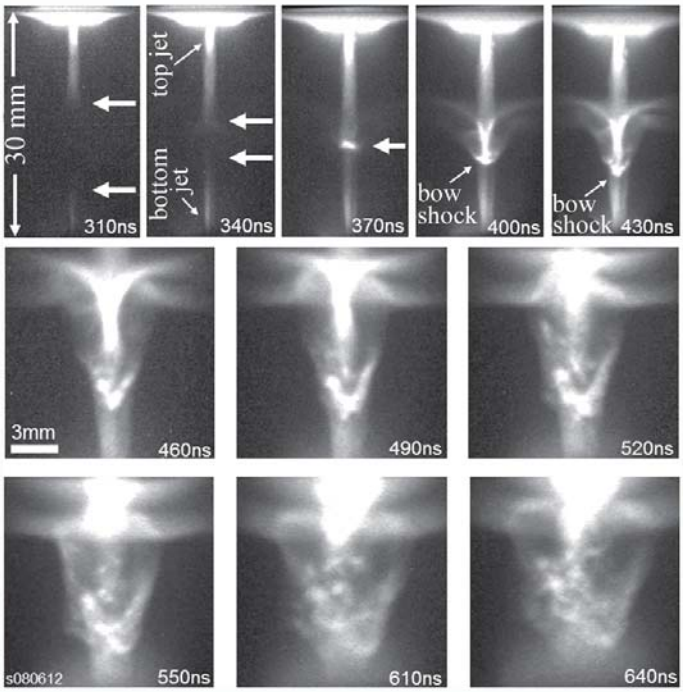

FIG. 37. Counterstreaming jet interaction results from optical self-emission of the plasma obtained from the same experiment. The arrows in the first three frames indicate the position of the tip of both jets (visibility dependent on image contrast levels), with their collision highlighted at 370 ns. The last six frames are focused on the bow shock region, which is seen to fragment most evidently in the last three times. (Suzuki-Vidal *et al*., 2015).

objects, while the observed spatial scales (between ~100um and ~1mm) correspond to 3-30 AU. It was noted in this paper that the size of the larger scale non-uniformities is consistent with the size of the new knots appearing in HH 1 object (Hartigan *et al*., 2011).

Experiments with colliding plasma jets in which the jets were produced by two conical wire arrays are reported in Valenzuela et al. (2015). These experiments also show development of clumpy structures, consistent with development of cooling instabilities in which the cooling time is shorter than the flow dynamical time.

Besides the jets produced in wire arrays and foils, the pulsed-power technique allows for a great variety of other configurations, with other plasma parameters. An interesting example is the interaction of plasma jets formed in the railguns (Moser and Hsu, 2015; Merritt *et al*., 2014). Well-collimated plasma streams with velocity of 35-45 km/s, Mach number of 3-10, initial density of $(1\text{-}2)\cdot 10^{16}$ cm^{-3}, electron temperature of 1-2 eV, diameter of 5 cm, and length of 20 cm have been produced. The working gas was hydrogen with heavier admixtures of argon, and other gases.

Several experiments on the collision of the plasma jets produced by two individual guns were performed. One experiment was made for the geometry where two such jets collided head-on in the middle of a large (2.7 m diameter) vacuum chamber, as illustrated in Fig. 38. Due to high directed energy of the ions, the Coulomb collisions between the ions of the two jets correspond initially to a long mean-free-path, greatly exceeding the length of either of the jets. However, the friction between the common electron population (in the overlap zone of the two jets) and the streaming ions is very high (Ross *et al*., 2012). The electrons are then rapidly heated driving sufficient ionization of the initially singly charged ions to the higher Z states. Then, as the ion-ion collision cross-section scales as Z^4, the mean-free path becomes low and a rapid braking of the stream occurs. Therefore a transition from initially collisionless interpenetration

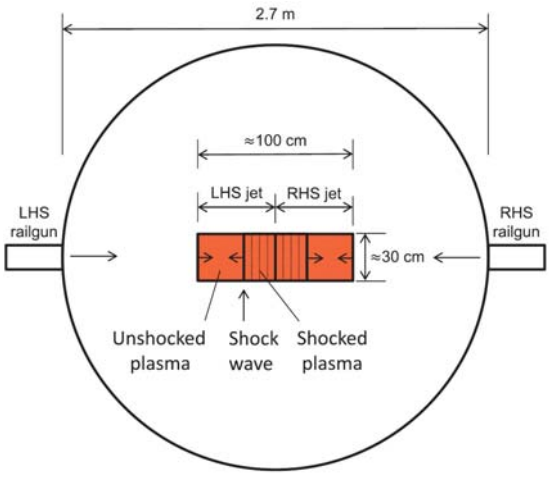

FIG. 38. Schematic of the experiment with two counter-propagating, high Mach numbers plasma bunches from the right-hand-side (RHS) and left-hand –side (LHS) railguns. Note the size of the spherical vacuum chamber (2.7 m in diameter). Courtesy A. Moser.

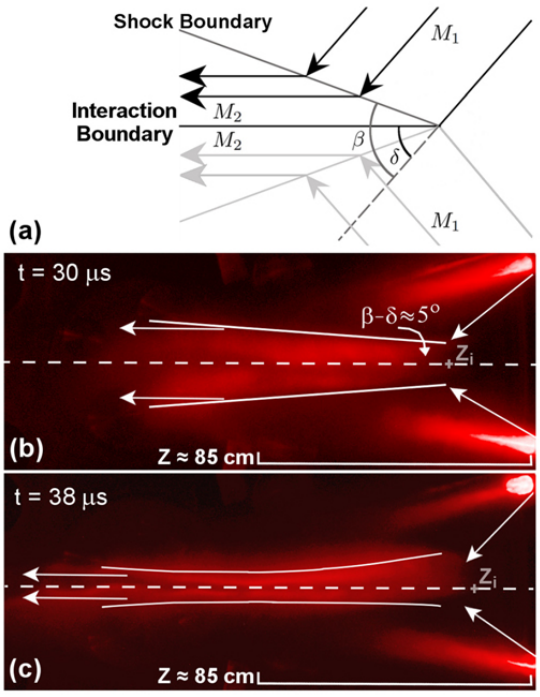

FIG. 39. Oblique merging of the two high-Mach number jets. False-color optical image for two instants of time. The notation is explained in panel (a). Courtesy E. Merritt

changes to a strong collisional interaction. In astrophysics this would correspond to the onset of enhanced particle scattering driven by plasma microinstabilities (i.e., formation of shocks in the initially collisionless system).

In another set of experiments Merritt *et al*. (2014) used different set of ports for injecting the jets creating an oblique collision of the two jets. The relative velocity of ions of the two identical jets was now small due to a small intersection angle and, although the common "parallel" velocity was large, the merging of the jets was collisional and gave rise to formation of collisional oblique shocks, as illustrated in Fig. 39. We remind the reader that such flows represented some of the earliest models for jet formation in the astrophysical literature (Canto *et al*., 1988).

Similar structures were earlier observed and analyzed in Swadling *et al*. (2013) in conjunction with the merging of the jets emanating from the wires in wire arrays. In this latter case the spatial scale was in the range of a millimeter, compared to tens of centimeters of Fig. 39. This is one more example of the scalability of hydrodynamic equations (the change of scale by a factor of 30 maintains even the finest features of the flows).

D. Introducing magnetic fields

The presence of the magnetic field adds a new degree of freedom to the dynamic processes occurring in complex plasma flows. In Lebedev *et al*. (2014), interaction of a magnetized plasma flow with an obstacle was studied. The schematic of the experiment

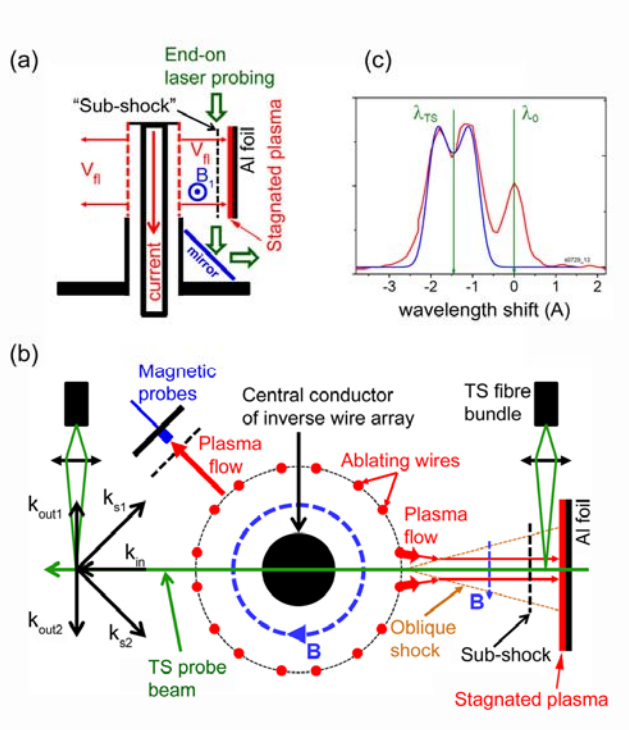

FIG. 40. Schematic of an experiment investigating interaction of a magnetized plasma flow with a planar conducting obstacle (thin Al foil). (a) Side-on and (b) end-on views of the set-up and diagnostics; (c) The Doppler shift of the TS spectra measured in the upstream plasma was used to determine plasma flow velocity and temperature. (Lebedev *et al.*, 2014)

is shown in Fig. 40. The cylindrically-diverging plasma flow is produced in the inverse-pinch configuration discussed earlier (Sec. II.A). The flow carries an azimuthal magnetic field B_1 ~ 2T measured by miniature magnetic probes. Plasma density along vertical lines of sight is measured interferometrically, whereas the flow velocity and temperature of the electrons and ions are measured by Thomson scattering. The parameters of the upstream flow are summarized in Table VIII.

This well-diagnosed experiment produced some unanticipated results. When an obstacle in the form of a rectangular Aluminum foil (0.5cm×1cm or 1cm×1cm, 17 μm thick) was introduced to the flow, one could anticipate the formation of a reverse shock propagating away from the foil, with parameters determined by MHD shock conditions (Landau and Lifshitz, 1984). In particular, the density should have increased by a factor of 4 or more, depending on the details of the equation of state. Experimentally, however, the density jump didn't exceed a factor of 2 (we call this shock-like structure a "sub-shock"). Other peculiarities of this flow configuration are discussed later.

To understand the flow a parameter called the ion-ion m.f.p. can be evaluated for the directed energy of the incoming ions (~700 eV for the incoming flow). It determines the width of the shock front: the incoming ions get scattered on and "mixed" with the shocked ions at this distance. An estimate in table VIII is rather crude, as it does not account for the density increase behind the shock. Still, it indicates that the collisional shock thickness will be no less than a few millimeters, whereas the distance between the aluminum foil and the sub-shock is also ~ a few millimeters.

TABLE VIII. Characteristic parameters of the upstream plasma flow in experiments by Lebedev *et al*. (2014). n_e - electron density; Te – electron temperature; $\bar{Z}$ - average ion charge; V_{fl} – flow velocity; λ_{ii} – ion-ion m.f.p.; λ_{ii_V} – ion-ion m.f.p. for the directed energy*; D_M – magnetic diffusivity; M – Mach number; M_A – Alfvenic Mach number; Re – Reynolds number; Re_M – magnetic Reynolds number.

n_e	T_e	$\bar{Z}$	V_{fl}	λ_{ii}	λ_{ii_V} *	D_M	M	M_A	Re	Re_M
10^{18} cm^{-3}	20 eV	3	10^7 cm/s	<1 μm	2 cm	3×10^5 cm^2	5	2	10^5	20

* See explanations in the text

Interestingly, the ion gyro-radius for the incoming flow in a 2 T magnetic field is ~ 3-4 mm, so that the magnetic field can affect the formation of the observed transition e.g. via two-fluid plasma effects; several examples of the importance of two-fluid MHD effects in astrophysical settings can be found in Kurlsrud *et al*., 1997; Königl, 2010; Gregori *et al*., 2012. We note that experiment is also relevant to on-going discussion of the relation and transition between the collisional and collisionless effects in shock formation (e.g. Ross *et al*, 2017).

E. Interaction of magnetized streams with clumps and globules

The interaction of supersonic flows with clumps of various nature is of a significant interest for astrophysics (e.g., Klein, *et al*. 1994, Hartquist and Dyson, 1996, Jones, *et al*. 1996, Hartigan, 2005, Yirak, *et al*. 2010). In particular, the issue of clump destruction processes by shear flow instabilities is still an active area of research. Some experiments based on the use of high-power lasers have been performed (e.g. Klein *et al*., 2003, Poludnenko *et al*., 2004, Hansen *et al*., 2007), but with no magnetic field. Astrophysical flows are, however, likely to carry significant embedded magnetic fields. Pulsed power techniques allow one to simulate both the effect of a magnetic field and radiation on the flow-clump interaction. This can be done via converging or diverging, magnetized plasma streams produced by a standard or an inverse wire arrays (see Sec. II). In this way the first experiments on flows around small obstacles have been recently carried out.

Ampleford *et al*. (2010) investigated formation of bow shocks in experiments where the plasma stream was produced in the standard Z-pinch configuration and propagated inward. This flow then collided with wires of a target array (Al, 15 μm diameter) positioned inside main, ablating wire array (Fig. 41). The current in each wire of the inner array could be varied and made sufficiently large to create a dynamically-significant magnetic field of up to ~40 T. The flow of Al plasma with Z~5, n_e~3×10^{18} cm^{-3}, and velocity of V=1.5×10^7cm/s emerging from the outer array collided with the inner array and produced a set of intersecting bow shocks. The dimensionless parameters characterizing the bow shock formation in these experiments were: M = 4-12; M_A = 1-5; β =0.1-5; Re_M = 4-10 (Ampleford *et al*., 2010). Reduction of the current (magnetic field) in the inner array resulted in the smaller apparent size of the obstruction, indicating that the magnetic field is an essential factor in the formation of the shock structure. Transition

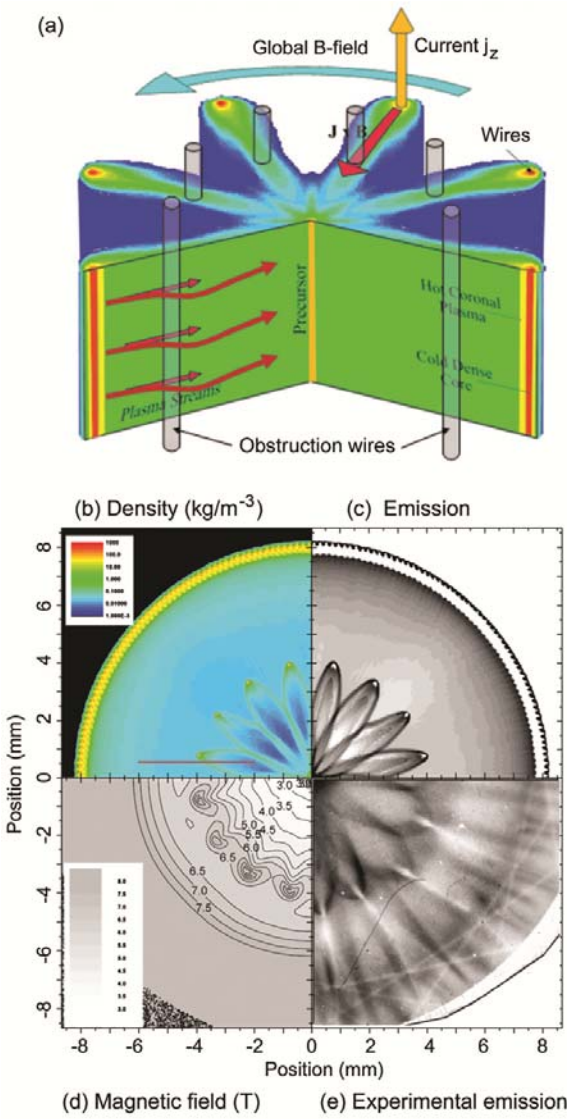

FIG. 41. (a) MHD simulations showing density distribution of ablation streams inside a cylindrical wire array and positions of obstacles for formation of bow shocks. Simulated maps of density (b); XUV emission (c); magnetic field (d), and emission map (e) recorded in experiment. (Ampleford *et al*., 2010).

from Al wires to W wires in the outer array caused significant decrease of the Mach angle compatible with increased radiation losses.

This work also included a detailed and, in general, favourable comparison of the experimental results with simulations by numerical code GORGON (Chittenden *et al*., 2004, Ciardi *et al*., 2007), widely used for simulation of astrophysics-related experiments on pulsed-power devices. Example of such comparison is presented in Fig. 41 for the case of plasma flow from Al wires. The simulations reproduced reasonably well the formation of the bow shocks around the wires of the target array, including the dependence of the shock angle on the strength of radiative cooling. However, the experimentally observed angles of the bow shocks were a factor of ~2 larger than those found in the simulations. The reasons for this discrepancy were not further investigated in that paper, in part due to the difficulties in obtaining detailed measurements of the plasma parameters of the incoming plasma and of the formed shocks, as the diagnostic access in this set-up were limited to probing only along the axial direction.

Significantly improved diagnostic access, allowing more detailed characterisation of the bow shock formation and evolution, was achieved using plasma flows from "inverse wire array" z-pinch configurations, similar to shown in Fig.40.

Experiments of Bott-Suzuki *et al*. (2015), based on the pulse-power generator XP at Cornell University, generated currents of 260 kA (Kalantar, 1993). Since the current was relatively low in these studies the authors used an array made of only two wires. Each wire (made of tungsten) then produced a plasma stream propagating radially, away from the central post, and carried with it a magnetic field embedded in the flow in

the vicinity of the wire. The stream was, therefore, interacting with an obstruction made of another wire (Al, 25 μm diameter), bent in such a way as to allow unhindered diagnostic access along the *z* axis. The characteristic flow parameters in these studies were: temperature T~15 eV; flow velocity V~10^7 cm/s; average charge state *Z*~10 (A=184); electron density n_e~10^{18}cm^{-3}. The magnetic field carried by the flow and measured in the absence of the obstruction (i.e. in the undisturbed flow) was ~ 5 T at the point where the obstruction would be inserted. A nice picture of the bow shock shrouding the obstruction was obtained by end-on interferometry (Fig. 42a). Gated pinhole images show the shock transition as a narrow but strong emitter of the hard UV, compatible with the anticipated post-shock temperature of ~ 50 eV. The presence of a diffuse emission region in front of the shock transition may be a sign of a radiative precursor, similar to that seen in Fig. 35.

Interestingly, the width of the shock transition - determined by the collisions of the incoming ions with the slower ions of the post-shock plasma - is rather large. Indeed, the upstream tungsten ions have the energy of 9 keV, so that the shock width is at a scale of a few mm, quite large compared to the obstruction diameter. The ion charge state in the shocked material may have become higher than 10 thus increasing the ion-ion Coulomb cross-section and making the width consistent with the observations.

The magnetic diffusivity for a *Z*=10, *T*=15 eV plasma is D_M=6×10^5 cm^2/s. For a flow velocity of V=10^7 cm/s, this would correspond to a penetration distance δ of the shock-compressed magnetic field into the upstream region $\delta \sim D_M/V \sim 0.6$ mm. Even for the higher temperature of the shocked plasma (T~50eV) the magnetic diffusivity remains high, ~10^5 cm^2/s, so that δ stays well beyond the wire diameter. As the size of the obstruction is much smaller than δ, it is hard to imagine a strong compression of the magnetic field behind the shock. In other words, the magnetic field in the shock transition stays at its pre-shock level. It may still play a role in setting the shock structure, as the electrons, heated to ~ 50 eV behind the shock, start to become magnetized even by this relatively weak field, $\lambda_{ei} \sim 7\mu m; \rho_e \sim 5\mu m$, and the electron heat conduction is suppressed.

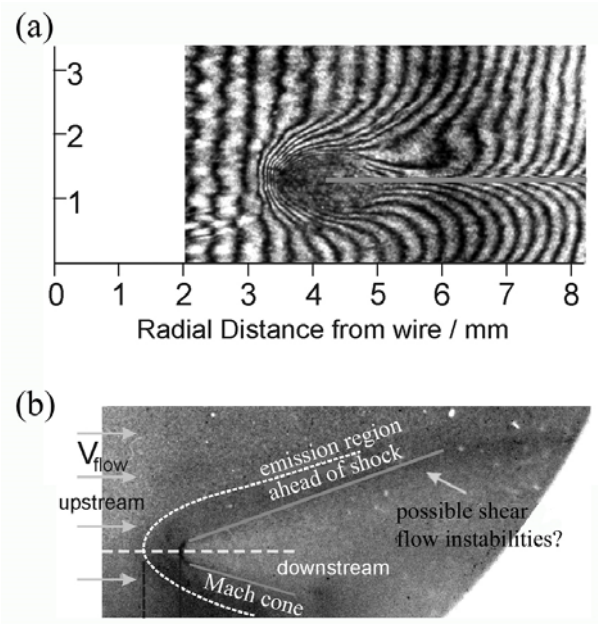

FIG. 42. (a) Interferometric image of the flow around the cylindrical obstruction placed at 4 mm from the plasma source; (b) a gated pinhole image of the same structure in the extreme UV range $h\nu$>80 eV (Courtesy Bott-Suzuki).

An experiment of Burdiak *et al*. (2017) investigated how the level of magnetic field pile-up at an obstacle affects the structure of bow shocks. Supersonic plasma flow (M_S = V_{flow}/C_S =5; M_A = V_{flow} / V_A =2-2.5), produced with an inverse wire array set-up similar to shown in

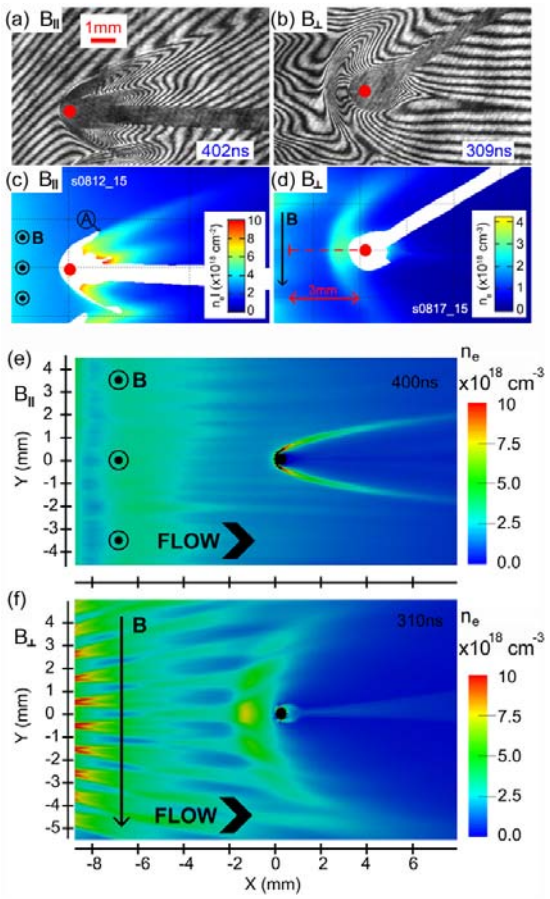

FIG. 43. Interferometric images (a,b) of bow shocks formed around cylindrical obstacles (red spots indicate diameter and position of the obstacles) and derived electron density maps (c,d) for the of the flows with magnetic field oriented parallel (a,c) and perpendicular (b,d) to the obstacles. Panels (e,f) show 2-D electron density slices from 3-D GORGON MHD simulations for parallel and perpendicular orientations, respectively (Courtesy G. Burdiak).

Fig.40. This flow interacted with conducting cylindrical obstacles oriented parallel or perpendicular to the magnetic field which was frozen (Re_M =20) into the plasma flow. It was found that both the orientation and the conductivity of the obstacles significantly affected the shape of the bow shock and the stand-off distance from the obstacles (Fig.43). For cylindrical obstacles oriented along the magnetic field (Fig.43a,c), the measured angle of the bow shock was consistent with the fast-magneto sonic Mach number of the plasma flow. The presence of magnetic field has been seen to be affecting the plasma compressibility. The stand-off distance in this case was, however, small due to the limited pile-up of magnetic field at the obstacle. Both the plasma and B-field were able to slip past the small-diameter obstacle. For the parallel orientation of B-field (with respect to the obstacle axis) both the shock curvature radius and the stand-off distance were much larger (Fig.43b,d), indicating a significant pile-up and draping of field-lines over the obstacle.

The set-up and diagnostics used in this experiment allowed detailed measurements of the bow shock structure and plasma parameters. These included spatially resolved measurements of flow velocities and plasma temperatures via Thomson scattering diagnostics, measurements of the density distributions with intereferometry and of the magnetic field with miniature magnetic probes. From these measurements detailed comparisons of the experimental results with 3-D resistive MHD simulations performed with GORGON code (Chittenden *et al*., 2004, Ciardi *et al*, 2007) could be carried out. For the B_{II} case, the simulations (Fig. 43e) reproduced the history of the shock formation observed in the experiments, including the small values of the shock opening angle and the small stand-off distance. For the $B_{\perp}$ case, however, the simulations did not reproduce the initial stages of the shock formation. In simulations the shock is first formed at the obstacle surface, as would be expected for an MHD shock, and then gradually moves away from the obstacle due to pile-up of the advected magnetic flux. In experiments, the shock in this time-dependent

flow was formed not at the obstacle, but at a large (~1.5mm) stand-off distance from the obstacle via a gradual steepening of the density perturbation. At the start of the interaction the ion-ion m.f.p. is large and the streaming ion flow is quite collisionless, and therefore one should not expect an MHD model to fully capture the formation dynamics. Instead the initial interaction is governed by 2-fluid plasma effects, when the magnetised electrons are decelerated by the piled-up magnetic field while the non-magnetized ions are decelerated by the cross-shock electric field. The thickness of the layer where the de-coupling of the electron and ion velocities is possible is the ion-inertial length (c/ω_{pi}). The value of the ion-inertial length agrees well with the stand-off distance of the shock at the formation time. We note that inspite not being able to correctly reproduce the initial phases of the shock formation, the MHD modelling reproduces very well the structure of the shock for the later times (Fig. 43f).

VI. Non-MHD effects

In this chapter we go beyond the single-fluid magnetohydrodynamics and discuss two astrophysically relevant extensions. The first is the Hall effect which is significant in objects such as astrophysical shocks and stellar flares. The second is generation of fast particles by the disruption of the current-carrying plasma columns. We conclude with a discussion of astrophysical systems where such effects can take place and consider their scaling to laboratory experiments.

A. Hall effect

In some cases of astrophysical significance a magneto-hydrodynamical description requires a refinement that would amend MHD equations with terms accounting for the Hall effect. This effect appears in two-fluid MHD (Braginski, 1965), which has separate equations for the mass, momentum, and energy of both electron and ion components of the plasma. The Hall effect stems from the electron momentum equation, which reads:

$$0 = -\nabla p_e - en_e\left(\boldsymbol{E} + \mathbf{v_e} \times \boldsymbol{B}\right) + F_{ei}\,. \qquad (6.1)$$

Here p_e, n_e and $\mathbf{v}_e$ are the electron pressure, particle density and velocity, respectively, and $\boldsymbol{F}_{ei}$ is a friction force between the electrons and ions. The latter is, in particular, responsible for the plasma resistivity. In Eq. (6.1) we neglected the electron inertia due to the small electron mass.

In the absence of the electron pressure gradient and electron-ion friction, Eq. (6.1) becomes a familiar line-tying equation, $\boldsymbol{E} + \mathbf{v_e} \times \boldsymbol{B} = 0$. Note however an important qualification, the magnetic field is line-tied to the *electron* fluid.

One can express $\mathbf{v}_e$ in terms of the mass velocity $\mathbf{v}$ of the plasma, which to a high accuracy is equal to the ion velocity $\mathbf{v}_i$, and the plasma current $\boldsymbol{j}$. To do that, one uses an expression for the current density, $\boldsymbol{j}=en_e(\mathbf{v}_i - \mathbf{v}_e)$, solves it for $\mathbf{v}_e$, and substitutes the latter to Eq. (6.1), with the understanding that $\mathbf{v}_i \approx \mathbf{v}$. The result reads:

$$\boldsymbol{E} + \mathbf{v} \times \boldsymbol{B} = \frac{\boldsymbol{j} \times \boldsymbol{B}}{en_e} + \frac{\boldsymbol{F}_{ei}}{en_e} - \frac{\nabla p_e}{en_e}\,. \qquad (6.2)$$

We assume that plasma is quasi-neutral. In the case of one ion species with a charge Z, the quasineutrality constraint implies $n_i=n_e/Z$. The electron-ion friction force can be

expressed in terms of the plasma current density, $\boldsymbol{F}_{ei} = ne\boldsymbol{j}/\sigma$, where σ is electrical conductivity.

For a medium at rest and without a pressure gradient one finds a textbook relation describing the Hall effect in a resting conducting medium (like solid metal):

$$\boldsymbol{j} = \sigma\left(\boldsymbol{E} - \frac{\boldsymbol{j}\times\boldsymbol{B}}{en_e}\right). \tag{6.3}$$

This equation indicates that if an electric field is applied to a solid conductor immersed in a magnetic field, the current generated will acquire a component flowing perpendicularly to the electric field – a textbook setting for the Hall effect.

In an environment of a conducting medium experiencing a complex and sometimes turbulent motion, the Hall effect may acquire new significance. As mentioned above, in terms of MHD problems, the change brought by this effect comes from the fact that the magnetic field is frozen into electron fluid, whose velocity may differ from the mass velocity at sufficiently high current density. If this is the case, the magnetic field interacts with the mass flow very differently compared to a single-fluid MHD, where the r.h.s. of Eq. (6.2) is dropped and the magnetic field is advected with hydrodynamic velocity.

We focus here on fully ionized plasmas, where the role of neutral particles in the plasma dynamics and magnetic field evolution is negligible. In a weakly ionized plasma one needs to consider the dynamics of all three components (electrons, ions, neutrals), this leading to a variety of additional effects. For example the friction of gravitationally unstable, collapsing molecular clumps against magnetically supported ionized gas may play significant role in star formation (Mckee and Zweibel, 1992 and Zweibel, 2002), and the Hall effect may contribute to this process (Wardle, 2004; Bai, 2014; Tassis and Mouschovias, 2005). The presence of a neutral component in these problems means a low temperature of the plasma and makes it difficult to simulate them in pulsed-power experiments. So, we consider below only the case where the neutral density is negligible.

The difference between velocities of the two components, $\boldsymbol{u}$, can be expressed in terms of the current density: $\boldsymbol{u} = \mathbf{v}_e - \mathbf{v} = -\boldsymbol{j}/n_e e$. It is convenient to characterize the role of the Hall effect by the dimensionless parameter *Ha*, "the Hall number," that indicates by how much the velocities of the two plasma components differ,

$$Ha \equiv u/\mathrm{v} = j/n_e e\mathrm{v}. \tag{6.4}$$

One can express it in terms of the characteristic values of the magnetic field B and the spatial scale of the system L. From equation, $\nabla\times\boldsymbol{B} = \mu_0\boldsymbol{j}$, we get $j \sim B/\mu_0 L$, so that

$$Ha = B/\mu_0 n_e e\mathrm{v}L. \tag{6.5}$$

One sees that favorable conditions for the observation of the Hall effect include small spatial scales, low densities, and slow hydrodynamic motions.

Due to very large spatial scales of the astrophysical systems, the Hall number is typically very small for them. As an example, one can take the inferred parameters of a typical Herbig-Haro outflow (Reipurth *et al*., 2002): B~10^{-7} T, n_e~10^{-9} m^{-3}, L~10^{15} m, v~10^6 m/s (see Table IX in Sec. VI.C). This yields the Hall number of 6×10^{-10}. However, the Hall parameter can be large in the systems like astrophysical MHD shocks, where the small spatial scale is associated with the shock thickness. The Hall effect is significant in

the space environment, as well in environments such as the Solar wind and its interaction with the Earth magnetosphere (see, e.g., Xu *et al*., 2015).

An interesting feature of the Hall effect is that it breaks the symmetry properties of a single-fluid MHD. Equations of single-fluid MHD allow for the transformation $\boldsymbol{B}\rightarrow-\boldsymbol{B}$; $\mathbf{v}\rightarrow\mathbf{v}$, or, similarly, $\boldsymbol{j}\rightarrow-\boldsymbol{j}$; $\mathbf{v}\rightarrow\mathbf{v}$. This means, in particular, that if one changes polarity of electrodes, the system evolves in exactly the same manner as for the initial polarity, just with the signs of the current and the magnetic field change. On the other hand, if the Hall effect is present, this symmetry breaks down: the evolution of two systems of different polarity differs substantially.

The polarity effect was tested experimentally in Gourdain and Seyler (2013) in the radial foil configuration (Cf. Sec. III). The heating of the foil by a high current causes the appearance of the plasma on the outer side of the foil. This plasma intercepts part of the radial current and gets accelerated in the upward direction. The current sheath moves upward, with the current closing through a central column.

When the "normal" polarity was reversed (with the central post becoming an anode), the jet parameters experienced detectable changes (Gourdain and Seyler, 2013): the jet became more collimated near the axis and faster than in the normal polarity. This is interpreted as a result of the sign change of the Hall contribution to the radial current: in the "normal" case, it is directed oppositely to the radial current formed due to plasma inertia. In the reverse case the currents add up, increasing the upward "push." This is illustrated in Fig. 44. The characteristic plasma parameters that define the value of the Hall number (6.5) were (Gourdain and Seyler, 2013, 2014): $n_e=5\times10^{19}\text{cm}^{-3}$, $L=2\times10^{-2}$ cm, $B=10^5$ G, $v=10^7$ cm/s. This yields a modest value of $Ha\sim1/15$, sufficient to detect the difference between two cases.

In problems where one considers turbulent dynamos and amplification of initially very weak magnetic fields, the Hall effect is negligible, and the polarity effect does not show up. In other words, a given turbulent velocity field will enhance in the same way initial magnetic fields of opposite polarity. Thus, if one wants to see effects of the broken symmetry, one has to assume that the magnetic field is sufficiently strong from the outset. On the other hand, there exists an observationally proven correlation between the vector of angular velocity of the AGN accretion disc and the Faraday rotation measure, making the Hall effect one of the potential explanations (Königl, 2010).

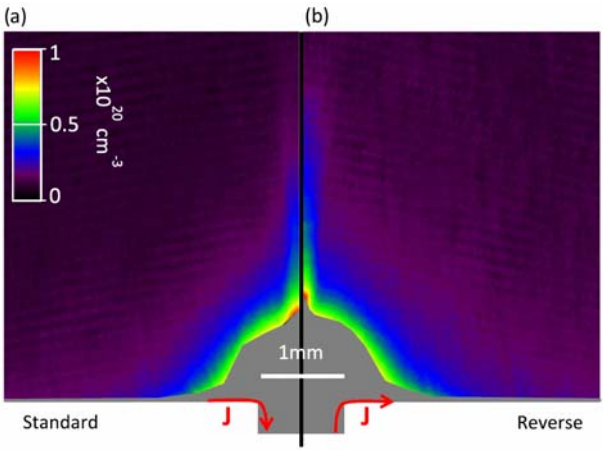

FIG. 44. Density distribution of the jets generated in Gourdain and Seyler (2013). This figure is a combination of two "halves": the left one is a left half of the density distribution in the normal polarity, whereas the right is a right half in the reverse polarity. The results are obtained by the Abel inversion of interferometric column densities. Courtesy P.-A. Gourdain.

The polarity effect was demonstrated in a very graphic form in Suzuki-Vidal *et al*. (2015), where

two oppositely-directed jets were driven in exactly the same configurations, but with opposite polarities, in conjunction with the bow-shock experiment (Sec. V.C).

In the laboratory experiments there exist other polarity effects, not related to the Hall effect. In particular, if an experiment includes interfaces between plasmas and condensed matter, the electron/ion emission from the interface may significantly depend on the polarity. A significant polarity effect was observed in Bland *et al*. (2005), where the experimental design allowed one to see the effect of the *radial* electric field polarity on the performance of the wire array. This circumstance may obscure the presence of the Hall effect.

B. Generation of energetic particles

It has long been understood that in astrophysical environments there may exist natural sources of localized current channels driven by the motion of conducting medium with embedded (possibly, self-generated) magnetic fields. Examples where these currents would naturally appear include stellar atmospheres, stellar outflows, accretion discs and giant planets (Severnyi, 1959; Hardee, 1982; Trubnikov, 1992; Szego *et al*., 2015). These currents may experience disruptions caused by the development of various instabilities, in particular, the sausage and kink instabilities driven by the combination of Rayleigh-Taylor and field-line curvature mechanisms. Particularly interesting is the sausage instability that causes formation of narrow "necks" in the current channel, and corresponding increase of the current density that may lead to a rapid growth of kinetic instabilities, onset of high anomalous resistance, and corresponding spikes in the voltage across the neck. Note that this mechanism is different from the Fermi-like acceleration occurring outside the current channel, in the cocoon area of the tower jets and described in Sec. III.B. Here we have acceleration occurring right at the neck, with a combination of direct, one step beam acceleration and, possibly, electromagnetic microturbulence leading to fast formation of the ion tail in the neck area (not considered here).

The plausibility of this chain of events became clear in an extensive set of laboratory studies using Z-pinches, plasma foci and X-pinches (Pikuz *et al*., 2015a, 2015b). Although not motivated by astrophysical connections, these studies revealed effects that could be of relevance to astrophysics: the formation of energetic, non-thermal ion populations, and generation of particle beams. Among the most important manifestations of such processes may be the conjectured current disruptions in filamentary structures (Trubnikov, 1990) observed near the center of our Galaxy (depicted in Fig.3 of Introduction, Yusef-Zadeh *et al*., 1984) .

In the remaining part of this section, we briefly summarize the experimental findings relevant to fast particle formation in current disruptions. We then discuss (still tentative) theoretical models for this process and speculate about the scaling of these results to their possible astrophysical counterparts. We emphasize again that this is a different mechanism from the one discussed in Sec. III.B.

We base our discussion on recent publications on the subject (Bakshaev *et al*., 2014; Klir *et al*., 2016; Shelkovenko *et al*., 2016), which contains an extensive list of the earlier papers. Information on the ion distribution function was obtained mostly via the neutron measurements in deuterium discharges (Klir *et al*., 2016). The ion spectrum and its anisotropy were related to neutron time-of-flight measurements along multiple chords.

By fitting the power spectrum of deuterons to the observed neutron spectrum, the authors have concluded that the neutron data can be explained by the time-integrated deuteron energy spectrum of the form $const/E^n$ with n being 2.5 – 3. The anisotropy was related to the orbit effect of the deuterons moving along the pinch in an azimuthal magnetic field (Fig.1 in Haines, 1983; Fig.10 in Bakshaev *et al*., 2014): for isotropic ion population near the axis, the larger fraction would leave the constriction towards the cathode than towards the anode. The characteristic "temperature" of these deuterons was ~ 10 keV.

In addition to the main group of the ions, there can be generated also much higher-energy ions, forming a weakly diverging stream detected at the cathode by the use of a radiochromic film (Klir *et al*., 2016). The ion energy in this stream reached tens of MeV.

Alongside with the fast ions, fast electrons are also formed in the pinched plasma, with the energies exceeding 300 keV, thereby approaching the relativistic domain. The most recent results as well as the earlier references are presented in Shelkovenko *et al*. (2016).

In all cases, the formation of high-energy ion tails and electron beams was correlated with the formation of "hot spots" near the constrictions of the axial current. Note also that, despite high plasma density in the constrictions, the mean-free paths of fast particles (ions, electrons) were much greater than the constriction size. This indicates that the collisionless description of the formation process may be adequate.

The appearance of fast particles in pulsed-power devices, and the astrophysical significance of this effect has recently gained attention from the research community. We note a recent study (Takezaki *et al*., 2016), where fast ions were formed in the interaction of plasma flow generated in a plasma focus device, with a perpendicular magnetic field and indicating one more mechanism of fast ion formation that may have astrophysical relevance.

C. Energetic electrons produced by current disruptions and conjectured scaling

In this section we discuss a specific model of the fast particles generation by the "necking" effect and attempt to scale the experimentally observed characteristics of the fast particles to the corresponding characteristics in the analogous astrophysical systems. Despite the presence of many uncertainties, this exercise may serve as a useful template for similar future studies based on more detailed analyses.

When the constriction starts to develop, as shown in the schematic form in Fig. 46 the total current within a column remains almost constant due to a high inductance. The azimuthal magnetic field in the constriction area must therefore increase. Ions are heated due to compression and their pressure increases to match the increased magnetic pressure. They are pushed out of the constriction zone along the axis (both ways). It is not certain what limits the width of the "neck" from below.

As the current remains constant, the shrinking of the "neck" radius leads in parallel to increase of the relative velocity u of the electrons and ions. When u exceeds a threshold for the development of micro-instabilities of ion-acoustic and/or lower-hybrid type, the micro-fluctuations cause enhanced scattering of the electrons and may lead to a rapid growth of the anomalous plasma resistivity (see references in Sec.VII.B of Ryutov *et al*., 2000). To sustain the current, the electric field increases, reaching a runaway

threshold for the electrons on axis. The electrons may form a beam with the energy ~*eEa* in the direction of the anode. The combination of these effects creates a complex and not yet fully understood picture.

To relate laboratory observation to possible astrophysical counterparts, we assume that the underlying physics of the laboratory and astrophysical pinches and their disruptions is the same. In particular, we assume that the shrinking of the constriction occurs with a non-relativistic velocity (i.e., $v_A<c$), as is the case in the laboratory experiments. Accordingly, we can extend our similarity consideration only to those astrophysical phenomena where $v_A<c$. This does not mean that we cannot have relativistic electron beams formed in the neck, as these beams still do not change the overall nonrelativistic evolution of the constriction zone, and the energy taken away by relativistic electrons is small.

The acceleration mechanism discussed in this section is directly related to the formation of very high electric fields and the rapid collapse of a constriction. This is the situation usually met in the laboratory experiments with Z- and X-pinches and plasma foci. In the astrophysical tower jets, as well as in their laboratory counterparts, additional mechanisms can work for the ion acceleration related to a long wandering of the ions in the magnetic field outside the central jet but inside the return current shroud (see Sec. III.B). Here the acceleration will be a gradual Fermi-like one and may lead to formation of long ion tails (Sec. III.B). This should favor ion acceleration as the ions go through a longer non-relativistic phase, which the electrons may not survive due to their much stronger attachment to the field lines and a rapid loss through a "leaky" magnetic field prior to reaching relativistic energies. Direct electron acceleration by the enormous inductive voltage in the disrupting current-carrying column may contribute to the appearance of highly relativistic electrons observed in a number of astrophysical sources.

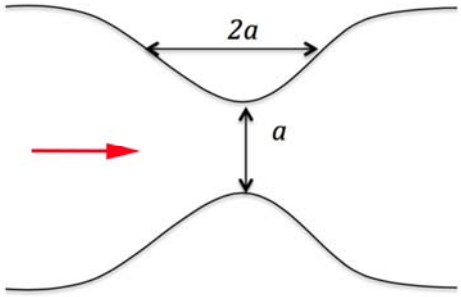

FIG. 45. Geometry of constriction. Effects of particle heating and acceleration occur predominantly in the zone of the neck with the length comparable to its diameter. The hot ions are ejected both ways, whereas the electron (ion) beam is directed towards anode (cathode) situated far to the left and right and not shown in the figure. The red arrow shows direction of the current flow. The characteristic evolutionary time of the constriction is $\tau \sim a / v_A$, where Alfven velocity v_A is evaluated for the magnetic field and plasma density in the neck area.

The pinch length l will be assumed significantly larger than its radius, and the processes in the constriction can be characterized by the length-scale a (Fig. 45) related to the constriction size. The ratio $\xi = l / a >> 1$ will be called an aspect ratio. The time can be measured in the units of the Alfvenic time a/v_A. As we are not going to develop a comprehensive theory model, but rather use the experimentally determined energy of fast electrons to scale it to the corresponding values in an astrophysical problem, we can skip the numerical coefficients in the scaling relations that follow.

The time scales will be related as the Alfvenic time-scales, so that

$$\tau_{astro} = \tau_{lab} \frac{\left(B / a\sqrt{n}\right)_{lab}}{\left(B / a\sqrt{n}\right)_{astro}}, \tag{6.6}$$

Now we consider the energy of accelerated electrons. Inductive accelerating voltage U appears with the onset of the anomalous resistance and resulting rapid current decrease:

$$U \sim L\Delta I / \tau \equiv LI \times (\Delta I / I) \times (1/\tau), \tag{6.7}$$

where L is inductance of the column. One has

$$\frac{L_{astro}}{L_{lab}} = \frac{(a\xi)_{astro}}{(a\xi)_{lab}} \tag{6.8}$$

We present also relation for the pinch current:

$$I_{astro} = I_{lab} \frac{(aB)_{astro}}{(aB)_{lab}}. \tag{6.9}$$

There are two dimensionless parameters that characterize both systems. Those are an aspect ratio ξ and the current drop $\Delta I/I$. Combining Eqs. (6.6) – (6.10), we find scaling for the energy W_e=eU of the electron beam generated at the constriction:

$$\frac{(W_e)_{astro}}{(W_e)_{lab}} = \frac{\left(aB_\varphi^2 / \sqrt{n}\right)_{astro}}{\left(aB_\varphi^2 / \sqrt{n}\right)_{lab}} \times \frac{\xi_{astro}}{\xi_{lab}} \times \frac{(\Delta I / I)_{astro}}{(\Delta I / I)_{lab}} \tag{6.10}$$

We assumed that the relative current drop $\Delta I / I$ and aspect ratio ξ are the same for both systems. If the identification of the acceleration mechanism is correct, then the assumption of the same relative current drop in the pinch columns with the same aspect ratio is natural. We emphasize that this is an assumption.

The laboratory experiments allow one to verify the scaling (6.10) by comparing the energies of accelerated electrons between pinches of various currents and plasma densities. This would offer an experimental test of the scaling. We are not aware of such experimental comparisons made to this date.

To get some impression of the parameters involved, we present in Table IX a comparison of some generic mid-size pinch and a plasma jets described in Reipurth *et al*. (2002) and visible in the lower part of Fig. 1 of the Introduction.

TABLE IX. Comparison of the characteristic parameters of laboratory and astrophysical pinches

Parameter	Lab	Astro
Aspect ratio ξ	10-20	10-20
Pinch radius, a (cm)	0.1	10^{17}
Magnetic field, B(G)	10^{6}	10^{-6}
Plasma density, n (cm^{-3})	10^{22}	10^{-3}
Pinch current, I (MA)	1	10^{6}
Alfven velocity, v_A (cm/s)	$3\cdot10^{6}$	$6\cdot10^{6}$
Evolution time, τ (s)	$3\cdot10^{-8}$	10^{10}
Electron beam energy, W_e(keV)	300	10^{9}

If the scalings presented above can be supported by a more thorough analysis, one can predict that the pinches associated with currents flowing along the central part of a young star jet may serve as a source of synchrotron radiation by the GeV-range electrons.

VII. Magnetic Reconnection

Magnetic reconnection is one of the most basic processes affecting many astrophysical phenomena. Pulsed-power devices open up the possibility to study this process in collisional resistive plasmas in well characterized environments. After a brief general introduction we describe first steps in the development of relevant experimental platforms.

Magnetic reconnection is phenomenon by which the global topology of the magnetic field can be changed by localized redistribution of the electric current. The idea of reconnection can be traced back to ground-breaking works by Parker (1957) and Dungey (1958); in a cartoon form, it can be illustrated by Fig. 46.

Imagine two magnetic flux-tubes as shown in Fig. 46a immersed in an ambient plasma and initially separated by some distance in the direction normal to the figure. Imagine then that the motion of the ambient plasma brings the tubes closer in this direction, and they "touch" each other. Then, in the contact zone, the components of the magnetic field directed oppositely to each other would annihilate, and the configuration would change to that shown in Fig. 46b. Remarkably, the local rearrangement of the field in a contact zone leads to a global change of the topology: the points 1 and 2 that were not initially connected along the magnetic field lines, become connected. This global change may give rise to a number of secondary processes. In particular, the electron heat conductivity between points 1 and 2 takes the parallel form. The other important consequence is that the field tension causes a "sling-shot" effect and may lead to straightening of the flux tubes. This "cartoon" picture may actually be realized in the stellar convective zones. In other settings, in particular, in the Solar corona, the geometry may be more complex.

Besides its ability to change the topology of the system, magnetic reconnection can also occur very rapidly, on time-scales much shorter than the resistive diffusion time in the initial configuration. In a number of situations, the reconnection process involves small spatial scales associated with collisionless instabilities driven by the plasma current. The plasma turbulence that starts at the largest-scale magnetic islands, produced by the resistive tearing instability (Furth *et al*., 1963), cascades to scales as small as the anomalous skin depth (Drake *et al*., 2008; Yamada *et al*., 2010; Yamada *et al*., 2016).

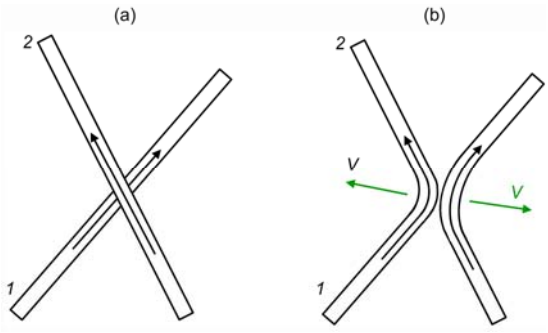

FIG. 46. Magnetic reconnection of two magnetic flux tubes immersed in an ambient slowly moving plasma.

Magnetic reconnection is a mechanism underlying Solar and stellar flares, and is thought to be a

significant player in a number of astrophysical phenomena: accretion discs; the interaction between accretion disks and the central object; in determining the thermal balance of the interstellar gas; and as an injection mechanism for particle acceleration (Zweibel and Yamada, 2009 and references therein).

In the case where initial plasma pressure is small compared to the magnetic pressure ($\beta << 1$) – a case typical for example in the solar flares – the magnetic field initially has a nearly force-free geometry and the plasma current is almost exactly parallel to the magnetic field. In this case the rapid dissipation of the magnetic field causes strong plasma heating, so that plasma pressure in the reconnection zone becomes comparable to the magnetic pressure. In the simplest geometry that is often used in the physics analyses of reconnection, one starts with a planar situation where the field has initially only *z* component, the current has only *y* component and all the parameters depend only on *x*. An array of instabilities then can occur starting from purely resistive tearing modes and going down to various current-driven collisionless microinstabilities.

In a more realistic version, one may have a situation where there is a uniform "guiding" magnetic field in the *z* direction and, overlaid with it, a "reconnecting component" that is directed along *y* and changes sign as a function of *x* (being, say, positive at $x>0$ and negative at $x<0$). Here the reconnection would release only the energy of the reconnecting component (Furth *et al*., 1963; Drake *et al*., 2008; Zweibel and Yamada, 2009; Yamada *et al*., 2010; Yamada *et al*., 2016).

Studies of magnetic reconnection in a $\beta << 1$ plasma are best suited for magnetic confinement devices. In these devices one can create and control magnetic configurations in the regimes where the plasma manifests its collisionless properties. The efficacy of this approach has been demonstrated, in particular, in beautiful experiments of the Princeton Plasma Physics Laboratory group (Yamada *et al*., 2010; Yamada *et al*., 2016).

But reconnection effects may also be important in $\beta \geq 1$ plasmas. These are likely to be quite common in many astrophysical settings where flows dominate the energetics but the fields can still play important roles. In these cases, the plasma heating becomes a subdominant effect, but there still remain two other important effects: 1) change of the magnetic topology; 2) dissipation of magnetic energy leading to slowing down and even destroying the magnetic dynamo. Z-pinches could naturally create plasmas of high beta and high collisionality and therefore open up a window to the processes not easily covered by the magnetic confinement facilities. High-beta reconnection regimes have been also produced with high-power lasers (see, e.g., Nilson *et al*., 2006; Fiksel *et al*., 2014 and Rosenberg *et al*., 2015).

In considering laboratory studies and astrophysical phenomena, it's important to note that magnetic reconnection is a multi-faceted phenomenon involving a tremendous range of scales, from global scales (thousands of kilometers in the stellar convective zones and parsecs in galactic accretion discs) to microscopic scales as small as micrometers (anomalous skin depth) in stellar interiors. The global scales are described by the MHD equations, whereas the processes in the reconnection zones are described by small-scale, sometimes kinetic, instabilities. One can introduce a large number of dimensionless parameters characterizing the relative role of all these processes. The most basic ones are the plasma beta and the plasma collisionality characterized by the ratio of the ion skin depth to the ion mean-free path. For one particular example these are shown later in this section, in Table X.

Below we focus on what pulsed power facilities have contributed and can contribute to *collisional* reconnection studies. An example comes from an experimental platform (Suttle *et al*., 2016; 2018; Hare *et al*., 2017a; 2017b; 2018) based on the use of MAGPIE pulsed power facility. This platform offers significant flexibility in controlling the parameters of the inflowing magnetized plasma flows. It also offers the opportunity to vary the dimensionless parameters characterizing the reconnection process, such as Lundquist number ($S = \mu_0 L V_A/\eta$) and plasma β.

The overall experimental setup is shown in Fig. 47; the details will be discussed later in this section. The basic element of this experiment is generation of a cylindrically-diverging, magnetized plasma flow using the inverse wire array z-pinch configuration (discussed in Section IIa). The magnetic reconnection setup involves two inverse arrays positioned side-by-side and driven in parallel by a 1.4MA, 500ns current pulse. The arrays produce radially divergent plasma flows which advect azimuthal magnetic fields. When the flows collide between the two arrays, the magnetic fields they carry are anti-parallel and magnetic reconnection occurs with formation of a long-lasting current sheet in which the magnetic field is annihilated. The 2-D magnetic reconnection configuration that forms is sustained in a quasi-stationary state by incoming plasma flows for more than 20 hydrodynamic crossing times.

This system manifests a number of interesting features briefly discussed below and has been very thoroughly characterized by a variety of diagnostics which provided detailed measurements of all of the key plasma parameters. Thomson scattering was used to measure spatial variations of the directed flow velocities, as well as the ion and electron temperatures. The magnetic field distribution in the reconnection plane was evaluated by laser polarimetry. The line-integrated density was obtained by the imaging laser interferometry, as illustrated in Fig.47b,c. As particle mean-free paths are much shorter than the global scale of the experiment, one can use the hydrodynamic picture of the flow. In the geometry of Fig. 47, the plasmas come along the *x*-axis from the left and right to interact in the *y*-*z* plane, where the radial flow stagnates. The plasma then flows out predominantly along the *y*-direction, and some plasma expansion can also occur in

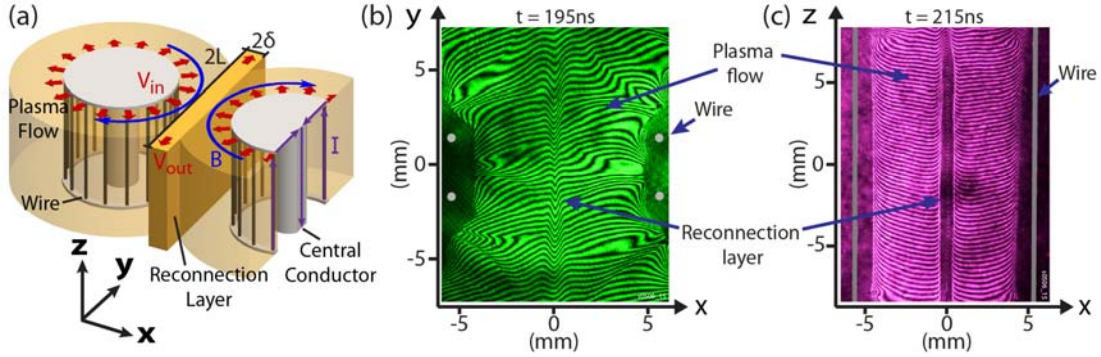

FIG. 47. (a) Experimental configuration of the reconnection experiment (with cut-away in the right wire array to show the current path). The current is applied in parallel to the two inverse wire arrays, producing magnetized plasma flows which collide to create a reconnection layer. Raw interferometry images of the reconnection layer along the *z*-direction (b) and along *y*-direction (c). In the explanations related to this figure, we use a Cartesian coordinate system shown in (a) with the origin in the mid-point of the annihilation layer. [Suttle et al. (2018)].

the *z*-direction at the top and the bottom edges of the reconnection layer.

For the further discussion, we present in Table X some important characteristics of the plasma in a reconnection layer formed from Al or Carbon plasma flows, including the derived dimensionless reconnection parameters. These characteristics change in space and time; the numbers given in the table roughly correspond to a central point of the layer at t = 215ns.

TABLE X. Characteristic plasma parameters in the magnetic reconnection layer. [Suttle *et al*., 2018; Hare *et al*., 2018]

Parameter	Symbol	Carbon plasma (A=6, Z=6)	Aluminium plasma (A=27, Z=7)
Physical parameters			
Electron density (cm^{-3})	n_e	$6x10^{17}$	$1x10^{18}$
Electron temperature (eV)	T_e	100	40
Ion temperature (eV)	T_i	600	300
Magnetic field (T)	B_0	3	2
Layer half-length (mm)	L	7	7
Layer half-thickness (mm)	δ	0.6	0.3
Inflow velocity (km/s)	V_0	50	50
Outflow velocity (km/s)	V_{out}	130	100
Derived plasma parameters			
Alfven speed (km/s)	V_A	70	20
Sound speed (km/s)	C_S	85	45
Ion skin depth (mm)	$d_i = c/\omega_{pi}$	0.4	0.35
Ion-ion m.f.p. (mm)	λ_{ii}	$3x10^{-3}$	$3x10^{-3}$
Electron-ion energy equilibration time (ns)	$\tau_{ei}^{(E)}$	140	40
Radiative cooling time (ns)	τ_{rad}	600	5
Magnetic diffusivity (cm^2/s)	D_M	10^4	$5x10^4$
Electron-ion relative velocity (km/s)	$u_e = B_0/\mu_0\delta en_e$	40	30
Dimensionless parameters			
Lundquist number	S	120	10
Inflow thermal Beta	$\beta_{th} = 2\mu_0 p/B_0^2$	0.4	1
Dynamic beta	$\beta_{dyn} = 2\mu_0\rho V^2/B_0^2$	1	10
Mach number	$M_A=V_0/V_A$	0.7	2.5
Dimensionless layer thickness	δ/d_i	1.5	0.85
Ion skin depth to ion-ion m.f.p. ratio	d_i / λ_{ii}	130	110
Dimensionless layer length	L/δ	>10	>20

The formation of the reconnection layer in Al and C plasmas has many features which are common for both materials: the layer thickness is comparable to the ion skin depth (δ/d_i ~1); the incoming plasma flows are re-directed and accelerated in the *y*-direction to velocities $V_y > V_A$; the plasma is strongly heated, and the ion temperature significantly exceeds both the electron temperature ($T_i \sim ZT_e$, with Z=6-7) and the kinetic energy of the incoming ions. Measurements show that the conversion of the magnetic

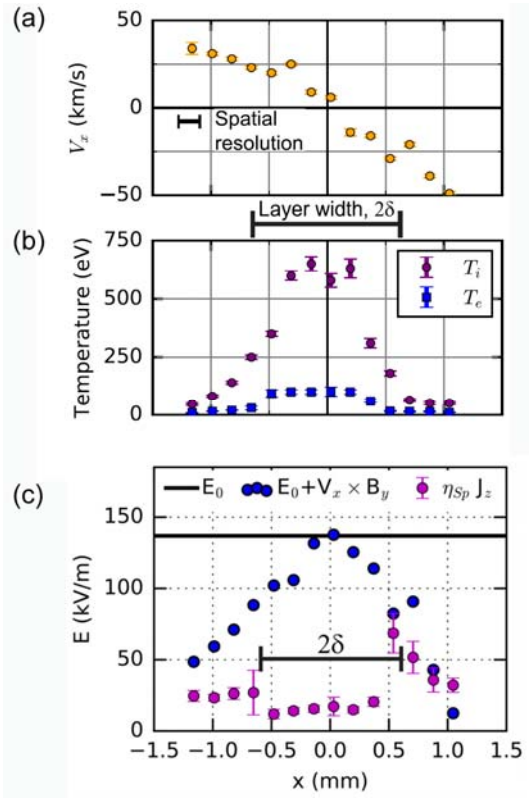

FIG. 48. Spatial profiles of the inflow velocity (a) and the electron and ion temperatures (b) measured by Thomson scattering in the reconnection layer for carbon plasma. (c) – components of the reconnecting electric field. From Hare *et al*. (2017b).

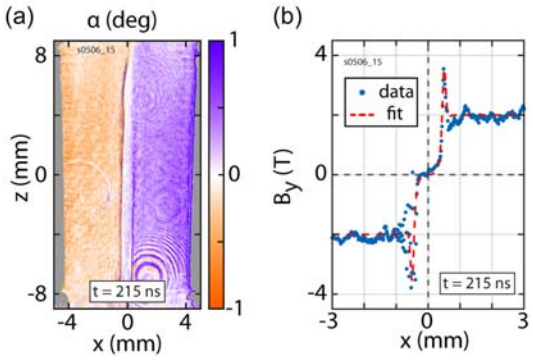

FIG. 49. The measured Faraday rotation angle (a) and the reconstructed profile of the *y* component of the magnetic field (b), showing a pile-up of the magnetic field at the boundary of the reconnection layer. From Suttle *et al*. (2018).

energy provides a significant contribution to the overall energy balance, ~50% for Carbon (Hare *et al*., 2017a). The mechanism responsible for the preferential ion heating in these experiments is still under investigation. The observed relation between the electron and the ion temperatures in the reconnection layer, T_i~ZT_e, and the large "current" drift velocity, comparable to the ion sound speed, suggests that the kinetic plasma effects could be responsible for the heating. The spatially resolved measurements of the plasma velocity and temperatures performed with Thomson scattering (Fig.48), combined with polarimetry measurements of the distribution of the magnetic field (similar to Fig.49), allow calculation of the electric field in the reconnection layer (Fig.48). For steady-state resistive MHD reconnection, the variation of the convective electric field (V_x x B_y) should be balanced by the variation in the resistive term ($\eta_{Sp}J_z$). Measurements show however, that the resistive component with Spitzer-Braginskii resistivity is a factor of ~10 smaller than necessary to support the reconnecting electric field.

There are also important differences in the behaviors of the reconnection layers formed in Al and C plasmas, arising from the differences in the inflow parameters (Mach numbers) and in the radiative cooling rates. Firstly, the inflows are super-Alfvenic (M_A=2.5) for Al, but sub-Alfvenic for Carbon (M_A=0.7). The stagnation of the Al flows lead to formation of two shocks whose separation sets the thickness of the hot plasma zone. Polarimetry measurements of magnetic field distribution (presented in Fig.49) show an increase (pile-up) of field at the layer boundary by a factor of two with respect to the field in the incoming flow

and a rapid decrease of field in the layer consistent with magnetic flux annihilation. Secondly, there is a significant difference in the importance of radiative cooling of plasma in the reconnection layer. Cooling is significant for Al (τ_{rad} ~5ns), but negligible for Carbon (τ_{rad} ~600ns). As a result, a much higher electron temperatures were observed in the case of Carbon (T_e =100eV for C versus 40eV for Al), with a corresponding increase of the Lundquist number to S=120 compared with ~10 in Al.

Measurements of the layer structure in the reconnection (x-y) plane showed that it is fairly uniform and steady in the case of Al, but highly unstable in the case of C. In the latter case the layer rapidly breaks up into a chain of plasmoids which are visible in the electron density maps (Fig. 50) and in multi-frame self-emission images (Hare *et al*., 2017a). Measurements with miniature magnetic probes (Hare *et al*., 2018) also indicate the presence of an O-point magnetic field structure as expected in a plasmoid. It is interesting to note that plasmoids in these experiments were observed at a relatively small Lundquist number of S~100. This is however consistent with theoretical predictions for the semi-collisional regime of plasmoid instability (Loureiro and Uzdensky, 2015), including the observed number of plasmoids and the characteristic growth time of the instability.

As Table X shows, the plasma in this experiment is strongly collisional with the ion mean-free path being shorter than their gyroradius and the electron mean-free path being comparable with their gyroradius. This means that the platform used is suitable for the reconnection studies in the poorly explored regimes of high plasma collisionality. In particular, a significant contribution of un-magnetized (i.e. strong) Nernst effect may eventually become identifiable.

In general, highly collisional reconnection regimes are of significant interest for magnetic field generation in stellar convective zones (e.g., Sec. V in Ryutov, 2015), where the collisionless effects are absent, but filamentation (tearing) instabilities (Furth *et al*., 1963) are still possible and may interfere with dynamo activity (Loureiro & Boldyrev, 2017). Direct observations of reconnection processes in stellar interiors are not possible and experimental results characterizing reconnection under such conditions would be helpful for benchmarking codes describing such phenomena. Table X illustrates the level of detailed information available on plasma parameters in experiments which, together with the information on the formation and evolution of spatial structures in the reconnection layer, can be used for comparison

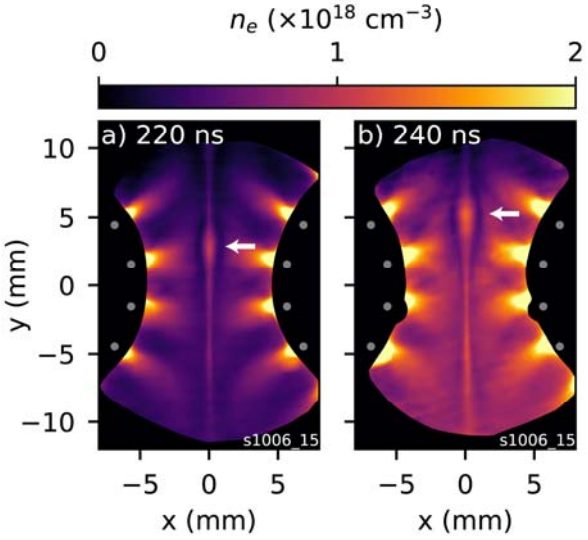

FIG. 50. Electron density maps obtained from laser interferometry (in the x-y) in the same experiment with a delay of 20ns, showing a reconnection layer at x=0 which extends across the entire field of view. Arrows indicate a plasmoid moving in the +y direction with velocity V_y=130km/s. From Hare *et al*. (2018).

with simulations. The relevant information regarding the tearing modes may be also obtained in experiments with thin metal foils with magnetic fields having opposite directions on the two sides of the foil (Zier et al., 2012). In this setting one should eliminate contamination from MRT instability, which can develop if the fields on the opposite sides of the foil are not quite equal in magnitude.

VIII. Summary and outlook

Achievements made with the use of pulsed power facilities are summarized and possible areas of future growth are identified.

This paper discusses achievements made in the area of experimental modeling of dynamical astrophysical phenomena via pulsed power techniques. The merit of these techniques is their capability to produce well-controlled plasma flows of desired geometries: jets; diverging or converging blast waves; rotating plasma discs; combinations of these structures. One of the advantages of pulsed power techniques is their intrinsic ability to introduce and control magnetic fields in the system. Plasma parameters can be controlled to change the plasma collisionality, the role of radiation, and ionization degree. Such control allows researchers to tailor the experiment in the best way for studying specific astrophysical phenomena. One characteristic example is the study of magnetic tower jets (Section III), where experimental studies provide support for the plausibility of models discussed in the astrophysical literature. Both the general morphology and dynamical characteristics of magnetic tower jets have now been reproduced in experiments. Other similar examples are discussed in this review.

In astrophysical environments hydrodynamic flows typically have very high Reynolds numbers. These are well in excess of the Reynolds numbers accessible in numerical simulations and limited by the numerical viscosity. Pulsed power experiments allow researchers to, at least partially, bridge this gap. They allow one to reach Reynolds numbers of order of 10^5, thereby providing necessary conditions for entering regimes with developed, high Re turbulence. The magnetic Reynolds number that characterizes the entraining of the magnetic field by the plasma flow ranges in the pulsed-power experiments between a few tens to a few hundreds, allowing access to the early stages of the field evolution in a turbulent plasma.

Progress in developing dedicated diagnostic instrumentation has opened up the possibility of resolving fine structures appearing within global flows: turbulent vortices (e.g., Fig.15c), multiple closely-spaced shocks (e.g., Fig. 9b), and magnetic reconnection current sheets (e.g., Fig. 50). These features are often not resolved in astrophysical images and their role is inferred only through MHD simulations. The scaled laboratory counterparts described in our review allow one to make direct comparisons between the "numerical" and real flows that have been experimentally produced and characterized in the laboratory.

As was recognized early in the laboratory astrophysics studies, hydrodynamic flows with subdominant dissipative processes allow scaling over tremendous range of spatial and temporal scales, provided the hydrodynamic description holds over this whole range. The similarity (called Euler similarity, see a summary in Appendix A) is

dynamical, i.e., it covers the whole spatio-temporal evolution of the system from some initial state, onward for several dynamical times. In this regard the Euler similarity is different from the similarities sometime used to find the scaling of some particular characteristics of the system (say, the friction force acting on the body, or the plasma confinement time in the fusion confinement experiments). In the Euler similarity we deal with the *whole dynamical process*. Importantly, the shocks and turbulence are covered by the Euler similarity as well. This critical similarity holds for the MHD flows too allowing one to make meaningful comparisons between astrophysical systems and their laboratory counterparts, including the presence of shocks.

Interestingly, Euler similarity may manifest itself in comparing two *laboratory experiments* of different scales. An example was discussed in Sec. V.C, where a very similar shock structures were observed in two experiments with the global scales differing by 2-3 orders of magnitude (~ 1m vs. ~ 1 mm). This (albeit unintended) synergy between laboratory experiments of disparate spatial scales provides additional support to the soundness of the general concept of scaling astrophysical structures to manageable laboratory models.

A promising development of recent years was the generation of an analogue of an accretion disc, where a rotating plasma disk is contained in the radial direction by the ram pressure of the incoming flow. The images of these discs reveal a rapid inward plasma transport occurring on time-scales much faster than classical diffusion time, possibly indicating the development of turbulent viscosity.

The generation of fast, suprathermal particles is a feature manifested by a number of pulsed-power facilities, most notably, z-pinches. Particles with the energies orders of magnitude greater than applied voltages have been observed in such experiments for decades. It is believed that their generation is related to disruptions of the pinch current by the sausage and kink instabilities, although details of related particle acceleration processes have not been fully understood. By assuming that the current disruptions in the current-carrying jets in astrophysics have the same underlying physics, one can produce a simple scaling from the laboratory to astrophysics. This scaling predicts that disrupting jets in astrophysics may produce copious amounts of multi-GeV electrons and, accordingly, be a source of intense synchrotron radiation.

A recent development in this area is an experimental detection of high-energy ions in tower jets (Sec. III. B). The ion energy reaches here 3 MeV, way above the values usually observed in Z-pinches and attributed, as mentioned above, to the ion compression in the "necking" area. We speculate that these ions get to high energy as they are confined in a larger magnetic structure of the tower jet, and experience the second- or first-order Fermi acceleration when bouncing in the whole cocoon. The jet "wiggling" near the axis creates temporal variations of the magnetic field in the cocoon, as needed for this acceleration mechanism. We further speculate that the maximum energy achievable by this mechanism is determined by the ions reaching large orbits and escaping the cavity. If so, the maximum attainable energy can be scaled to the astrophysical tower jets and falls into the range of tens of TeV.

Pulsed-power facilities with relatively dense and cold plasmas may offer an excellent platform for studies of resistive reconnection not involving development of microturbulence, anomalous resistivity and non-fluid effects. These regimes, beside their conceptual importance, may be the only ones available in the stellar convective zones

where plasma becomes nearly non-ideal and the standard separation of scales between collisionless and collisional processes loses its relevance. Such reconnection can be still fast, accelerated by the development of the hydrodynamic turbulence on the appropriate scales (Cf. the plasmoid model, e.g. Loureiro & Uzdensky, 2016).

The results summarized in this review have been mostly obtained on modest pulsed power facilities that have been and can be deployed in university-scale laboratories. The multiplicity of these facilities made possible a rapid progress and cross-checking of the results. The key factor that is also within the reach of the university laboratories is development and fielding of novel, inventive diagnostics. We anticipate a continuous flow of physics information needed for the development of comprehensive models of astrophysical phenomena and a strengthening the interaction between astrophysicists and practitioners of pulsed-power experiments.

IX. Acronyms

AGN – Active Galactic Nuclei

COBRA – Cornell Beam Research Accelerator

EOS – Equation Of State

HEDLA – High-Energy Density Laboratory Astrophysics

KH – Kelvin-Helmholtz (instability)

MAGPIE – Mega Ampere Generator for Plasma Implosion Experiments

m.f.p. – mean free path

MHD – Magneto-Hydro-Dynamics

MRT – Magneto-Rayleigh-Taylor (instability)

PF – Plasma Focus

PPPL – Princeton Plasma Physics Laboratory

YSO – Young Stellar Object

Acknowledgments

We acknowledge many helpful discussions with D.J. Ampleford, S.N. Bland, G.C. Burdiak, J.P. Chittenden, A. Ciardi, R.P. Drake, M.G. Haines (deceased), G.N. Hall, J.D. Hare, A.J. Harvey-Thompson, L.A. Pickworth, B.A. Remington, L.G. Suttle, F. Suzuki-Vidal and G.F. Swadling. SL and AF acknowledge support by the DOE Award No. DE-

SC-0001063. SL acknowledges support by EPSRC Grant No. EP/N013379/1 and by the DOE Award No. DE-F03-02NA00057. DR is grateful to Imperial College (London) for its kind hospitality during DR's visit in the fall of 2016. AF acknowledges support from the Laboratory for Laser Energerics, the Department of Energy grant GR523126, the National Science Foundation grant GR506177, and the Space Telescope Science Institute grant GR528562.

Appendix A. Similarity considerations

When establishing connections between a laboratory experiment and its astrophysical counterpart a natural question arises as to how one relates phenomena occurring on the enormous spatial and temporal scales of astrophysical objects to their laboratory models with the size of less than a centimeter and time-scale of less than a microsecond. In discussing this issue we focus on hydrodynamical and magnetohydrodynamical phenomena.

There is a large number of publications on scaling techniques, and among them comprehensive texts by Bridgman (1963), Barenblatt (1979), Sedov (1993) and Durst (2007). In conjunction with laboratory astrophysics these issues have been discussed in Arnett (2000), Ryutov & Remington (2002), Koepke (2008), and Hartigan et al (2009).

It goes without saying that, to build a meaningful laboratory experiment, one needs to have at least a general idea of the processes governing the observed natural phenomena. Then one can attempt to build a laboratory model replicating the same processes. Pulsed power technology is most suitable for imitating effects governed by MHD, whence the focus on this class of effects in our review.

An ability of the laboratory experiment to reach a morphological similarity with astrophysical images is encouraging and helpful: it signifies a correct identification of the underlying processes. [To be more precise, attaining a morphological similarity is a *necessary* condition for the correct identification.]

In what follows in this Appendix we present a brief summary of similarity issues for the magnetohydrodynamical (MHD) systems. We present a brief outline of the general approach and refer the reader to the publications containing more detailed analyses.

The similarity conditions for the hydrodynamical and magneto-hydrodynamical phenomena have been reviewed by Ryutov et al (2000) and Ryutov& Remington (2002). Here we present a brief summary of a so-called Euler similarity. We start from a set of ideal MHD equations for a polytropic gas,

$$\frac{\partial \rho}{\partial t} + \nabla \cdot \rho \mathbf{v} = 0, \tag{A.1}$$

$$\rho\left(\frac{\partial \mathbf{v}}{\partial t} + \mathbf{v} \cdot \nabla \mathbf{v}\right) = -\nabla p - \frac{\boldsymbol{B} \times \nabla \times \boldsymbol{B}}{4\pi}, \tag{A.2}$$

$$\frac{\partial B}{\partial t} = \nabla \times \mathbf{v} \times \boldsymbol{B}, \tag{A.3}$$

$$\frac{\partial p}{\partial t} + \mathbf{v} \cdot \nabla p = -\gamma p \nabla \cdot \mathbf{v}, \tag{A4}$$

where ρ and **v** are mass density and velocity, p is the pressure, and $\boldsymbol{B}$ is the magnetic field. There are no dissipative processes included in these equations (no viscosity, heat conductivity, and electrical resistivity); the role of dissipative processes is discussed later in this Appendix. The composition here is assumed to be uniform. MHD shocks with the standard relations between the downstream and upstream parameters on the shock transitions are allowed (Ryutov, Drake, Remington, 2000).

Initial conditions for the set of equations (A1) – (A4) read:

$$\rho_{t=0} = \rho^* f\left(\frac{\boldsymbol{r}}{L^*}\right);\quad p_{t=0} = p^* g\ \left(\frac{\boldsymbol{r}}{L^*}\right);$$
$$\mathbf{v}_{t=0} = \mathrm{v}^* \boldsymbol{h}\left(\frac{\boldsymbol{r}}{L^*}\right);\quad \boldsymbol{B}_{t=0} = B^* \boldsymbol{k}\left(\frac{\boldsymbol{r}}{L^*}\right). \tag{A5}$$

We present them above in a way suitable for subsequent use in dimensionless form. In particular, L^* is a characteristic scale of the problem, and ρ^* is a characteristic density. The function f is dimensionless and characterizes initial shape of the density distribution. The same relates to the rest of the initial conditions in (A5).

One can now introduce dimensionless representation of the set (A1)-(A4) by normalizing the variables ($\boldsymbol{r}$, t) and unknown functions (ρ, **v**, p, $\boldsymbol{B}$) using the same set of scale parameters:

$$\boldsymbol{r}' = \boldsymbol{r}/L^*,\quad t' = t\sqrt{\rho^*/p^*}/L,\quad \rho' = \rho/\rho^*,$$
$$p' = p/p^*,\quad \mathbf{v}' = \mathbf{v}\sqrt{\rho^*/p^*},\quad \boldsymbol{B}' = \boldsymbol{B}/\sqrt{p^*}. \tag{A6}$$

Substituting these relations to Eqs. (A1)-(A.4) we reduce the governing equations to dimensionless form:

$$\frac{\partial \rho'}{\partial t'} + \nabla' \cdot \rho' \mathbf{v}' = 0,$$
$$\rho'\left(\frac{\partial \mathbf{v}'}{\partial t'} + \mathbf{v}' \cdot \nabla' \mathbf{v}'\right) = -\nabla' p' - \frac{\boldsymbol{B}' \times \nabla' \times \boldsymbol{B}'}{4\pi},$$
$$\frac{\partial \boldsymbol{B}'}{\partial t'} = \nabla' \times \mathbf{v}' \times \boldsymbol{B}', \tag{A7}$$
$$\frac{\partial p'}{\partial t'} + \mathbf{v}' \cdot \nabla' p' = -\gamma p' \nabla \cdot \mathbf{v}'.$$

Likewise, the initial conditions (A6) become:

$$\rho'_{t=0} = f(\boldsymbol{r}');\quad p'_{t=0} = g(\boldsymbol{r}');$$
$$\mathbf{v}'_{t=0} = Eu\boldsymbol{h}(\boldsymbol{r}');\quad \boldsymbol{B}'_{t=0} = \sqrt{8\pi/\beta}\boldsymbol{k}(\boldsymbol{r}'). \tag{A8}$$

where

$$Eu \equiv \mathrm{v}^* \sqrt{\rho^*/p^*};\quad \beta \equiv 8\pi p^*/B^{*2} \tag{A9}$$

are two dimensionless parameters characterizing the problem.

The usefulness of this approach is in its universality: the set of dynamical equations (A7) does not contain any parameters characterizing the initial state. So, if the initial state in the simulation experiment has been chosen so as to have the

initial state to be geometrically similar to that of the natural one (i.e. the functions f, g, $\boldsymbol{h}$, and $\boldsymbol{k}$ in Eq. (A8) are the same) and two dimensionless parameters (A9), Eu and β, are the same, then any two initially geometrically-similar systems evolve in exactly the same way, despite a possible enormous differences in the dimensional factors p^*, ρ^*, v*, B^*, and L^*. Both systems may experience compression, recompression, shock formation, transition to the turbulent state – and all this will be covered by the same set of equations (A7). This universality makes the Euler similarity so attractive for laboratory astrophysics.

The similarity is quite broad, imposing only two constraints, the constancy of Eu and β, on five parameters (p^*, ρ*, v*, B^*, and L^*) that define the system. In some cases, the number of constraints becomes even lower. For a purely hydrodynamical (B=0), systems initially at rest ($\mathbf{v}$(t=0)=0) its further evolution remains similar for all geometrically-similar initial states, without any constraints on p^*, ρ*, and L^*). All this makes the Euler similarity attractive for designing experiments imitating dynamical astrophysical phenomena.

It goes without saying that set (A7)-(A8) contains all other, more specific similarities allowed by ideal hydrodynamics. In particular, if the system is spherically symmetric and a short-pulse point source of energy creates a highly heated zone in the otherwise cold gas, a self-similar blast-wave solution by Sedov and Taylor is recovered (Tang & Wang, 2009). If the system contains (or develops) shear flows, it may generate fluid turbulence with the inertial cascading to smaller scales and the Kolmogorov-Obukhov similarity solution in the inertial range is established (Ryutov & Remington, 2003; Ye Zhou, 2017). These are just two examples of many similarity solutions that can be found within the Euler similarity.

We emphasize that the Euler similarity is "tailored" to describe non-steady state processes (e.g., jet formation, development of RT instabilities of accelerated interfaces, evolution of supernova remnants, interaction of shocks with clumps, etc). In this regard it is different from similarities, designed to find characteristics of systems maintained in a quasi-steady state, like scaling for the viscous drag in Reynolds similarity, or plasma confinement scaling in fusion devices (Connor & Taylor, 1978).

Now we briefly discuss the role of dissipative processes: viscosity, thermal conductivity, magnetic diffusivity, and mutual diffusion of components in systems with variable composition. Those are characterized by the dimensionless parameters relating the rate of dissipation to the fluid advection rate. This yields familiar constraints on the Reynolds Number, Re, Peclet number, Pe, Magnetic Reynolds number, $\mathrm{Re_M}$, and mass Peclet number $\mathrm{Pe_m}$:

$$\mathrm{Re} = L^* \mathrm{v} / \nu; \quad \mathrm{Pe} = L^* \mathrm{v} / \chi; \; \mathrm{Pe}_{mass} = L^* \mathrm{v} / D; \; \mathrm{Re}_{magn} = L^* \mathrm{v} / D_{magn}, \quad \text{(A10)}$$

where L^* is a characteristic length-scale, and ν, χ, D, D_{magn} are, respectively, the kinematic viscosity, thermal diffusivity, mutual diffusion coefficient for two-component system, and magnetic diffusivity. If all of these dimensionless numbers are much larger than unity, the role of the corresponding dissipation process is not important for the global scale motion. In astrophysical setting these conditions are normally satisfied to a very large degree due to large scale of the astrophysical systems. In laboratory, however, special care has to be taken to choose the experimental parameters that yield large values

of these numbers though these are not necessarily the same as in real astrophysical systems. If they are large, then the motion on the global scales is not affected by dissipation.

One can expand the Euler similarity to include radiative cooling of the matter. In the case where radiative power per unit volume is a power law of p and ρ,

$$Q_{rad} = Ap^{\mu}\rho^{\nu}, \tag{A11}$$

one additional constraint has to be imposed, Ryutov et al (2001): a parameter $AL^* p^{*\mu-3/2} \rho^{*\nu-1/2}$ has to be kept constant between the two systems. In a simpler model, where the radiative loss is characterized by some cooling time τ, $Q_{rad} = p/(\gamma-1)\tau$, the similarity is observed if a parameter $(\tau/L)\sqrt{p^*/\rho^*}$ is invariant between the two systems.

Adding other dissipative processes to the set of equations (A1) – (A4) leads to appearance of additional constraints. A detailed analysis of these issues has been presented in Falize et al, 2009, 2011. Assuming that the radiative thermal diffusivity can be represented as a power-low function of p and ρ, one can find similarities for the diffusive radiative transport. For the situations where dynamic equations have to take into account too many dissipative processes (e.g., all four transport processes are important and have different dependences on the density and temperature), establishing a meaningful similarity may become impossible as the number of independent constraints exceeds the number of dimensional characteristics of the system, p^*, ρ*, v*, B^*, and L^*.

Scaled experiments play an important role in validation and verification of astrophysical codes used for detailed description of astrophysical phenomena: the ensuing MHD flows are notoriously difficult for simulations. Provided the scalability can be established, numerical simulations of the laboratory experiment with controlled initial conditions (which one can vary on the shot-to-shot basis) and numerous diagnostics, establishes a firm base for the code validation and verification. It is this area where considerable effort has been spent during the past decade (e.g., Calder et al, 2002, 2004; Valarde et al, 2006; Stehle et al, 2009; Kuranz et al, 2010, 2018).

In some cases, where a strongly reduced model is used, the similarity is easy to find. An example is scaling of the maximum energy of particles accelerated by the sausage instability of a current-carrying plasma column (Sec. VI.C). Applying such similarity to the set of laboratory experiments with varying input parameters (say, the current or geometrical dimensions) one can test the model itself, before attempting to apply it to astrophysics.

If one gets to collisionless regimes, then other types of similarities may show up, that enter the problem via the Vlasov equations for the electron and ion distribution functions and Maxwell equations. An example of the corresponding similarity is that for the collisionless shocks formation in two counter-streaming plasmas (Ryutov et al., 2012). This similarity covers both electrostatic and electromagnetic mechanisms. It allows also for scaling from hydrogen plasmas (as in astrophysical settings) to plasmas of heavier elements (like carbon or beryllium) often used in the laboratory experiments because of the fabrication issues of the initial setup.

As a general rule one may say that the simpler the set of equations is (with a smaller number of parameters characterizing the system), the easier it is to find a similarity. It must, however, be verified that the same physics (the same set of equations)

work for both laboratory and astrophysical system. For example, if the radiation transport is negligibly small in the astrophysical system, the parameters of the laboratory experiments have to be chosen so as to make radiative transport negligible.

REFERENCES

Agra-Amboage, V.; Dougados, C.; Cabrit, S.; et al., 2011, "Sub-arcsecond [Fe II] spectro-imaging of the DG Tauri jet Periodic bubbles and a dusty disk wind?", ASTRONOMY & ASTROPHYSICS **532**, A59

Aleksandrov, V. V. Volkov, G. S., Grabovski, E. V., Gritsuk , A. N., Laukhin, Ya. N. , Mitrofanov, K. N., Oleinik, G.M., Frolov, I.N., Shevel'ko, A. P., 2016, "Study of the formation, stability, and X-ray emission of the Z-pinch formed during implosion of fiber arrays at the Angara-5-1 facility". Plasma Physics Reports, **42**, 1024.

Ampleford, D.J., S.V. Lebedev, A. Ciardi, S.N. Bland, S.C. Bott, J.P. Chittenden, G. Hall, C.A. Jennings, J. Armitage, G. Blyth, S. Christie and l. Rutland, 2005," Formation of working surfaces in radiatively cooled laboratory jets", Astrophys. Space Sci. **298**, 241–246.

Ampleford, D. J., A. Ciardi, S. V. Lebedev, S. N. Bland, S. C. Bott · J. P. Chittenden, G. N. Hall, A. Frank, E. Blackman, 2007, "Jet Deflection by a Quasi-Steady-State Side Wind in the Laboratory." Astrophysics Space Science **307**, 29–34

Ampleford, D.J., S.V. Lebedev, A. Ciardi, S. N. Bland, S. C. Bott, G. N. Hall, N. Naz, C. A. Jennings, M. Sherlock, J. P. Chittenden, J. B. A. Palmer, A. Frank, and E. Blackman, 2008, "Supersonic radiatively cooled rotating flows and jets in the laboratory." Physical Review Letters **100**, 035001.

Ampleford, D. J., C. A. Jennings, G. N. Hall, S. V. Lebedev, S. N. Bland, S. C. Bott, F. Suzuki-Vidal, J. B. A. Palmer, J. P. Chittenden, M. E. Cuneo, A. Frank, and E. G. Blackman, 2010, "Bow shocks in ablated plasma streams for nested wire array z-pinches: a laboratory astrophysics testbed for radiatively cooled shocks", Phys. Plasmas **17**, 056315.

Arnett, David, Bruce Fryxell, and Ewald Mueller, 1989, "Instabilities and nonradial motion in SN 1987A." *The Astrophysical Journal* **341**, L63-L66.

Arnett, D., 1996, *Supernovae and Nucleosynthesis,* Princeton University Press, Princeton.

Arnett, D., 2000, "The relevance of HED lasers to astrophysics." Comptes Rendus de L'Academie des Sciences Serie IV, Physique Astrophysique, 1, # 6, 767.

Arnett, D., C. Meakin, P. A. Young, 2009, "Turbulent convection in stellar interiors. II. The velocity field." ApJ. **690**, 1715.

Bacciotti, F., R. Mundt, T.P. Ray, J. Eisloffel, J. Solf, M. Camezind, 2000, "Hubble space telescope STIS spectroscopy of the optical outflow from DG Tauri: structure and

kinematics on subarcsecond scales", ApJ, **537**, L49.

Bacciotti, F., T.P. Ray, R. Mundt, J. Eisloffel, J. Solf, 2002, "Hubble Space Telescope/STIS Spectroscopy of the Optical Outflow from DG Tauri: Indications for Rotation in the Initial Jet Channel." The Astrophysical Journal **576**, 222-231.

Bai, X-N. 2014, "Hall-effect-controlled gas dynamics in protoplanetary disks. I. Wind solutions at the inner disk" Astrophysical Journal, **791**, 137.

Bailey, J. E.; Rochau, Rochau, G. A. ; Iglesias, C. A.; Abdallah, J.,Jr.; MacFarlane, J. J.; Golovkin, I.; Wang, P. ; Mancini, R. C.; Lake, P.W.; Moore, T. C.; Bump, M.; Garcia, O.; Mazevet, S. (2007). "Iron-plasma transmission measurements at temperatures above 150 eV." Phys. Rev. Lett., **99**, 265002.

Bailey, J. E., T. Nagayama, G. P. Loisel, G. A. Rochau, C. Blancard, J. Colgan, Ph. Cosse, G. Faussurier, C. J. Fontes, F. Gilleron, I. Golovkin, S. B. Hansen, C. A. Iglesias, D. P. Kilcrease, J. J. MacFarlane, R. C. Mancini, S. N. Nahar, C. Orban, J.-C. Pain, A. K. Pradhan, M. Sherrill & B. G. Wilson, 2015, "A higher-than-predicted measurement of iron opacity at solar interior temperatures", Nature volume **517**, 56.

Bakshaev, Yu. L., V.A. Bryzgunov, V.V. Vikhrev, et al., 2014, "Generation and anisotropy of neutron emission from a condensed Z-pinch." Plasma Physics Reports, **40**, 437-450.

Balbus, S.A., J.F. Hawley, 1991, "A powerful local shear instability in weakly magnetized disks. I - Linear analysis. II - Nonlinear evolution", *Astrophysical Journal*, **376**, 214.

Balbus, S.A. and Henri, P., 2008, "On the magnetic Prandtl number behavior of accretion disks", The Astrophysical Journal, **674**, 408-414.

Balbus, S.A., 2011, "A turbulent matter." Nature **470**, 475-476.

Bamba, A., R. Yamazaki, M. Ueno, K. Koyama, 2003. "Small-scale structure of the SN 1006 shock with Chandra observations." Astrophysical Journal, **589**, 827.

Barenblatt, G.I., 1979, ""Similarity, self-similarity, and intermediate asymptotics." Consultants Bureau, New York and London.

Begelman, M.C., 1998, "Instability of Toroidal Magnetic Field in Jets and Plerions", ApJ, **493**, 291

Bellan, P. M., 2000, "*Spheromaks*." Imperial College Press, London.

Bellan, P.M., S. You, S. C. Hsu, 2005, "Simulating astrophysical jets in laboratory experiments." Astrophysics and Space Science **298**, 203.

Bellan, P.M., 2018a, "Experiments and models of MHD jets and their relevance to astrophysics and solar physics", Phys. Plasmas, **25**, 055601.

Bellan, P.M., 2018b, "Experiments relevant to astrophysical jets", J. Plasma Phys., **84**, 755840501

Benford, G., 1978, "Current-carrying beams in astrophysics: models for double radio sources and jets", Monthly Notices of the Royal Astronomical Society, **183**, 29–48.

Bennett, M.J., S.V. Lebedev, G.N. Hall, L. Suttle, G. Burdiak, F. Suzuki-Vidal, J. Hare, G. Swadling, S. Patankar, M. Bocchi, J.P. Chittenden, R. Smith, A. Frank, E. Blackman, R.P. Drake, A. Ciardi, 2015, "Formation of radiatively cooled, supersonically rotating, plasma flows in Z-pinch experiments: Towards the development of an experimental platform to study accretion disk physics in the laboratory." High Energy Density Physics **17**, 63.

Bennett, M., S.V. Lebedev, G. Swadling, L. Suttle, M. Bocchi, E. Blackman, G. Burdiak, J.P. Chittenden, A. Ciardi, R.P. Drake, A. Frank, G.N. Hall, J. Hare, S. Patankar, R. Smith, F.Suzuki-Vidal, 2018, "Development of turbulence in differentially rotating plasma disc". (In preparation.)

Bland, S. N., S. V. Lebedev, J. P. Chittenden, D. J. Ampleford, S. C. Bott, J. A. Gomez, M. G. Haines, G. N. Hall, D. A. Hammer, I. H. Mitchell, and J. B. A. Palmer, 2005, "Effect of Radial-Electric-Field Polarity on Wire-Array Z-Pinch Dynamics." Phys Rev Letters, **95**, 135001.

Blondin, J.M., B. A. Fryxell, and A. Konigl, 1990, "The structure and evolution of radiatively cooling jets." Astrophys. J. **360**, 370.

Bocchi, M., B. Ummels, J. P. Chittenden, S. V. Lebedev, A. Frank, and E. G. Blackman, 2013, "Numerical simulations of z-pinch experiments to create supersonic differentially rotating plasma flows." The Astrophysical Journal, **767**, 84.

Bosch-Ramon, V., Rieger, F.~M., 2012, "Exploring Particle Acceleration in Gamma-Ray Binaries", Astroparticle, Particle, Space Physics and Detectors For Physics Applications - Proceedings of the 13th ICATPP Conference.~Edited by Giani Simone et al.~Published by World Scientific Publishing Co.~Pte.~Ltd., 2012, pp.~219-225 219-225.

Bott-Suzuki, S. C., L. S. Caballero Bendixsen, S. W. Cordaro, I. C. Blesener, C. L. Hoyt, A. D. Cahill, B. R. Kusse, D. A. Hammer, P. A. Gourdain, C. E. Seyler, J. B. Greenly, J. P. Chittenden, N. Niasse, S. V. Lebedev, and D. J. Ampleford, 2015, "Investigation of radiative bow-shocks in magnetically accelerated plasma flows." Phys. Plasmas, **22**, 052710.

Braginski, S. I., 1965, "Transport processes in a plasma," in *Reviews of Plasma Physics*, M. A. Leontovich, Ed. New York, NY, USA: Consultants Bureau, p. 205.

Branch, D., J. C. Wheeler, 2017, Supernova Explosions, (Springer), Sec 9.5.

Bridgman, P.W., 1963, Dimensional analysis. (Yale University Press, New Haven).

Burdiak, G.C., S.V. Lebedev, R.P. Drake, A.J. Harvey-Thompson, G.F. Swadling, F. Suzuki-Vidal, J. Skidmore, L. Suttle, E. Khoory, L. Pickworth, P. de Grouchy, G.N. Hall, S.N. Bland, M. Weinwurm, J.P. Chittenden, 2013a, "The production and evolution of multiple converging radiative shock waves in gas-filled cylindrical liner z-pinch experiments," High Energy Density Physics **9** 52.

Burdiak, G. C., S. V. Lebedev, G. N. Hall, A. J. Harvey-Thompson, F. Suzuki-Vidal, G. F. Swadling, E. Khoory, L. Pickworth, S. N. Bland, P. de Grouchy, and J. Skidmore, 2013b, "Determination of the inductance of imploding wire array Z-pinches using measurements of load voltage ." Phys. Plasmas, **20**, 032705.

Burdiak, G. C., S. V. Lebedev, A. J. Harvey-Thompson, G. F. Swadling, F. Suzuki-Vidal, G. N. Hall, E. Khoory, L. Pickworth, S. N. Bland, P. de Grouchy, J. Skidmore, L. Suttle, M. Bennett, N. P. L. Niasse, R. J. R. Williams, K. Blesener, L. Atoyan, A. Cahill, C. Hoyt, W. Potter, E. Rosenberg, P. Schrafel, and B. Kusse, 2014, "Radiative precursors driven by converging blast waves in noble gases." Physics of Plasmas, **21**, 033302.

Burdiak, G. C., S. V. Lebedev, F. Suzuki-Vidal, G. F. Swadling, S. N. Bland, N. Niasse, L. Suttle, M. Bennet, J. Hare, M. Weinwurm, R. Rodriguez, J. Gil and G. Espinosa, 2015, "Cylindrical liner Z-pinch experiments for fusion research and high-energy-density physics.", J. Plasma Physics, **81**, 365810301.

Cabot, W.H., A. W. Cook, 2006, "Reynolds number effects on Rayleigh–Taylor instability with possible implications for type Ia supernovae." *Nature Physics* 2.8: 562-568.

Calder, A., B. Fryxell, T. Plewa, R. Rosner, L.J. Dursi, V.G. Weirs, T. Dupont, H.F. Robey, J.O. Kane, B.A. Remington, R.P. Drake, G. Dimonte, M. Zingale, F.X. Timmes, K. Olson, P. Ricker, P. McNeice, H.M. Tufo., 2002, "On validating an astrophysical simulation code." Astrophys. J., Suppl. Ser. 143, 201.

Canto, J., Tenorio-Tagle, G., & Rozyczka, M., 1988 "The formation of interstellar jets by the convergence of supersonic conical flows."A&A, **192**, 287.

Canto, J., A. Raga, 1995, "The dynamics of a jet in a supersonic side wind." MNRAS, **277**, 1120.

Chevalier, R.A., J.M. Blondin, 1995, "Hydrodynamic instabilities in supernova remnants: early radiative cooling." Astrophysical Journal, **444**, 312.

Chittenden, J. P., S. V. Lebedev, C. A. Jennings, S. N. Bland, and A. Ciardi, 2004, "X-ray generation mechanisms in three-dimensional simulations of wire array Z-pinches", Plasma Phys. Controlled Fusion **46**, B457-B476.

Ciardi, A., Lebedev, S. V., Chittenden, J. P., & Bland, S. N., 2002, "Modeling of supersonic jet formation in conical wire array Z-pinches." Laser Part. Beams, **20**, 255.

Ciardi A., Lebedev S.V., Frank A., Blackman E.G., Chittenden J.P., Jennings C., Ampleford D.J., Bland S.N., Bott S.C., Rapley J., Hall G., Suzuki-Vidal F. A., Marocchino A., Lery T., C. Stehle, 2007, "The evolution of magnetic tower jets in the laboratory", Physics of Plasmas, **14**, 056501.

Ciardi, A., D.J. Ampleford, S.V. Lebedev, C. Stehle, 2008, "Curved Herbig-Haro jets: simulations and experiments " The Astrophysical Journal, **678**, 968-973.

Ciardi, A., Sergey V. Lebedev, Adam Frank, Francisco Suzuki-Vidal, Gareth N. Hall, Simon N. Bland, Adam Harvey-Thompson, Eric G. Blackman, and Max Camenzind, 2009, "Episodic magnetic bubbles and jets: astrophysical implications from laboratory experiments." The Astrophysical Journal, **691**, L147–L150.

Ciardi, Andrea; Hennebelle, Patrick, 2010, "Outflows and mass accretion in collapsing

dense cores with misaligned rotation axis and magnetic field", MONTHLY NOTICES OF THE ROYAL ASTRONOMICAL SOCIETY, **409**, L39-L43.

Coffey, D., Bacciotti, F.,Woitas, J., Ray, T. P., & Eisloffel, J. 2004, "Rotation of jets from young stars: new clues from the Hubble space telescope imaging spectrograph", The Astrophysical Journal **604**, 758.

Coffey, D., C. Dougados, S. Cabrit, J. Pety, F. Bacciotti, 2015., "A Search for Consistent Jet and Disk Rotation Signatures in RY Tau.", The Astrophysical Journal **804**, 2.

Comisso, L., M. Lingam, Y.-M. Huang, A. Bhattacharjee, 2016, "General theory of the plasmoid instability", Phys. Plasmas **23**, 100702.

Connor, J.W., J.B. Taylor, 1977, "Scaling laws for plasma confinement." Nuclear Fusion, **17**, 5.

Cuneo, M.E., D.B. Sinars, E.M. Waisman, D.E. Bliss, W.A. Stygar, R.A. Vesey, R.W. Lemke, I.C. Smith, P.K. Rambo, J.L. Porter, G.A. Chandler, T.J. Nash, M. G. Mazarakis, R.G. Adams, E.P. Yu, K.W. Struve, T.A. Mehlhorn, S.V. Lebedev, J.P. Chittenden, C.A. Jennings, 2006, "Compact single and nested tungsten-wire-array dynamics at 14-19 MA and applications to inertial confinement fusion." Phys. Plasmas, **13**, 056318.

Dougados, C, Cabrit, S., Lavalley-Fouquet, C., Menard, F., 2000, "T Tauri stars microjets resolved by adaptive optics" A&A, **357**, L61.

Drake, R. P., 1999, "Laboratory experiments to simulate the hydrodynamics of supernova remnants and supernovae," J. Geophys. Res. 104, 14505–14515.

Drake, R.P., 2006, *High-Energy-Density Physics*. Springer, Berlin-Heidelberg.

Drake, J. F., M. A. Shay, M. Swisdak, 2008, "The Hall fields and fast magnetic reconnection." Physics of Plasmas, **15**, 042306.

Dungey, J. W., 1958, *Cosmic Electrodynamics*. London, U.K.: Cambridge Univ. Press.

Durst, F., 2007, *Fluid Mechanics*, Chapter 7, Springer

Falize, E., C. Michaut, S. Bouquet. 2009, "Scaling laws for radiating fluids: the pillar of laboratory astrophysics." Astrophysics and Space Science, 322, 107.

Falize, E., C. Michaut, S. Bouquet, 2011, "Similarity properties and scaling laws of radiation hydrodynamic flows in laboratory astrophysics." ApJ, **730**, 96.

Farley, D. R., K. G. Estabrook, S. G. Glendinning, S. H. Glenzer, B. A. Remington, K. Shigemori, J. M. Stone, R. J. Wallace, G. B. Zimmerman, J. A. Harte, 1999, "Radiative Jet Experiments of Astrophysical Interest Using Intense Lasers." Phys. Rev. Lett., **83**, 1982.

Federrath, Christoph; Schroen, Martin; Banerjee, Robi; et al., 2014, "Modeling jet and outflow feedback during star cluster formation", ASTROPHYSICAL JOURNAL, **790**, 128.

Ferreira, J., C. Dougados, S. Cabrit, 2006, "Which jet launching mechanism(s) in T Tauri

stars?", Astronomy and Astrophysics **453**, 785-796.

Fiksel, G., W. Fox, A. Bhattacharjee, D. H. Barnak, P.-Y. Chang, K. Germaschewski, S. X. Hu, and P. M. Nilson, 2014, "Magnetic Reconnection between Colliding Magnetized Laser-Produced Plasma Plumes", Phys. Rev. Lett. **113**, 105003.

Fleischer, R.L., P.B. Price, R.M. Walker, 1965, "Ion explosion spike mechanism for formation of charged-particle tracks in solids." J. Appl. Phys., **36** 3645.

Foster, J. M., B. H. Wilde, P. A. Rosen, R. J. R. Williams, B. E. Blue, R. F. Coker, R. P. Drake, A. Frank, P. A. Keiter, A. M. Khokhlov, J. P. Knauer, T. S. Perry, 2005, "High-energy-density laboratory astrophysics studies of jets and bow shocks." The Astrophysical Journal, **634**, L77–L80.

Fox, W. Fiksel, G.; Bhattacharjee, A.; Chang, P.-Y.; Germaschewski, K.; Hu, S. X.; Nilson, P. M., 2013, "Filamentation instability of counterstreaming laser-driven plasmas", Phys. Rev. Lett. **111,** 225002.

Frank, A., Balick, B., & Livio, M., 1996, "A mechanism for the production of jets and ansae in planetary nebulae." ApJ, **471**, L53.

Frank, A., Ray, T. P., Cabrit, S., Hartigan, P.; Arce, H. G.; Bacciotti, F.; Bally, J.; Benisty, M.; Eislöffel, J.; Güdel, M.; Lebedev, S.; Nisini, B.; Raga, A., 2014, "Jets and Outflows from Star to Cloud: Observations Confront Theory.", in *Protostars and Planets VI*, edited by H. Beuther, R.S. Klessen, C.P. Dullemond, and T. Henning (University of Arizona Press, Tucson), p.451-474.

Furth, H.P., J. Killeen, M.N. Rosenbluth, 1963, "Finite-Resistivity Instabilities of a Sheet Pinch." Phys. Fluids, **6**, 459.

Ghavamian, P., P.F. Winkler, J.C. Raymond, K.S. Long. 2002. "The optical spectrum of the SN 1006 supernova remnant revisited." Astrophysical Journal, **572**, 888.

G. Gregori, A. Ravasio, C. D. Murphy, K. Schaar, A. Baird, A. R. Bell, A. Benuzzi-Mounaix, R. Bingham, C. Constantin, R. P. Drake, M. Edwards, E. T. Everson, C. D. Gregory, Y. Kuramitsu, W. Lau, J. Mithen, C. Niemann, H.-S. Park, B. A. Remington, B. Reville, A. P. L. Robinson, D. D. Ryutov, Y. Sakawa, S. Yang, N. C.Woolsey, M. Koenig & F. Miniati, 2012, "Generation of scaled protogalactic seed magnetic fields in laser-produced shock waves", Nature, **481**, 480.

Goodson, A. P., R. M. Winglee, and K. H. Böhm, 1997, "Time-dependent accretion by magnetic young stellar objects as a launching mechanism for stellar jets", Astrophys. J., **489**, 199.

Goodson, A. P., K. H. Böhm, and R. M. Winglee, 1999, "Jets from accreting magnetic young stellar objects. I. Comparison of observations and high-resolution simulation results", Astrophys. J., **524**, 142.

Goodson A. P. and R. M. Winglee, 1999, "Jets from accreting magnetic young stellar objects. Ii. Mechanism physics", Astrophys. J., **524**, 159.

Gourdain, P.-A., I. C. Blesener, J. B. Greenly, D. A. Hammer, P. F. Knapp, B. R. Kusse,

and P. C. Schrafel, 2010, “Initial experiments using radial foils on the Cornell Beam Research Accelerator pulsed power generator .”Physics of Plasmas **17**, 012706.

Gourdain, P.-A., J. B. Greenly, D. A. Hammer, B. R. Kusse, S.A. Pikuz, C.E. Seyler, T.C. Shelkovenko, P. F. Knapp, 2012, “Magnetohydrodynamic instabilities in radial foil configuration.” Phys. Plasmas, **19**, 022701.

Gourdain, P.-A. and C. E. Seyler, 2013, “Impact of the Hall Effect on High-Energy-Density Plasma Jets.” Physical Review Letter, **110**, 015002.

Gourdain, P-A and C E Seyler, 2014, “Modeling of strongly collimated jets produced by high energy density plasmas on COBRA.” Plasma Phys. Control. Fusion **56** 035002.

Gourdain, P-A and C E Seyler, 2017, “The impact of three dimensional MHD instabilities on the generation of warm dense matter using a MA-class linear transformer driver”, High Energy Density Physics **24**, 50.

Haines, M., 1983, “Ion-beam formation in an m = 0 unstable z-pinch.” Nuclear Instruments & Methods In Physics Research, **207**, 179-185.

Haines, M.G., 2011, “A review of the dense Z-pinch,” Plasma Phys. Controlled Fusion, **53**, 093001.

Hansen, E. C., A. Frank, P. Hartigan, S. V. Lebedev, 2017, “The Shock Dynamics of Heterogeneous YSO Jets: 3-D Simulations Meet Multi-Epoch Observations.” The Astrophysical Journal, **837**, 143.

Hare, J.D., L.G. Suttle, S.V. Lebedev, N. F. Loureiro, A. Ciardi, G. C. Burdiak, J. P. Chittenden, T. Clayson, C. Garcia, N. Niasse, T. Robinson, R. A. Smith, N. Stuart, F. Suzuki-Vidal, G. F. Swadling, J. Ma, J. Wu, and Q. Yang, 2017a, “Anomalous Heating and Plasmoid Formation in a Driven Magnetic Reconnection Experiment”, Phys. Rev. Letters, **118**, 085001.

Hare, J.D., L.G. Suttle, S.V. Lebedev, N. F. Loureiro, A. Ciardi, G. C. Burdiak, J. P. Chittenden, T. Clayson, S.J. Eardley, C. Garcia, J.W.D. Halliday, N. Niasse, T. Robinson, R. A. Smith, N. Stuart, F. Suzuki-Vidal, G. F. Swadling, J. Ma, J. Wu, 2017b, “Formation and Structure of a Current Sheet in Pulsed-Power Driven Magnetic Reconnection Experiments”, Physics of Plasmas, **24**, 102703.

Hare, J. D., L. G. Suttle, S. V. Lebedev, N. F. Loureiro, A. Ciardi, J. P. Chittenden, T. Clayson, S. J. Eardley, C. Garcia, J. W. D. Halliday, T. Robinson, R. A. Smith, N. Stuart, F. Suzuki-Vidal, and E. R. Tubman, 2018, “An experimental platform for pulsed-power driven magnetic reconnection”, Physics of Plasmas, **25**, 055703

Hardee, P.E., 1982, "Helical and pinching instability of supersonic expanding jets in extragalactic radio sources". Astrophysical Journal. **257**, 509–526.

Hartigan, P., 2005, “Laboratory experiments of stellar jets from the perspective of an observer.” Astrophys. Space Sci., **298**, 99.

Hartigan, Patrick, Adam Frank, Peggy Varnie´re and Eric G. Blackman, 2007, “Magnetic fields in stellar jets”, ApJ, **661**, 910-918.

Hartigan, P.; Foster, J. M.; Wilde, B. H.; et al. , 2009, “Laboratory experiments, numerical simulations, and astronomical observations of deflected supersonic jets: application to HH 110.” Astrophysical Journal, 705, 1073.

Hartigan, P., A. Frank, J. M. Foster, B. H. Wilde, M. Douglas, P. A. Rosen, R. F. Coker, B. E. Blue, J. F. Hansen, 2011, “Fluid dynamics of stellar jets in real time: third epoch *HUBBLE SPACE TELESCOPE* images of HH 1, HH 34, and HH 47.” The Astrophysical Journal, **736**, 29.

Hartquist, T.W., J.E. Dyson, 1996. “Flows in Clumpy Planetary Nebulae”, Astrophysics and Space Science **245**, 263-273.

Harvey-Thompson, A. J., S. V. Lebedev, S. N. Bland, J. P. Chittenden, G. N. Hall, A. Marocchino, F. Suzuki-Vidal, S. C. Bott, J. B. A. Palmer, and C. Ning, 2009, “Quantitative analysis of plasma ablation using inverse wire array Z pinches”, Phys. Plasmas 16, 022701.

Hillas, A.M. (1984). “The origin of ultra-high-energy cosmic rays.” Ann. Rev. Astron. Astrophys. **22**, 425.

Hsu, S. C., P. M. Bellan, 2002, “A laboratory plasma experiment for studying magnetic dynamics of accretion discs and jets.” Mon. Not. R. Astron. Soc. **334**, 257–261.

Huarte-Espinosa, M., A. Frank, E. G. Blackman, A. Ciardi, P. Hartigan, S. V. Lebedev, and J. P. Chittenden, 2012, “On the structure and stability of magnetic tower jets.” ApJ, **757**, 66.

Huntington, C., F. Fiuza, J.S. Ross, A. Zylstra, R. P. Drake, D. Froula, G. Gregori, N. Kugland, C. Kuranz, M. Levy, C. Li, J. Meinecke, T. Morita, R. Petrasso, C. Plechaty, B. Remington, D. Ryutov, Y. Sakawa, A. Spitkovsky, H. Takabe, and H.-S. Park, 2015, "Observation of magnetic field generation via the Weibel instability in interpenetrating plasma flows." Nature Physics, **11**, 173-176.

Jones, T.W., D. Ryu, I.L. Tregillis, 1996, “The Magnetohydrodynamics of Supersonic Gas Clouds: MHD Cosmic Bullets and Wind-swept Clumps”, The Astrophysical Journal **473**, 365.

Kadomtsev, B. B., 1965, “Plasma Stability.” In: Reviews of Plasma Physics, edited by M. A. Leontovich, (Consultants Bureau, NY,), Vol. 2, p. 153.

Kalantar, D. H., 1993, Ph.D. dissertation, Cornell University.

Kane, J. O., D. Arnett, B. A. Remington, S. G. Glendinning, J. Castor, R. Wallace, A. Rubenchik, and B. A. Fryxell, 1997, “Supernova-relevant hydrodynamic instability experiments on the Nova laser,” Astrophys. J. Lett. 478, L175–L178.

Käpylä, P.J., A.Brandenburg, M.J.Korpi, J.E.Snellman, R.Narayan, 2010, “Angular momentum transport in convectively unstable shear flows.” Astrophysical Journal **719** 67-76.

Kasen, D.; L. Bildsten, 2010, "Supernova Light Curves Powered by Young Magnetars". Astrophysical Journal. **717**: 245–249.

Kato, Y., Hayashi, M.R., Matsumoto, R., 2004, "Formation of Semirelativistic Jets from Magnetospheres of Accreting Neutron Stars: Injection of Hot Bubbles into a Magnetic Tower." The Astrophysical Journal **600**, 338.

Kifonidis, K., T. Plewa, H.T. Janka, E. Muller, 2003, "Non-spherical core collapse supernovae - I. Neutrino-driven convection, Rayleigh-Taylor instabilities, and the formation and propagation of metal clumps." Astronomy & Astrophysics, **408**, 621.

Klein, R.I., C.F. McKee, P. Colella, 1994, "On the hydrodynamic interaction of shock waves with interstellar clouds. 1: Nonradiative shocks in small clouds", The Astrophysical Journal **420**, 213-236.

Klein, R.I., K. S. Budil, T. S. Perry, and D. R. Bach, 2003, "The interaction of supernova remnants with interstellar clouds: Experiments on the Nova laser," Astrophys. J. **583**, 245–259.

Klir, D., A. V. Shishlov, V. A. Kokshenev, P. Kubes, A. Yu. Labetsky, K. Rezac, R. K. Cherdizov, J. Cikhardt, B. Cikhardtova, G. N. Dudkin, F. I. Fursov, A. A. Garapatsky, B. M. Kovalchuk, J. Krasa, J. Kravarik, N. E. Kurmaev, H. Orcikova, V. N. Padalko, N. A. Ratakhin, O. Sila, K. Turek, V. A. Varlachev, A. Velyhan, and R. Wagner, 2016, "Deuterium z-pinch as a powerful source of multi-MeV ions and neutrons for advanced applications", Phys. Plasmas, **23**, 032702.

Knudson MD; Hanson, DL; Bailey, JE; Hall, CA; Asay, JR; Anderson, WW. (2001). Equation of state measurements in liquid deuterium to 70 GPa. Phys. Rev. Lett, **87**, 225501.

Knudson, M. D., M. P. Desjarlais, A. Becker, R. W. Lemke, K. R. Cochrane, M. E. Savage, D. E. Bliss, T. R. Mattsson, R. Redmer, 2015, "Direct observation of an abrupt insulator-to-metal transition in dense liquid deuterium", Science, **348**, p. 1455.

Koepke, M. E., 2008, "Interrelated laboratory and space plasma experiments", Reviews of Geophysics, 46, RG3001.

Königl, Arieh, 2010, "On the interpretation of the apparent existence of a preferred magnetic field in extragalactic jet sources", MNRAS, **407**, L79-L83.

Kubes, P., M. Paduch, B. Cikhardtova, J. Cikhardt, D. Klir, J. Kravarik, K. Rezac, E. Zielinska, D. Zaloga, M. J. Sadowski, and K. Tomaszewski, 2016, "Influence of the Al wire placed in the anode axis on the transformation of the deuterium plasma column in the plasma focus discharge", Physics of Plasmas **23**, 062702.

Kurlsrud R.M. Cen, R. Ostriker, J.P. & Ryut, D., 1997, "The protogalactic origin for cosmic magnetic fields." Astrophys. J., **480**, 481-491.

Kuranz, C., Drake, R. P., Grosskopf, M. J., Fryxell, B., Budde, A., Hansen, J.F., Miles, A., R., Plewa, T., Hearn, N., Knauer, 2010, "Spike morphology in blast-wave-driven instability experiments." Phys. Plasmas, 17, 052709.

Kuranz C.C. , H.-S. Park, C.M. Huntington, A.R. Miles, B.A. Remington, T. Pleva, M.R. Trantham, H.F. Robey, D. Shvarts, A. Shimony, K. Raman, S. MacLaren et al, 2018,

"How high energy fluxes may affect Rayleigh–Taylor instability growth in young supernova remnants" Nature Communications, 9, Article number: 1564.

Landau, L. D. and E. M. Lifshitz, 1987, *Fluid Mechanics*, (Pergamon Press, New York).

Landau, L. D. and E. M. Lifshitz, 1984, *Electrodynamics of Continuous Media,* (Pergamon Press, New York).

Lebedev, S. V., I. H. Mitchell, R. Aliaga-Rossel, S. N. Bland, J. P. Chittenden, A. E. Dangor, and M. G. Haines, 1998, "Azimuthal structure and global instability in the implosion phase of wire array Z-pinch experiments." Phys. Rev. Lett. **81**, 4152.

Lebedev, S. V., R. Aliaga-Rossel, S. N. Bland, J. P. Chittenden, A. E. Dangor, M. G. Haines, and I. H. Mitchell, 1999, "The dynamics of wire array Z-pinch implosions", Phys. Plasmas **6**, 2016.

Lebedev, S.V., F. N. Beg, S. N. Bland, J. P. Chittenden, A. E. Dangor, M. G. Haines, K. H. Kwek, S. A. Pikuz, T. A. Shelkovenko, 2001, "Effect of discrete wires on the implosion dynamics of wire array Z pinches", Phys Plasmas, **8**, 3734.

Lebedev, S.V., J.P. Chittenden, F.N. Beg, S.N. Bland, A. Ciardi, D. Ampleford, S.Hughes, M.G. Haines, A. Frank, E.G. Blackman, T. Gardiner, 2002, "Laboratory astrophysics and collimated stellar outflows: The production of radiatively cooled hypersonic plasma jets." Astrophysical Journal, **564**, 113.

Lebedev, S.V., D. Ampleford, A. Ciardi, S. N. Bland, J. P. Chittenden, M. G. Haines, A. Frank, E. G. Blackman, and A. Cunningham, 2004, "Jet deflection via crosswinds: laboratory astrophysical studies", ApJ **616**, 988–997.

Lebedev, S.V, A Ciardi, D J Ampleford, S N Bland, S C Bott, J P Chittenden, G N Hall, J Rapley, C Jennings, M Sherlock, A Frank, E G Blackman, 2005a, "Production of radiatively cooled hypersonic plasma jets and links to astrophysical jets", Plasma Phys. Control. Fusion 47, B465–B479.

Lebedev, S. V., A. Ciardi, D. J. Ampleford, S. N. Bland, S. C. Bott, J. P. Chittenden, G. N. Hall, J. Rapley, C. A. Jennings, A. Frank, E. G. Blackman, T. Lery, 2005b, Magnetic tower outflows from a radial wire array Z-pinch. Mon. Not. R. Astron. Soc. **361**, 97–108.

Lebedev, S. V., L. Suttle, G. F. Swadling, M. Bennett, S. N. Bland, G. C. Burdiak, D. Burgess, J. P. Chittenden, A. Ciardi, A. Clemens, P. de Grouchy, G. N. Hall, J. D. Hare, N. Kalmoni, N. Niasse, S. Patankar, L. Sheng, R. A. Smith, F. Suzuki-Vidal, J. Yuan, A. Frank, E. G. Blackman, and R. P. Drake, 2014, "The formation of reverse shocks in magnetized high energy density supersonic plasma flows, Phys. Plasmas, **21**, 056305.

LeBlanc, J.M., J.R. Wilson, 1970, "A numerical example of collapse of a rotating magnetized star", ASTROPHYSICAL JOURNAL, **161**, 541.

Lee, C.-F., Ho, P.T.P., Li, Z.Y., Hirano, N., Zhang, Q., Shang, H., 2017., "A rotating protostellar jet launched from the innermost disk of HH 212", Nature Astronomy **1**, 0152.

Longair, M.S. (2011). "High Energy Astrophysics." Cambridge University Press, Cambridge UK.

Lord Rayleigh, 1900, Scientific Papers, V.II (Cambridge Univ. Press, Cambridge, England), p. 200

Lovelace, R. V. E., H. Li, A. V. Koldoba, G. V. Ustyugova, M. M. Romanova, 2002, "Poynting jets from accretion disks," ApJ, **572**, 445.

Loureiro, N F and D A Uzdensky, 2016, "Magnetic reconnection: from the Sweet–Parker model to stochastic plasmoid chains." Plasma Phys. Control. Fusion, **58**, 014021.

Loureiro, N F and S. Boldyrev, 2017, "Role of Magnetic Reconnection in Magnetohydrodynamic Turbulence", Phys. Rev. Lett., **118**, 245101

Lynden-Bell D., 1996, "Magnetic collimation by accretion discs of quasars and stars", MNRAS, **279**, 389.

Lynden-Bell D., 2003, "On why discs generate magnetic towers and collimate jets", MNRAS, **341**, 1360.

Madlener, D., S. Wolf, A. Dutrey, S. Guilloteau, 2012, "The circumstellar disk of HH 30: Searching for signs of disk evolution with multi-wavelength modeling." Astronomy and Astrophysics, **543**, A81.

Mandt, M. E., R. E. Denton, J. F. Drake, 1994, "Transition to whistler mediated magnetic reconnection", Geophys. Res. Lett. **21**, 73.

Matzen, M.K., C. Deeney, R.J. Leeper, J.L. Porter, R.B. Spielman, G.A. Chandler, M.S. Derzon, M.R. Douglas, D.L. Fehl, D.E. Hebron, T. Nash, R.E. Olson, L.E. Ruggles, T.W.L. Sanford, J.F. Seamen, K.W. Struve, W.A. Stygar, D.L. Peterson, 1999, "Fast z-pinches as dense plasma, intense x-ray sources for plasma physics and fusion applications." Plasma Physics and Controlled Fusion, **41**, A175-A184.

Mckee, C.F., E.G. Zweibel, 1992, "On the virial-theorem for turbulent molecular clouds", Astrophysical Journal **399**, 551-562.

McKinney, Jonathan C.; Blandford, Roger D., 2009, "Stability of relativistic jets from rotating, accreting black holes via fully three-dimensional magnetohydrodynamic simulations", MONTHLY NOTICES OF THE ROYAL ASTRONOMICAL SOCIETY, **394**, L126-L130.

Mereghetti, S., 2008, "The strongest cosmic magnets: soft gamma-ray repeaters and anomalous X-ray pulsars." The Astronomy and Astrophysics Review. **15**, 225.

Merritt, E. C., A. L. Moser, S. C. Hsu, Colin S. Adams, John P. Dunn, A. M. Holgado, M. A. Gilmore, 2014, "Experimental evidence for collisional shock formation via two obliquely merging supersonic plasma jets." Phys. Plasmas, **21**, 055703.

Metzger, B.D., Margalit, B., Kasen, D., Quataert, E., 2015, "The diversity of transients from magnetar birth in core collapse supernovae" MONTHLY NOTICES OF THE ROYAL ASTRONOMICAL SOCIETY. **454**, 3311.

Moffatt, H.K., 1978, *Magnetic Field Generation in Electrically Conducting Fluids* (Cambridge University Press, Cambridge).

Moll, R., 2010, " Large jets from small-scale magnetic fields", ASTRONOMY & ASTROPHYSICS, **512** , A5.

Moser, A.L., P. M. Bellan, 2012, "Magnetic reconnection from a multiscale instability cascade." Nature, **482**, 379.

Moser, A. L., S. C. Hsu, 2015, "Experimental characterization of a transition from collisionless to collisional interaction between head-on-merging supersonic plasma jets." Phys. Plasmas, **22**, 055707.

Nakamura, M. & Meier, D. L., 2004, "Poynting flux-dominated jets in decreasing density atmospheres. I. The nonrelativitic current-driven Kink instability and the formation of 'Wiggled' structures", Astrophys. J. **617**, 123–154

Nakamura, Masanori, A., Hui Li, Shengtai Li, 2007, "Stability properties of magnetic tower jets", The Astrophysical Journal, **656**,721–732.

Nicolaï, Ph., C. Stenz, A. Kasperczuk et al., 2008, "Studies of supersonic, radiative plasma jet interaction with gases at the Prague Asterix Laser System facility", PHYSICS OF PLASMAS **15**, 082701.

Nilson, P. M., L. Willingale, M. C. Kaluza, C. Kamperidis, S. Minardi, M. S. Wei, P. Fernandes, M. Notley, S. Bandyopadhyay, M. Sherlock, R. J. Kingham, M. Tatarakis, Z. Najmudin, W. Rozmus, R. G. Evans, M. G. Haines, A. E. Dangor, and K. Krushelnick, 2006, "Magnetic Reconnection and Plasma Dynamics in Two-Beam Laser-Solid Interactions", Phys. Rev. Lett. **97**, 255001.

Ostriker, J. P. and C. F. McKee, 1988, "Astrophysical blast waves." Rev. Mod. Phys. **60**, 1.

Parker, E. N., 1957, "Sweet's mechanism for merging magnetic fields in conducting fluids," J. Geophys. Res., **62**, no. 4, pp. 509–520.

Pascoli, G.; Lahoche, L, 2010, "A Magnetohydrodynamic Model for the AGB Star: Preplanetary Nebula Symbiosis", PUBLICATIONS OF THE ASTRONOMICAL SOCIETY OF THE PACIFIC, v. **122**, Issue: 897, 1334-1340.

Pikuz, S. A., T. A. Shelkovenko, D. A. Hammer, 2015a, "X-Pinch. Part I". Plasma Physics Reports, **41**, pp. 291–342.

Pikuz, S. A., T. A. Shelkovenko, D. A. Hammer, 2015b, "X-Pinch. Part II". Plasma Physics Reports, **41**, pp. 445–491.

Pohl, M., Yan, H., & Lazarian, A., 2005, "Magnetically limited X-ray filaments in young supernova remnants" ApJ, **626**, L101.

Poludnenko, A.Y., K. K. Dannenberg, R. P. Drake, A. Frank, J. Knauer, D. D. Meyerhofer, M. Furnish, J. R. Asay, and S. Mitran, 2004, "A laboratory investigation of supersonic clumpy flows: experimental design and theoretical analysis", The

Astrophysical Journal, **604**, 213.

Prager, S.C., R. Rosner, H.T. Ji and F. Cattaneo, 2010, *Research Opportunities in Plasma Astrophysics* (Princeton, NJ: Princeton Plasma Physics Laboratory) http://www.pppl.gov/conferences/2010/WOPA/index.html

Pringle, E.J., 1981, "Accretion Discs in Astrophysics", Annual Review of Astronomy and Astrophysics, **19**, 137.

Pudritz, R.E., R. Quyed, C. Fendt, A. Brandenburg, 2007, In: "Protostars and Planets V', B. Reipurth, D. Jewitt, K.Keil – Eds., (University of Arizona Press, Tucson,), p. 277.

Raga. A.C., E. M. de Gouveia Dal Pino, A. Noriega-Crespo, P. D. Mininni, and P. F. Vel´azquez, 2002, "Jet/cloud collision, 3D gasdynamic simulations of HH 110", Astron. Astrophys. **392,** 267-276.

Ray, T., C. Dougados, F. Bacciotti, J. Eislöffel, A. Chrisostomou, 2007, In: "Protostars and Planets V', B. Reipurth, D. Jewitt, K.Keil – Eds., (University of Arizona Press, Tucson,), p. 231.

Reipurth, B., J. Bally, 2001, "Herbig-Haro flows: probes of early stellar evolution." Annu. Rev. Astron. Astrophys. **39,** 403–55.

Reipurth, B., S. Heathcote, J. Morse, P. Hartigan, J. Bally, 2002, "Hubble Space Telescope images of the HH 34 jet and bow shock: structure and proper motions." The Astronomical Journal, **123**, 362.

Remington, B. A., J. Kane, R. P. Drake, S. G. Glendinning, K. Estabrook, R. London, J. Castor, R. J. Wallace, D. Arnett, E. Liang, R. McCray, A. Rubenchik, and B. Fryxell, 1997, "Supernova hydrodynamics experiments on the Nova laser," Phys. Plasmas **4**, 1994.

Remington, B.A., R.P. Drake, D.D. Ryutov, 2006, "Experimental astrophysics with high-power lasers and Z pinches", Rev. Mod. Phys., **78,** 755-807.

Robey, H. F., J. O. Kane, B. A. Remington, R. P. Drake, O. A. Hurricane, H. Louis, R. J. Wallace, J. Knauer, P. Keiter, D. Arnett, and D. D. Ryutov, 2001, "An experimental testbed for the study of hydrodynamic issues in supernovae," Phys. Plasmas 8, 2446–2453.

Rochau, G. A, J. E. Bailey, R. E. Falcon, G. P. Loisel, T. Nagayama, R. C. Mancini, I. Hall, D. E. Winget, M. H. Montgomery, and D. A. Liedahl, 2014, "ZAPP: The Z Astrophysical Plasma Properties collaboration", Physics of Plasmas **21**, 056308 (2014).

Rochau, G.A., J.E. Bailey, Y. Maron, G.A. Chandler, G.S. Dunham, D.V. Fisher, V.I. Fisher, R.W. Lemke, J.J. MacFarlane, K.J. Peterson, D.G. Schroen, S.A. Slutz, E. Stambulchik, 2008, "Radiating shock measurements in the z-pinch dynamic hohlraum." Physical Review Letters, **100,** 125004.

Rodriguez R., J.M. Gil, G. Espinosa, R. Florido, J.G. Rubiano, M.A. Mendoza, P. Martel, E. Minguez, D.R. Symes, M. Hohenberger, R.A. Smith, 2012, "Determination and analysis of plasma parameters for simulations of radiative blast waves launched in

clusters of xenon and krypton", Plasma Phys. Control. Fusion **54**, 045012

Romanova, M.M., Ustyugova, G.V., Koldoba, A.V., Lovelace, R.V.E., 2004, "Three-dimensional Simulations of Disk Accretion to an Inclined Dipole. II. Hot Spots and Variability." The Astrophysical Journal **610**, 920-932.

Romanova, M. M., A. Kulkarni, M. Long, R. V. E. Lovelace, J. V. Wick, G.V. Ustyugova, and A. V. Koldoba, 2006, Adv. Space Res. **38**, 2887.

Rosenberg, M. J., C. K. Li, W. Fox, A. B. Zylstra, C. Stoeckl, F. H. Séguin, J. A. Frenje, and R. D. Petrasso, 2015, Slowing of Magnetic Reconnection Concurrent with Weakening Plasma Inflows and Increasing Collisionality in Strongly Driven Laser-Plasma Experiments, Phys. Rev. Lett. 114, 205004.

Rosenbluth, M. N. and C. L. Longmire, 1957, "Stability of Plasmas Confined by Magnetic Fields.".Ann. Phys. **1**, 120.

Rosner, R., D.A. Hammer, 2010, *Basic Research Needs for High Energy Density Laboratory Physics* (Washington, DC: US Department of Energy) http://www.science.energy.gov/fes/news-and-resources/workshop-reports/

Ross, J. S., S. H. Glenzer, P. Amendt, R. Berger, L. Divol, N. L. Kugland, O. L. Landen, C. Plechaty, B. Remington, D. Ryutov, W. Rozmus, D. H. Froula, G. Fiksel, C. Sorce, Y. Kuramitsu, T. Morita, Y. Sakawa, H. Takabe, R. P. Drake, M. Grosskopf, C. Kuranz, G. Gregori, J. Meinecke, C. D. Murphy, M. Koenig, A. Pelka, A. Ravasio, T. Vinci, E. Liang, R. Presura. A. Spitkovsky, F. Miniati, and H.-S. Park, 2012, "Characterizing counter-streaming interpenetrating plasmas relevant to astrophysical collisionless shocks." Phys. Plasmas, **19**. 056501.

Ross, J.S., D. P. Higginson, D. Ryutov, F. Fiuza, R. Hatarik, C. M. Huntington, D. H. Kalantar, A. Link, B. B. Pollock, B. A. Remington, H. G. Rinderknecht, G. F. Swadling, D. P. Turnbull, S. Weber, S. Wilks, D. H. Froula, M. J. Rosenberg, T. Morita, Y. Sakawa, H. Takabe, R. P. Drake, C. Kuranz, G. Gregori, J. Meinecke, M. C. Levy, M. Koenig, A. Spitkovsky, R. D. Petrasso, C. K. Li, H. Sio, B. Lahmann, A. B. Zylstra, and H.-S. Park, 2017, "Transition from Collisional to Collisionless Regimes in Interpenetrating Plasma Flows on the National Ignition Facility." Phys. Rev. Lett. **118**, 185003.

Ryutov, D.D., R. P. Drake, J. Kane, E. Liang, B. A. Remington, and W.M. Wood-Vasey, 1999, "Similarity criteria for the laboratory simulation of supernova hydrodynamics." Astrophysical Journal, **518**, 821.

Ryutov, D.D., M.S. Derzon, M.K. Matzen, 2000, "The physics of fast Z pinches." Rev. Mod. Phys., **72**, 167.

Ryutov, D.D., R.P. Drake and B.A. Remington, 2000, "Criteria for scaled laboratory simulations of astrophysical MHD phenomena." Astrophysical Journal - Supplement, **127**, 465.

Ryutov, D.D., B.A. Remington, H.F. Robey, R.P. Drake, 2001, "Magnetohydrodynamic scaling: from astrophysics to the laboratory," Phys. Plasmas, **8**, 1804.

Ryutov, D.D., 2011, "Using Intense Lasers to Simulate Aspects of Accretion Discs and Outflows in Astrophysics" Astrophys. Space Sci, **336**, 21.

Ryutov, D.D., N. L. Kugland, H.-S. Park, C. Plechaty, B.A. Remington, J. S. Ross, 2012, "Basic scalings for collisionless shock experiments", PPCF, **54**, 105021.

Ryutov, D.D., 2015, "Characterizing the Plasmas of Z-Pinches (Mini-Tutorial)", IEEE Transactions on Plasma Science, **43**, 2363.

Sagdeev, R. Z., C. F. Kennel, 1991, "Collisionless shock waves", Scientific American, April, p. 106.

Sawai, H., K. Kotake, S. Yamada, 2005, "Core-Collapse Supernovae with Nonuniform Magnetic Fields", The Astrophysical Journal **631**, 446-455.

Savin, D. W., N. S. Brickhouse, J. J. Cowan, et al., 2012, "The impact of recent advances in laboratory astrophysics on our understanding of the cosmos." Reports on Progress in Physics **75**, 036901.

Sedov, L. "Similarity and Dimensional Methods in Mechanics" (10th ed. CRC Press, 1993)

Severnyi, A.B., 1959, "On the Appearance of Cosmics Rays in the Pinch Effect in Solar Flares". Soviet Astronomy. **3**, 887.

Shakura, N.I., R.A. Sunyaev, 1973, "Black Holes in Binary Systems. Observational Appearance." Astronomy & Astrophysics, **24**, 337.

Shelkovenko, T. A., S. A. Pikuz, C. L. Hoyt, A. D. Cahill, L. Atoyan, D. A. Hammer, I. N. Tilikin, A. R. Mingaleev, V. M. Romanova, and A. V. Agafonov, 2016, "A source of hard X-ray radiation based on hybrid X pinches." Phys. Plasmas, **23**, 103303.

Shigemori, K., R. Kodama, D. R. Farley, T. Koase, K. G. Estabrook, B. A. Remington, D. D. Ryutov, Y. Ochi, H. Azechi, J. Stone, and N. Turner, 2000, "Experiments on radiative collapse in laser-produced plasmas relevant to astrophysical jets", PHYSICAL REVIEW E, **62**, 8838.

Shumlak, U., B. A. Nelson, B. Balick, 2007, "Plasma Jet Studies via the Flow Z-Pinch." Astrophys Space Sci, **307**, 41–45.

Shumlak, U., B. A. Nelson, E. L. Claveau, E. G. Forbes, R. P. Golingo, M. C. Hughes, R. J. Oberto, M. P. Ross, T. R. Weber, 2017, "Increasing plasma parameters using sheared flow stabilization of a Z-pinch", PHYSICS OF PLASMAS **24**, 055702.

Stehle, C., A. Ciardi, J.-P. Colombier, et al., 2009, "Scaling stellar jets to the laboratory: The power of simulations." Laser and Particle Beams, 27 709.

Stone, J.M. and M.L. Norman, 1993a, "Numerical simulations of protostellar jets with nonequilibrium cooling.1. Method and 2-dimensional results." Astrophys. J., **413**, 198.

Stone, J.M. and M.L. Norman, 1993b, Numerical simulations of protostellar jets with nonequilibrium cooling .2. Models of pulsed jets." Astrophys. J. **413**, 210.

Suttle, L.G., J. D. Hare, S. V. Lebedev, G. F. Swadling, G. C. Burdiak, A. Ciardi, J. P. Chittenden, N. F. Loureiro, N. Niasse, F. Suzuki-Vidal, J. Wu, Q. Yang, T. Clayson, A. Frank, T. S. Robinson, R. A. Smith, and N. Stuart, 2016, "Structure of a Magnetic

Flux Annihilation Layer Formed by the Collision of Supersonic, Magnetized Plasma Flows." Phys. Rev. Lett., **116**, 225001.

Suttle, L.G., J. D. Hare, S. V. Lebedev, A. Ciardi, N. F. Loureiro, G. C. Burdiak, J. P. Chittenden, T. Clayson, J. W. D. Halliday, N. Niasse, D. Russell, F. Suzuki-Vidal, E. Tubman, T. Lane, J. Ma, T. Robinson, R. A. Smith, and N. Stuart, 2018, "Ion heating and magnetic flux pile-up in a magnetic reconnection experiment with super-Alfvénic plasma inflows", Physics of Plasmas, **25**, 042108.

Suzuki-Vidal, F., S.V. Lebedev, A. Ciardi, S.N. Bland, J.P. Chittenden, G.N. Hall, A. Harvey-Thompson, A. Marocchino, C. Ning, C. Stehle, A. Frank, E.G. Blackman, S.C. Bott, T. Ray, 2009, "Formation of episodic magnetically driven radiatively cooled plasma jets in the laboratory." Astrophys Space Sci, **322**, 19.

Suzuki-Vidal, F., S. V. Lebedev, S. Bland, G.N. Hall, A.J. Harvey-Thompson, J.P.Chittenden, A. Marocchin, S.C. Bott, J.B.A. Palmer, A. Ciardi, 2010a, "Effect of Wire Diameter and Addition of an Axial Magnetic Field on the Dynamics of Radial Wire Array Z-Pinches." IEEE Transactions on Plasma Science, **38**, 581.

Suzuki-Vidal, Francisco, Sergey V. Lebedev, Simon N. Bland, Gareth N. Hall, George Swadling, Adam J. Harvey- Thompson, Jeremy P. Chittenden, Alberto Marocchino, Andrea Ciardi, Adam Frank, Eric G. Blackman, and Simon C. Bott, 2010b, "Generation of episodic magnetically driven plasma jets in a radial foil Z-pinch." Phys Plasmas, **17**, 112708.

Suzuki-Vidal, F., S.V. Lebedev, S.N. Bland, G.N. Hall, G. Swadling, A.J. Harvey-Thompson, G. Burdiak, P. de Grouchy, J.P. Chittenden, A. Marocchino, M. Bocchi, A. Ciardi, A. Frank, S.C. Bott, 2011, "Experimental Studies of Magnetically Driven Plasma Jets." Astrophys Space Sci **336**, 41–46.

Suzuki-Vidal, F., F. Suzuki-Vidal, M. Bocchi, S. V. Lebedev, G. F. Swadling, G. Burdiak, S. N. Bland, P. de Grouchy, G. N. Hall, A. J. Harvey-Thompson, E. Khoory, S. Patankar, L. Pickworth, J. Skidmore, R. Smith, J. P. Chittenden, M. Krishnan, R. E. Madden, K. Wilson-Elliot, A. Ciardi, and A. Frank, 2012, "Interaction of a supersonic, radiatively cooled plasma jet with an ambient medium" Phys. Plasmas **19**, 022708.

Suzuki-Vidal, F., S.V. Lebedev, M. Krishnan, J. Skidmore, G.F. Swadling, M. Bocchi, A.J. Harvey-Thompson, S. Patankar, G.C. Burdiak, P. de Grouchy, L. Pickworth, S.J.P. Stafford, L. Suttle, M. Bennett, S.N. Bland, J.P. Chittenden, G.N. Hall, E. Khoory, R.A. Smith, A. Ciardi, A. Frank, R.E. Madden, K. Wilson-Elliot, P. Coleman, 2013a, "Interaction of radiatively cooled plasma jets with neutral gases for laboratory astrophysics studies", High Energy Density Physics **9**, 141.

Suzuki-Vidal, F, S Patankar, S V Lebedev, S N Bland, H Doyle, D Bigourd, G Burdiak, P. de Grouchy, G N Hall, A J Harvey-Thompson, E Khoory, L Pickworth, J Skidmore, R A Smith, G F Swadling, 2013b, Observation of energetic protons trapped in laboratory magnetic-tower jets", New Journal of Physics**, 15**, 125008.

Suzuki-Vidal, F., S. V. Lebedev , A. Ciardi , L. A. Pickworth , R. Rodriguez, J. M. Gil , G. Espinosa , P. Hartigan , G.F.Swadling , J.Skidmore, G.N.Hall, M.Bennett, S.N.Bland,G. Burdiak, P.deGrouchy ,J.Music, L. Suttle , E. Hansen , and A. Frank,

2015, “Bow shock fragmentation driven by a thermal instability in laboratory astrophysics experiments”, Astrophysical Journal, **815**, 96.

Swadling, G. F., S. V. Lebedev, N. Niasse, J. P. Chittenden, G. N. Hall, F. Suzuki-Vidal, G. Burdiak, A. J. Harvey-Thompson, S. N. Bland, P. De Grouchy, E. Khoory, L. Pickworth, J. Skidmore, and L. Suttle, 2013, “Oblique shock structures formed during the ablation phase of aluminium wire array z- pinches”, Phys. Plasmas, **20**, 022705.

Szego, Karoly et al., 2015, “*The Magnetodiscs and Aurorae of Giant Planets*”, Springer.

Takezaki, Taichi, Kazumasa Takahashi, Toru Sasaki, Takashi Kikuchi, and Nob Harada, 2016, “Accelerated ions from pulsed-power-driven fast plasma flow in perpendicular magnetic field” Phys. Plasmas, **23**, 062904.

Tang, S., Q.D. Wang, 2009, “Scalability of supernova remnant simulations.” Monthly Notices of the Royal Astronomical Society, 397, 2106.

Tassis K., T,C. Mouschovias, 2005, “Ambipolar-diffusion timescale, star formation timescale, and the ages of molecular clouds: Is there a discrepancy?” ASTROPHYSICAL JOURNAL **616**, 283.

Taylor, G., 1950, “The instability of liquid surfaces when accelerated in a direction perpendicular to their planes. 1.” Proceedings of the Royal Society of London Series A-Mathematical and Physical Sciences **201**, 192-196.

Thompson, M. J. (ed.), 2006, *An Introduction to Astrophysical Fluid Dynamics* (Imperial College Press, London), Chapters 8 and 9.

Trubnikov, B.A., 1990, “On the possible generation of cosmic rays in plasma pinches.” Sov. Phys. Usp. **33**, 1061.

Trubnikov, B. A., 1992, "A new hypothesis of cosmic ray generation in plasma pinches". IEEE Transactions on Plasma Science. **20** , 898–904.

Valenzuela, C., G.W. Collins IV, T. Zick, J. Narkis, I. Krasheninnikov, F.N. Beg, 2015, “Counter-propagating plasma jet collision and shock formation on a compact current driver”, HEDP, **17**, 140-145.

Velikhov, E. P., 1959, “Stability of an ideally conducting liquid flowing between cylinders rotating in a magnetic field.” Soviet Physics – JETP, **36**, 995-998.

Vink, J., & Laming, J. M., 2003, “On the magnetic fields and particle acceleration in Cassiopeia A.” ApJ, **584**, 758.

Vishniac E.T., 1983, “The dynamic and gravitational instabilities of spherical shocks.” Astrophysical Journal, **274**, 152-167.

Uzdensky, D.A., A.I. MacFadyen, 2006, “Stellar Explosions by magnetic towers”, The Astrophysical Journal, **647**, 1192–1212.

Uzdensky, D.A., A.I. MacFadyen, 2007, “Magnetically dominated jets inside collapsing stars as a model for gamma-ray bursts and supernova explosions”, Physics of Plasmas,

14, 056506.

Walters, W., 1998, *Fundamentals of Shaped Charges*. (CMCPress, Baltimore, Maryland, ISBN 0-471-62172-2.)

Wardle, M., 2004, “Star formation and the Hall effect.” Astrophysics and Space Science **292**: 317–323.

Wheeler, J. Craig, David L. Meier, and James R. Wilson, 2002, “Asymmetric Supernovae from Magnetocentrifugal Jets”, The Astrophysical Journal, **568**, 807.

White, M. C.; Bicknell, G. V.; McGregor, P. J.; et al., 2014, “Multi-epoch subarcsecond [Fe II] spectroimaging of the DG Tau outflows with NIFS - II. On the nature of the bipolar outflow asymmetry”, MONTHLY NOTICES OF THE ROYAL ASTRONOMICAL SOCIETY, **442**, 28-42.

Woosley, S., S., 2010, "Bright Supernovae From Magnetar Birth". Astrophysical Journal Letters. **719**, L204.

Xu, Qiang, Jiakun Dan, Guilin Wang, Shuai Guo, Siqun Zhang, Hongchun Cai, Xiao Ren, Kunlun Wang, Shaotong Zhou, Zhaohui Zhang, and Xianbin Huang, 2017, “The magnetically driven plasma jet produces a pressure of 33 GPa on PTS.” Phys. Plasmas, **24**, 010701.

Xu, Xiaojun, Yi Wan, Fengsi Wei, Xueshang Feng, Xiaohua Deng, Yonghui Ma, Meng Zhou, Ye Pang & Hon-Cheng Wong, 2015, “Direct evidence for kinetic effects associated with solar wind reconnection.” Nature Scientific Reports, **5**, 8080.

Yamada, M., R. Kulsrud, and H. Ji, 2010, “Magnetic reconnection,” *Rev. Modern Phys.*, vol. **82**, pp. 603–664.

Yamada, M., J. Yoo, and C. Myers, 2016, “Understanding the dynamics and energetics of magnetic reconnection in a laboratory plasma: Review of recent progress on selected fronts . Physics of Plasmas, **23**, 055402.

Yirak, K., A. Frank, A.J. Cunningham, 2010, “Self-convergence of Radiatively Cooling Clumps in the Interstellar Medium”, The Astrophysical Journal **722**, 412-424.

You, S., J. von der Linden, E. S. Lavine, E. G. Carroll, A. Card, M. Quinley, M. Azuara-Rosales, 2018, “The Mochi LabJet Experiment for Measurements of Canonical Helicity Injection in a Laboratory Astrophysical Jet, The Astrophysical Journal Supplement Series, **236**, 29.

Yusef-Zadeh, F., M. Morris, and D. Chance, 1984, “Large, highly organized radio structures near the galactic-center.” Nature **310**, 557.

Yusef-Zadeh, F., J.W. Hewitt, W. Cotton, 2004, “A 20 centimeter survey of the galactic center region. i. detection of numerous linear filaments”, The Astrophysical Journal Supplement Series, **155**, 421.

Zhai, X., P. M. Bellan, 2016, “A hybrid Rayleigh-Taylor-current-driven coupled instability in a magnetohydrodynamically collimated cylindrical plasma with lateral gravity.” Phys. Plasmas, **23**, 032121.

Zhou, Ye. “Rayleigh–Taylor and Richtmyer-Meshkov instability induced flow, turbulence, and mixing.“ I: Physics Reports, 720–722, 1; II: Physics Reports, 723–725, 1 (2017)

Zier, J. C., R. M. Gilgenbach, D. A. Chalenski, Y. Y. Lau, D. M. French, M. R. Gomez, S. G. Patel, I. M. Rittersdorf, A. M. Steiner, M. Weis, P. Zhang, M. Mazarakis, M. E. Cuneo, and M. Lopez, 2012, “Magneto-Rayleigh-Taylor experiments on a MegaAmpere linear transformer driver.” Phys. Plasmas, **19**, 032701.

Zweibel, E.G., 2002, “Ambipolar drift in a turbulent medium.”Astrophysical Journal, **567,** 962-970.

Zweibel, E. G., M. Yamada, 2009, “Magnetic Reconnection in Astrophysical and Laboratory Plasmas”, Annual Review of Astronomy and Astrophysics, 47, 291.